CALIFORNIA
ENERGY COMMISSION

Energy Research and Development Division

FINAL PROJECT REPORT

Low-Cost, Large-Diameter Shallow Ground Loops for Ground-Coupled Heat Pumps

Gavin Newsom, Governor
February 2021 | CEC-500-2021-009

PREPARED BY:

Primary Author:
Curtis Harrington, Antash Najib, Vinod Narayanan, Mitchal Dichter

UC Davis Western Cooling Efficiency Center
215 Sage Street, Suite 100
Davis, CA 95616
(530) 754-7670
wcec.ucdavis.edu

David Springer, Michael Slater, Peter Grant, Ada Liu, James Haile

Frontier Energy
123 C Street
Davis, CA 95616
(530) 322-9143
FrontierEnergy.com

Moncef Krarti, Joseph Huang

White Box Technologies
346 Rheem Boulevard, Suite 205A
Moraga CA 94556
(925) 388-0265
yjhuang@whiteboxtechnologies.com

Contract Number: EPC-15-019

PREPARED FOR:
California Energy Commission

Abigail Jacob
Project Manager

Virginia Lew
Office Manager
ENERGY EFFICIENCY RESEARCH OFFICE

Laurie ten Hope
Deputy Director
ENERGY RESEARCH AND DEVELOPMENT DIVISION

Drew Bohan
Executive Director

ACKNOWLEDGEMENTS

The authors acknowledge the role of Professor Angelo Zarrella from University of Padova, Italy, in the development of the CaRM and assistance with using and modifying the CaRM model. Prof. Zarrella was committed to advancing this research and provided a significant contribution by reviewing work and collaborating on model improvements.

We also acknowledge Dick Bourne from Integrated Comfort Inc. who provided guidance on helical heat exchanger design, best practices for installation, and costing information for digging and installing the helical ground heat exchanger.

Finally, the project team acknowledges the members of our Technical Advisory Committee: Bill Martin with the California Geothermal Heat Pump Association, Dick Bourne with Integrated Comfort Inc., Rick Beier with Oklahoma State University, Larry Froess and Garry Maurath with the California Energy Commission, and Angelo Zarrella with the University of Padova, Italy.

PREFACE

The California Energy Commission's (CEC) Energy Research and Development Division supports energy research and development programs to spur innovation in energy efficiency, renewable energy and advanced clean generation, energy-related environmental protection, energy transmission and distribution and transportation.

In 2012, the Electric Program Investment Charge (EPIC) was established by the California Public Utilities Commission to fund public investments in research to create and advance new energy solutions, foster regional innovation and bring ideas from the lab to the marketplace. The CEC and the state's three largest investor-owned utilities—Pacific Gas and Electric Company, San Diego Gas & Electric Company and Southern California Edison Company—were selected to administer the EPIC funds and advance novel technologies, tools, and strategies that provide benefits to their electric ratepayers.

The CEC is committed to ensuring public participation in its research and development programs that promote greater reliability, lower costs, and increase safety for the California electric ratepayer and include:

- Providing societal benefits.
- Reducing greenhouse gas emission in the electricity sector at the lowest possible cost.
- Supporting California's loading order to meet energy needs first with energy efficiency and demand response, next with renewable energy (distributed generation and utility scale), and finally with clean, conventional electricity supply.
- Supporting low-emission vehicles and transportation.
- Providing economic development.
- Using ratepayer funds efficiently.

Low-Cost, Large-Diameter Shallow Ground Loops for Ground-Coupled Heat Pumps is the final report for Contract Number EPC-15-019 conducted by University of California, Davis. The information from this project contributes to the Energy Research and Development Division's EPIC Program.

For more information about the Energy Research and Development Division, please visit the CEC's research website (www.energy.ca.gov/research/) or contact the CEC at ERDD@energy.ca.gov.

ABSTRACT

This project developed and validated modeling tools for simulating a ground heat exchanger technology that provides a less expensive method for implementing ground-source heat pumps and significantly reduces energy use in many California climate zones, furthering attainment of California's energy goals. It is well documented that properly sized and installed ground-source heat pumps enjoy higher system efficiencies than conventional air-source systems by exchanging heat with the ground rather than with ambient air. Ambient air temperatures are hottest when cooling is most required and coldest when heating is most required. Exchanging heat with the ground reduces the temperature extremes and improves heat pump performance.

Market adoption of ground-source heat pump technology has been slow largely due to the significant cost of installing the ground heat exchangers. This technology generally requires drilling deep to place the heat exchanger. Typical California valley soil conditions require 200-foot-deep bores for each ton of heat pump capacity, so a three-ton system would require three 200-foot bores, costing at least $9,000. The large-diameter shallow bore technology studied in this project, however, costs roughly one-third the cost of the deep bore technology.

To evaluate the benefits to California ratepayers, this project performed an analysis using EnergyPlus, and considered the effect of using the large-diameter shallow bore ground-source heat pump on heating and cooling energy end uses for a prototypical single-family home located in each of California's 16 climate zones. Simulations show a significant reduction in energy use for many California climate zones, with an average heating and cooling energy savings of 20 percent and 23 percent, respectively. Based on a general cost of $0.20 per kilowatt-hour, the annual savings for California ratepayers would be more than $100 for eight of the 16 climate zones and more than $300 for climate zone 16.

Keywords: Ground source heat pump systems, ground heat exchanger, helical shape, numerical simulation, computational fluid dynamics, shallow bore hole

Please use the following citation for this report:

Harrington, Curtis, Antash Najib, Vinod Narayanan, David Springer, Michael Slater, Peter Grant, Ada Liu, James Haile, Moncef Krarti, and Joseph Huang. 2021. *Low Cost, Large Diameter Shallow Ground Loops for Ground-Coupled Heat Pumps*. California Energy Commission. Publication Number: CEC-500-2021-009.

TABLE OF CONTENTS

Page

ACKNOWLEDGEMENTS i

PREFACE ii

ABSTRACT iii

EXECUTIVE SUMMARY 1

Introduction 1

Project Purpose 1

Project Approach 1

Project Results 3

Technology/Knowledge Transfer/Market Adoption (Advancing the Research to Market) 3

Benefits to California 4

CHAPTER 1: Introduction 7

California Energy Commission Initiatives and Legislative Background 8

CHAPTER 2: Project Approach 10

Existing Ground Heat Exchanger Installations 10

Lab Testing of Ground Heat Exchangers 11

Goals of Lab Testing 12

Davis Lab Design and Test Matrix 12

Test Matrix 17

Computational Model Development 19

CaRM-He Tool 21

CFD model 22

Boundary Conditions 24

Modifications to the CaRM-He Model (CaRM-He v2) 28

G-Function Development 30

General Equation for Long-Term G-function 30

Short Term g-functions 30

Modification in g-function Formula for Shallow Helical GHEs 30

Effect of Surface Boundary Condition 31

Initialization 31

Temporal Discretization 33

System and Site-Specific Inputs 34

G-function for Multiple Bores 34
Validation Results 35
G-function for T_{amb} = T_g= 59°F (15°C): 36
Mean Fluid Temperature or Cases T_{amb} ≠ T_g= 59°F (15°C): 39
EnergyPlus Integration 40
California Climate Zones 42
CHAPTER 3: Project Results 45
Lab Testing Results 45
Results from Single Bore Testing 45
Results from Multiple Bore Testing 50
Model Validation 51
Model Calibration with Existing Field Data and Validation with Detailed CFD Model 51
Model Validation with Laboratory Data 57
Ground Heat Exchanger Parametric Analysis 61
CHAPTER 4: Technology/Knowledge/Market Transfer Activities 74
CHAPTER 5: Conclusions and Recommendations 76
CHAPTER 6: Benefits to Ratepayers 78
Analyzing Ratepayer Benefits 78
LIST OF ACRONYMS 80
REFERENCES 81
APPENDIX A: Excerpts from Energy Commission Documents and Other References A-1
APPENDIX B: Detailed Equations B-1
APPENDIX C: Design and Installation Guide C-1
APPENDIX D: Additional Advantages of GSHP Systems D-1
APPENDIX E: LDSB-GSHP Integration User Guide for EnergyPlus E-1

LIST OF FIGURES

Page

Figure 1: Schematic of Laboratory Test Bore Field....13
Figure 2: Installation of Ground Heat Exchanger into Bore....14
Figure 3: Ground Heat Exchanger Load Control Scheme....17
Figure 4: Illustration of Ground Heat Exchanger Configurations....20
Figure 5: Model Schematic....21
Figure 6: Bore hole Model....22
Figure 7: Field Data from Honda Smart Home Helical Ground Heat Exchanger....23
Figure 8: Ground Temperature Profiles from CFD Simulations with Fine and Coarse Mesh....24
Figure 9: Boundary Conditions for Models....25
Figure 10: Ground Temperature Profile from CaRM-He Original and CFD....27
Figure 11: Approach of the New CaRM-He V2....29
Figure 12: Scheme Showing the Superposition Method....31
Figure 13: Ambient Hourly Temperature Comparison....32
Figure 14: G-Function Generated Using Parameters from Kusuda and Achenback (1965) Method....33
Figure 15: Ground Heat Exchanger Boundary Conditions, Type 1 to Type 4 Used in CaRM....35
Figure 16: Nine Ground Heat Exchangers Row Used for Simulation....35
Figure 17: Long-Term and Short-Term G-Functions for Types 1 and 2b with $T_{amb}=T_g=59°F$ (15°C)....36
Figure 18: Long-Term G-Functions for Types 1 and 2b Under Different Configurations and Loads....37
Figure 19: Mean Fluid Temperature Calculated at Different Ambient Conditions....40
Figure 20: Rendering of Detached Home Model Used for EnergyPlus Modeling....41
Figure 21: Map of 16 California Climate Zones....43
Figure 22: Test at 1200W with a Dry Bore....45
Figure 23: Single Bore Test at 300W and 1 gpm....46
Figure 24: Single Bore Test at 600W and 1 gpm....46
Figure 25: Single Bore Test at 900W and 1 gpm....47
Figure 26: Single Bore Test at 1200W and 1 gpm....47
Figure 27: Single Bore Test at 600W and 1.2 gpm....48

Figure 28: Single Bore Test at 600W and 0.8 gpm 48
Figure 29: Single Bore Test at 1200W, 1 gpm Constant Load Long Term 49
Figure 30: Single Bore 1200w Intermittent Load Test 50
Figure 31: Bore Performance in Multiple Bore Testing at 1200W per Bore 51
Figure 32: Modeled Temperature Predictions Compared to Measured Data 52
Figure 33: Short-Term Ground Temperature Profile from Models 53
Figure 34: Long-Term Ground Temperature Profile from Models 54
Figure 35: Core Temperatures Predicted by Models 55
Figure 36: Bore wall Temperatures Predicted by Models 56
Figure 37: Soil Thermal Conductivity Testing 57
Figure 38: Measured and Modeled Inlet and Outlet Temperature for Single Bore with Cyclic Loading 58
Figure 39: Measured and Modeled Bore hole Wall Temperature 59
Figure 40: Measured and Modeled Inlet and Outlet Temperature for Multiple Bore with Constant Loading 60
Figure 41: Measured and Modeled Bore hole Wall Temperature for Multiple Bore with Constant Loading 60
Figure 42: Ambient Air, Dry Bulb Temperature for Climate Zone 12 and Periodic Temperature Curve Fitted to Data 62
Figure 43: Hourly and Cumulative Seasonal Load Profiles for Model Home in Climate Zone 12 63
Figure 44: Ambient Air, Dry Bulb Temperature for Climate Zone 10 and Periodic Temperature Curve Fitted to Data 64
Figure 45: Hourly and Cumulative Seasonal Load Profiles for Model Home in Climate Zone 10 65
Figure 46: Land Area Considerations Based on Bore hole Configuration 68
Figure 47: Results from Parametric Study for Climate Zone 12 69
Figure 48: Climate Zone 12 Annual Heating and Cooling Season Electricity Consumption 71
Figure 49. Results from Parametric Study for CZ 10 (Riverside) 72
Figure 50: Climate Zone 10 Annual Heating and Cooling Season Electricity Consumption 73
Figure E-1: The Variation of G-Function as a Function of Ln(T/Ts) E-2
Figure E-2: Equations Used for Applying G-Functions Predicting Mean Fluid Temperature E-3

LIST OF TABLES

Page

Table 1: Ground Heat Exchanger Geometry 15
Table 2: General Sensor Specifications 16
Table 3: Original Test Matrix 18
Table 4: Mesh Parameters for Grid Independence Study 22
Table 5: CFD Model Parameters 23
Table 6: Common Parameters Used in CFD and CaRM-He Models 24
Table 7: Ground Properties for Yolo Silt Loam Based on Moisture 26
Table 8: Temporal Parameters for G-Functions 34
Table 9: G-Functions at 21 Points for Ground Heat Exchangers of All Six Types 38
Table 10: G-functions for Row of 9 and 16 Ground Heat Exchangers 39
Table 11: Basic Features of Detached Home Model Used for Simulation Analysis 42
Table 12: Summary of Annual Heating and Cooling Degree Days 44
Table 13: Basic Characteristics of Home Model Used 61
Table 14: Parametric Variables Used in Simulations 66
Table B-1: Example of Site-Specific Data Required for Simulationx B-3
Table C-1: Installation Guide for Bore Field Sizing Bore Hole Quantity per Ton for 15' Deep Holes C-2
Table C-2: Installation Guide for Bore Field Sizing Bore Hole Quantity per Ton for 22' Deep Holes C-2
Table C-3: Manifold Maximum One-Way Length in Feet vs. Connecting Pipe Size System Size, Tons C-3
Table C-4: Ground-Source Heat Pump Standards from AHRI 330-1998 ..... C-5
Table D-1: AHP/GHP Performance Comparison D-2
Table D-2: Other Considerations* D-2

EXECUTIVE SUMMARY

Introduction

Ground-source heat pumps take advantage of moderate ground temperatures to reduce energy required by pumps to heat and cool buildings. Traditional air-source heat pumps and air conditioners exchange heat with outside air, which is hottest when air conditioning demand is high and lowest when heat pump heating demand is high. This leads to inherent inefficiency from the large temperature difference between the inside and outside of the building. Ground temperatures, on the other hand, have a more stable temperature, which means using the ground as a heat sink/source can improve the efficiency of heat pumps.

Ground-source heat pumps have been around for decades but have traditionally involved drilling deep into the earth to place the ground heat exchanger. A demonstration and commercialization project co-sponsored by the California Energy Commission, Pacific Gas and Electric Company, and the National Geothermal Heat Pump Consortium in the 1990s (the California GeoExchange Project) determined that the cost to install vertical ground loops was greater than $10 per foot, and costs reported in 2010 were about $15 per foot. For typical central valley soil conditions, 200-foot-deep bores are required for each ton of heat pump capacity, so a three-ton system would require three 200-foot bores, costing at least $9,000. Installing ground heat exchangers at that depth also requires special equipment for drilling and grouting not commonly available in California. Consequently, drillers frequently must transport equipment from out of state, adding logistical complications and complexity to using this technology. The high cost of ground heat exchangers is the reason this technology is not more commonly used.

This project investigates an alternative ground heat exchanger design that is significantly cheaper to install. The large-diameter shallow bore heat exchanger is a helix design that is installed at much shallower depths, thus reducing excavation costs. The large-diameter shallow bore design has been slow to penetrate the market due to the lack of clear design guidelines and modeling tools for simulating performance.

Project Purpose

This project developed and validated modeling tools for simulating performance of the large-diameter shallow bore ground-source heat pump system. These tools enable proper sizing of bore hole arrays to optimize performance and installation cost. In addition, accurate estimates of performance for a specific design enable calculation of appropriate returns on investment relative to other technologies. These tools are expected to improve market adoption of this technology by giving installers more confidence in the energy performance of their designs. Field and lab data were used to validate the models and confirm accuracy.

Project Approach

The research team was led by the University of California, Davis Western Cooling Efficiency Center, which is part of the UC Davis Energy and Efficiency Institute. Frontier Energy was a subcontractor that directed the field and laboratory work, and White Box Technologies, another subcontractor, provided guidance on the EnergyPlus simulations. Integrated Comfort

is an equipment manufacturing partner that provided expertise on large-diameter shallow bore installations and cost.

An independent technical advisory committee provided input on the research design. The technical advisory committee members represented the California Energy Commission, academia, and an equipment manufacturer.

The project included a thorough review of existing research, field data collection, laboratory testing, and modeling calibration.

The literature review considered prior research related to ground-source heat pump installations and modeling strategies. This included traditional ground heat exchanger types and helical-type (i.e., coil shaped) heat exchangers. Through the literature review, the research team discovered previous modeling techniques for shallow, helical ground heat exchanger designs. The investigator of that work, Angelo Zarrella from the University of Padova in Italy, collaborated with the research team on this project to further improve modeling predictions.

The field testing collected data on three existing large-diameter shallow bore ground-source heat pump systems (LDSB-GSHP) to observe the temperature response from the ground heat exchangers. The first is the Honda Smart Home, a net-zero energy demonstration house located in Davis, California. The second is a small condo building in Davis, California called Parkview Place. Finally, the third installation is a single-family house located in Vacaville, California. These three sites used similar ground-coupled heat exchangers, with notable differences in design. Short-term and long-term testing were conducted to evaluate the performance. Data collected on the field test sites primarily consisted of water temperature entering and exiting the bores and water flow rate. Other than the Honda Smart Home, which included a significant monitoring system, the field test sites in Northern California could only provide minimal information for model validation purposes. It became clear from the field testing that known soil properties are extremely important for validating model predictions.

The laboratory testing for this project was ultimately used for model validation. The researchers installed an arrangement of four helical ground heat exchangers that was then connected to laboratory equipment to provide specific thermal loads to the ground heat exchangers. The arrangement enabled testing of multiple bores in common bore hole configurations. The soil properties at the laboratory test site as well as the backfill material were tested for thermal conductivity, density, and specific heat. The bore field was instrumented with temperature sensors and moisture sensors to measure the distribution of temperature in the ground for comparison to model predictions. Several lab tests validated the numerical simulation of ground heat transfer between a helical ground heat exchanger and the ground.

Model calibration was performed at multiple points during this project and using multiple sources. First, the Honda Smart Home site, which provided the most detailed monitoring instrumentation, was used for the initial validation. However, soil thermal properties were not known and had to be adjusted from original assumptions. Second, a detailed three-dimensional computation model was developed to further validate the numerical model using the same soil thermal properties. Lastly, the laboratory testing provided a final calibration where soil properties were known and model predictions for exiting water temperature from the ground heat exchanger and ground temperatures could be verified.

Project Results

The primary objective of this project was to develop tools for simulating large-diameter shallow bore ground-source heat pump systems. The capacitance-resistance model (CaRM-He) was improved by this effort, enabling better prediction of fluid temperatures in the bore. The model developed has shown good agreement with field and laboratory data, providing a valuable resource for the industry. The CaRM-He model was used to develop response factors (G-functions) for use in open-source software programs such as EnergyPlus, enabling practitioners and other stakeholders to perform specific simulations for their projects.

Validation efforts demonstrated the improved CaRM-He model agreed with laboratory test data. The outlet temperature from the bore was predicted to within 1.8°F (1°C) of the measured result in single-bore and multi-bore configurations. This outlet temperature is the key parameter affecting heat pump performance since this is the sink/source temperature from which heating and cooling is provided. An accurate outlet temperature provides accurate estimates of energy use for a heat pump. As one point of reference, the heat pump equipment referenced for the simulations in this project showed that a 1.8°F difference in outlet temperature resulted in only a 3.0% difference in efficiency.

Using the CaRM-He model, parametric simulations were performed to assess the effect on heating and cooling energy use when varying design conditions, including number of ground heat exchangers, soil thermal properties, bore hole arrangement including spacing and configuration, and cost. The simulations were performed in California climate zones 10 and 12 using building loads generated from CBECC-Res (2013), which is the compliance software used by the 2019 California Building Energy Efficiency Standards – Title 24. Climate zone 10 is in Southern California with a reference city of Riverside while climate zone 12 is in the central valley with a reference city of Sacramento. The analysis of the two valley climate zones indicates that the ground-source system outperformed the air-source system in all configurations tested. The parametric analysis found the optimal bore design based on installation cost and energy performance. Using the results, the research team calculated the cost per kilowatt-hour of electricity saved annually, which was $4.35 and $3.72 per kilowatt-hour for climate zones 10 and 12, respectively. This metric was developed to better compare the trade-off between different bore field designs and system efficiency (e.g., more bores provide better efficiency but at a higher installation cost.) This metric also allows the GSHP technology to be compared to other technologies such as photovoltaic system to determine the better investment.

Technology/Knowledge Transfer/Market Adoption (Advancing the Research to Market)

Stakeholder outreach was conducted throughout the project to disseminate results. This information reached a much broader audience than would ordinarily seek out research related to ground-source heat pumps. The Western Cooling Efficiency Center conducts numerous tours, which include a poster presentation on this project. Visitors from all over the world are able to hear about the work and the potential for the technology.

This project also produced several publications. Papers have been published in Applied Thermal Engineering and presented at the 2019 and 2020 American Society of Heating,

Refrigerating and Air-Conditioning Engineers (ASHRAE) annual conferences, the largest heating, ventilation, and air conditioning-related conference in the world. ASHRAE and its members focus on building systems, energy efficiency, indoor air quality, refrigeration, and sustainability in buildings. Antash Najib, the graduate student researcher on this project, was awarded multiple awards, including the College of Fellows award from ASHRAE and the Kirk T. Mescher Award.

The project team also worked closely with Integrated Comfort Inc. which provided detailed cost information, which was used in the parametric analysis, and consulted on the design and installation guide. The company plans to use the modeling results from this project to market ground source heat pump technology in California.

Another impediment to technologies making a significant impact in the California housing market is whether they can be accurately simulated in the California code compliance software. EnergyPlus is used as the simulation engine for commercial buildings but residential building rely on the California Simulation Engine (CSE) through CBECC-Res. According to the 2019 Residential Alternative Calculation Method (ACM) Reference Manual, ground-source heat pumps are currently simulated as a minimum efficiency split-system equivalent to the standard design. This clearly does not capture the efficiency improvement potential of ground-source heat pumps and does not allow for designers to qualify for incentives for installing the technology. Discussions with the California Building Standards Office highlighted that future versions of the ACM will include improved performance maps which might accommodate ground-source heat pumps. A similar approach could be applied as used for variable capacity heat pumps (VCHPs) or "mini-splits" wherein a percentage improvement over minimum standard efficiencies could be used. Designs would have to meet specific eligibility criteria for ground heat exchanger design. The problem with this method is that there is a much wider variation in ground-source heat pump performance than for VCHPs (COPs range from 3.1 to 5.6 and EERs from 13.8 to 42). The efficiency adjustments could be developed using the modeling approaches developed in this project along with a heat pump model, or EnergyPlus simulations.

Benefits to California

The research team used EnergyPlus simulations to evaluate the benefits to California ratepayers. The simulations compared total heating, ventilation, and air conditioning energy use between the air-source heat pump and the large-diameter shallow bore ground-source heat pump.

The results show lower energy consumption for the large-diameter shallow bore ground-source heat pump system in all climate zones except climate zone 15. Climate zone 15 is the hottest climate zone with the largest cooling loads and very minimal heating loads. This unbalanced load results in poorer performance for the large-diameter shallow bore ground-source heat pump system. The climate zone with the largest savings was climate zone 16. While this climate zone is also unbalanced with much higher heating loads than cooling loads, the very low ambient temperatures result in poor performance from the air-source system while the large-diameter shallow bore ground-source heat pump system does not experience the same temperature extremes when exchanging heat with the ground.

The reduction in energy use is significant for many California climate zones. The simulations show roughly 20 percent heating and cooling energy savings for many climate zones and up to 27 percent in certain regions. Based on a general cost of $0.20 per kilowatt-hour, simulations show annual cost savings for California ratepayers of more than $100 for 9 of the 16 climate zones and more than $300 for climate zone 16.

CHAPTER 1: Introduction

The goal of this project was to produce tools and materials needed to remove the barriers that currently prevent widespread adoption of a less expensive method for implementing ground-source heat pump technology. Air conditioners and air-source heat pumps reject heat to the hottest air when demand for cooling is greatest and absorb heat from the coldest air when demand for heating is greatest. These conditions result in average efficiencies far below their rated seasonal energy efficiency ratio (SEER) and heating seasonal performance factor (HSPF). By exchanging heat at the mild temperatures found deep in the soil, ground-coupled heat pumps transcend the performance limitations of air-source systems. It is well documented that properly sized and installed ground-source heat pumps (GSHPs) enjoy higher system efficiencies than conventional air-source systems.

With these proven energy savings, why are ground-coupled heat pumps not prevalent in California? The primary answer is the high cost of the ground heat exchangers. A demonstration and commercialization project co-sponsored by the California Energy Commission (CEC), Pacific Gas and Electric Company (PG&E), and the National Geothermal Heat Pump Consortium in the 1990s (the California GeoExchange Project) determined that the cost to install vertical ground loops was greater than $10 per foot, and costs reported in 2010 were about $15 per foot (Davis Energy Group 2010). For typical central valley soil conditions, 200-foot-deep bores are required for each ton of heat pump capacity, so a three-ton system would require three 200-foot bores, costing at least $9,000. Installing ground heat exchangers (GHE) at that depth also requires special equipment for drilling and grouting not commonly available in California. Consequently, drillers frequently must transport equipment from out of state, adding logistical complications and complexity to employing this technology.

The California GeoExchange project afforded the opportunity to explore lower cost alternatives to standard vertical bores, and a large-diameter shallow bore (LDSB) heat exchanger was developed, tested, and applied to student housing on the University of California, Davis campus (Villages at La Rue) in the mid-1990s. These GHEs used a 30’ deep by 36” diameter hole drilled using readily available auger equipment, and a ½” diameter high density polyethylene helical coil heat exchanger. The ground loops performed satisfactorily, but the project ended before the technology could be developed to the point of commercialization. Subsequently, similar installations have been completed at the Honda Smart Home (also on the UC Davis campus) and at a small retirement community (Parkview Place) in downtown Davis. Each of these installations employed slightly different GHE designs.

This project further explores the promise of the large-diameter shallow bore ground heat exchanger (LDSB GHE) design through a series of efforts. The tasks for this project included gathering data on existing installations, developing modeling tools for simulating performance, installing, and testing GHEs to measure performance for model validation, and performing building energy modeling of the system in multiple California climate zones.

Heat transfer to and from the soil can be affected by the design of the system, the amount of heat transferred between the GHE and the bore, the length of delay periods between heat

transfer events, and the soil moisture content of the bore. To evaluate the LDSB GHE design, the project team first collected basic data on existing installations such as heat load and flow rates. Since the performance of the GHE depends on several parameters, including soil properties, a more detailed and controlled lab experiment was implemented as a part of the project. The goal of the lab data collection was to measure the heat transfer performance between the GHE and the ground. The lab data also provided a dataset for validating the computational model that was developed for LDSB GHEs. The model was used to perform parametric analysis of the heat exchanger design to optimize performance with variables of depth, diameter, backfill material, and bore spacing and configuration. The validated computational model was also used to develop non-dimensional soil resistance functions, called g-functions, which were in turn used in coupled building simulation models to predict the energy savings by use of a water-source GHE heat pump compared to an air-source heat pump.

California Energy Commission Initiatives and Legislative Background

The CEC has been involved with proceedings related to geothermal resources, including high temperature geothermal and low temperature applications using heat pumps, for over 20 years. Recent activity is listed below.

Assembly Bill 2339 (Williams, 2012) required the CEC to evaluate policies to overcome barriers to the use of geothermal heat pump and ground-loop technologies in California, and to include evaluations and recommendations in the 2013 Integrated Energy Policy Report (IEPR). The CEC held a workshop in March 2013 and developed a working group to evaluate current policies.

A staff paper reviewing the issues was published in July 2014 (CEC-400-019). A barrier identified by the geothermal heat pump industry during the proceedings was that building standard models do not accurately reflect geothermal heat pump characteristics. Consequently, builders and building owners could not qualify for incentives because incentive programs are based on energy savings predicted by compliance models. The industry requested that a set of modeling rules specific to geothermal heat pumps be created. CEC staff determined that the Warren-Alquist Act required that it be the responsibility of industry to develop compliance options for technologies not explicitly covered by the standards. Recognizing that this process can take more than one year, staff suggested that design engineers confirm the efficiency of ground-coupled heat pump (GSHP) systems and develop protocols for site inspections in the interim. Industry representatives countered that it should be the responsibility of the CEC take the lead in developing an Alternative Calculation Method (ACM) compliance option.

A 2012 CEC staff report assessed geothermal heat pump efficiencies by climate zone concluded "Such systems are among the most efficient and cost-effective means for conditioning interior air and use 25 percent to 50 percent less electricity than conventional heating and cooling systems." The report also concluded that the absence of an assessment that measures the applicability of GSHP systems to California's diverse geology and climate zones, and insufficient analysis of the benefits these systems could provide to help California comply with a Renewables Performance Standard (RPS) and Assembly Bill 32 (AB 32), which

mandates reductions in greenhouse gas (GHG) emissions contributed to the minimal development progress.

These prior activities clearly show that there is interest and value in overcoming barriers to GSHP technologies. The shallow-bore technology shows that the industry is continuing to develop GSHP products for the market and this project is critical for developing the necessary tools for evaluating that technology.

Additional excerpts from CEC Documents, as well as other references used, can be found in Appendix A.

CHAPTER 2:
Project Approach

Existing Ground Heat Exchanger Installations

Large-diameter shallow bore ground-coupled heat exchangers use a helical design to provide a length of heat exchanger tubing equivalent to traditional U-tube designs without requiring deep bore installations. These systems are typically installed in the top 25 feet of soil, compared to the 150 to 300 feet common in traditional U-tube designs (California Energy Commission 2014). By remaining closer to the surface, large-diameter shallow bore ground-coupled heat exchangers can significantly reduce installation costs through using less expensive equipment and avoid groundwater contamination issues.

This field study included both short-term and long-term monitoring at three separate sites in the Sacramento region of California. The first is the Honda Smart Home, a net-zero energy demonstration house located in Davis, California. The second is a small condo building in Davis, California called Parkview Place. Finally, the third installation is a single-family house located in Vacaville, California. These three sites used similar ground-coupled heat exchangers, with notable differences in design. Changes include the length of the heat exchanger, the type of backfill used, the number of heat exchangers installed, and the distance between the heat exchangers.

Short-term monitoring featured one day of testing at the Vacaville site while the system was still under construction. An external test apparatus was used to add heat to the bore while monitoring the supply, return, and ground temperatures in the system. Results indicated approximately a 7°Fahrenheit (F) (3.9°Celsius [C]) temperature drop across the heat exchanger when operated at 1 gallon per minute (gpm) of flow. Theoretical calculations showed temperature drop represents a heat exchanger effectiveness of 30 percent. Calculations for coefficient of performance of an attached heat pump indicated that the occupants should expect a range from 2.5 to 4 during typical cooling operation.

Long-term monitoring of the temperature drops and flow rate through each system identified some differences in performance. The systems at the Honda Smart Home and Parkview Place have appropriate temperature drops across the loop, ranging from 4°F (2.2°C) to 21°F (12°C) depending on the operating conditions. The larger temperature drops were at Parkview Place, and it is believed this occurred because the flow rate through each individual heat exchanger was approximately 0.6 gallons/minute at that site, much lower than the 1.15 gallons/minute through each heat exchanger at the Honda Smart Home. The temperature drop at the Vacaville site was typically around 1 to 2°F (0.6 to 1.1°C), which is low for a system like this. Water flow rate monitoring was not feasible at this site, but it is suspected that the low temperature drop in the system may have been caused by a higher than anticipated flow rate.

The maximum and minimum fluid temperature returning from the ground loops at Parkview Place and the Honda Smart Home were examined to look for potentially dangerous operation, as well as predict likely heat pump efficiencies. The return temperatures at Parkview Place were more extreme, as is expected with the lower flow rates and higher temperature drops.

The maximum temperature reached as high as 120°F (49°C), which would return an anticipated heat pump coefficient of performance of 2. The minimum recorded temperature was 36°F (2°C). While this temperature is not cold enough to cause a problem, including glycol in the system is recommended to avoid freezing the fluid and damaging the system in colder winters. Temperatures at the Honda Smart Home were more moderate, ranging from 46°F to 102°F (8° to 39°C). These more moderate temperatures would result in higher performance from the heat pump and lower risk of damage to the system.

Studying the heat transfer rate with the ground as a function of temperature difference between the supply water and average bore temperature at the Honda Smart Home showed decreased performance at high temperature differences. This could have been caused by two reasons: (1) the soil moisture content fell below the critical level, resulting in dramatically lower soil conductivity, or (2) the soil cracked, causing a gap to form between the heat exchanger and the soil, reducing performance. These potential issues could be solved by either irrigation systems adding water to the soil or by using different backfill materials, such as fine sand, to avoid the soil cracking.

Lab Testing of Ground Heat Exchangers

Laboratory experiments have been performed to address some of the limitations of the previous field monitoring data and have allowed for better validation of the computer simulation model. Field monitoring data was inadequate for a detailed validation of the GHE model. It was not possible to provide enough control of the data to validate all the detailed performance aspects of the system or of the simulation model. Field monitoring data collected previously on LDSBs were inadequate in the following ways:

1. The inability to obtain properties of the backfill and nearby soil created an uncertainty, where the model could be forced to match the data by adjusting the soil parameters. This does not allow appropriate validation of the model, as it is entirely possible that the wrong soil parameters were used to make an inaccurate model match the measured performance data.
2. None of the field installations had a good far-field soil temperature measurement. The Honda Smart Home did have a measurement, but it was situated between two bores. As a result, it was affected by the other bore and did not represent a true boundary condition. To determine boundary conditions, the far-field measurement provides a reference to distinguish the effects of surrounding bores from the effects of the ground itself.
3. Ground temperature profiles were only collected in the Honda Smart Home, which prevented adequate data for verifying simulation results.

Additionally, the field monitoring did not allow precise control of the water flow rate through the bores or to an irrigation system. Investigating irrigation of the bore hole or bore field was not part of the goal of the field monitoring plan, but there is potential for these techniques to increase the performance of the systems.

The laboratory testing in this project was designed to address these issues through data collection in a more controlled laboratory environment wherein simulated heat pump loads could be imposed on a single or on multiple GHEs.

Goals of Lab Testing

Lab test design and test plans were developed to ensure that there was an ability to: (1) assess the backfill and soil properties, (2) control the number and configuration of GHEs active at any given time, and (3) control the load profile of the heat exchangers.

A study of the performance of irrigation systems and the effect of rainfall was a fundamental part of this study. Performance degradation was observed during the summer in the field monitoring installations. On-site measurements in existing GHE installations were not adequate to determine the cause of this degradation; however, the prevailing theory was that low moisture in the soil caused either (1) the soil conductivity to dramatically decrease, or (2) the soil to crack, degrading the physical connection between the GHE and the soil. Rejecting heat drives moisture out of the soil, so it was proposed that there is some critical moisture content for a given type of soil below which efficacy falls off. For Yolo County loam, which is the soil for both the laboratory and the Honda Smart Home field measurements, this number is estimated at 20 percent (Hart and Couvillion 1986). Laboratory testing addressed this issue by (1) including soil moisture measurements in the bore and surrounding soil and (2) performing long term tests, intended to drive moisture out of the soil and cause a low performance situation.

The final research topic is a preliminary study on the flow rate of water through the GHEs. Lower water flow rates through the GHE would increase the residence time for water to exchange heat with the soil and would result in higher temperature drops across the heat exchanger. Theoretically this could result in more favorable temperatures at the heat pump and higher coefficient of performance (COP). The downside is that lower flow rates cause lower heat transfer rates, reducing the ability to exchange heat with the ground. This preliminary study will explore (1) whether lower flow rates can improve condensing temperature and COP of the, and (2) whether there is potential to design a controller that identifies the heat pump's need for heat exchange with the ground and adjusts flow rate to match that need by increasing or decreasing flow rate, as necessary. These two questions could lead to controllers for GHE systems that improve the COP of the attached heat pump by reducing the flow rate when possible.

Ultimately, through this project, a lab experiment was designed and built to appropriately test single and multiple GHEs, control loading conditions, and test bores in in-line and corner bore configurations. By varying the bore configuration, the effect of different types of boundary conditions could be assessed experimentally and used in model validation.

Davis Lab Design and Test Matrix

The laboratory was constructed near the UC Davis campus, at 17 Arboretum Drive, Davis California 95616. This is lab space used by Frontier Energy for several projects. The inside of the building contains some environmental chambers and various parts from previous projects. These parts are recycled as needed to accommodate the requirements of experiments and fit the experimental design. The dirt lot on the outside of the building was used as the location to dig the bores and bury the heat exchangers for this set of tests.

Lab Design

Davis is in Yolo County, which is in climate zone 12. It typically has a cooling season that lasts from early June to late September and a heating season that lasts from late November to mid-February. Tests for this project were completed during an off-peak and heating season from September to January. The lab's soil was Yolo County loam, which is compositionally similar to that at the Honda Smart Home. One benefit of doing soil analysis at this site was that the Honda Smart Home field tests could be better understood.

Bore Construction, Layout, and Monitoring Instrumentation Specifications

Figure 1 shows a schematic of the laboratory test apparatus. It has the following features:

1. Four test bores, with three in a straight line and a fourth adjacent to the center bore forming a T-shape. One of three configurations could be tested — the single central bore, three in-line bores or three bores in an L shape corresponding to a corner bore configuration.
2. Temperature measurements at five depths in the center of two test bores, on the edge (bore wall) of two test bores, and every 3.33 feet in between the monitored test bores.
3. Moisture sensors at three depths in the center of two test bores and every 3.33 feet between the two monitored test bores.
4. Five far-field temperature measurements and two far-field moisture measurements 10 feet away from the test bores.
5. Hot water supply and cold water return lines.

Figure 1: Schematic of Laboratory Test Bore Field

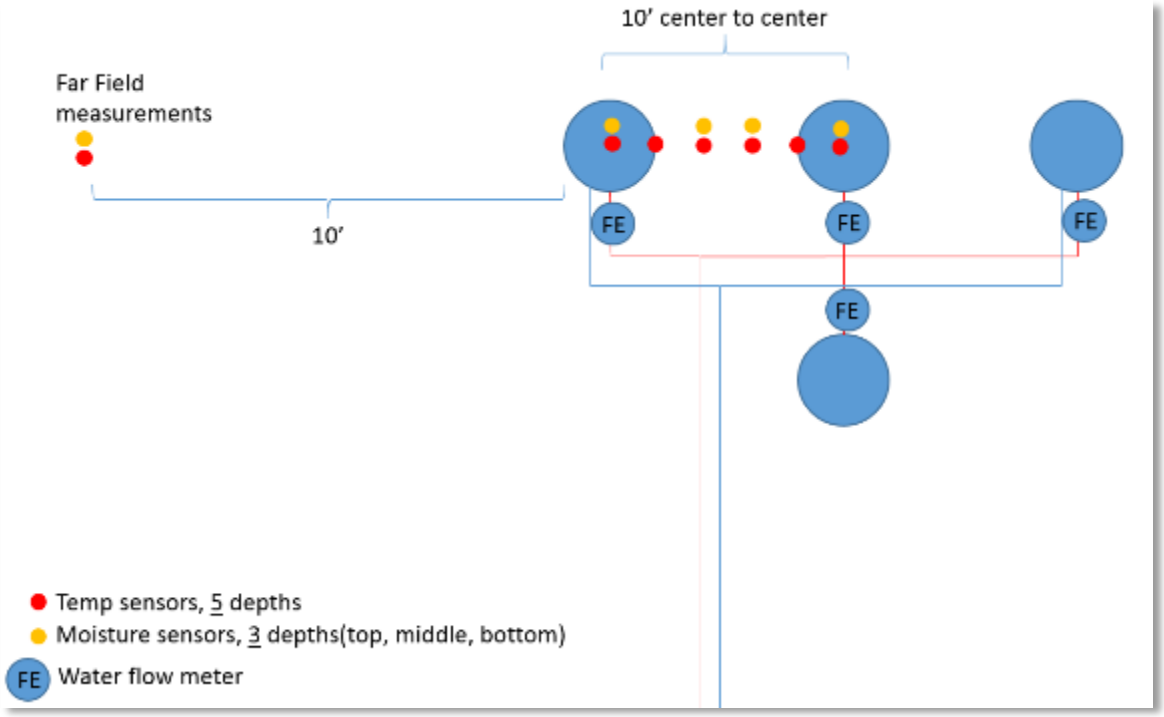

Source: University of California, Davis

Additional controls and sensors not shown in the schematic include:

1. Manual ball valves on each test bore hot water supply line that allowed control of which test bores are included in each test
2. Supply and return water temperature on each of the instrumented test bores
3. Automatic control of water flow rate to the test bores (presented in Figure 4.)
4. Automated control of the water temperature directed to the test bores (presented in Figure 4.)

The heat exchanger geometry and bore parameters are shown in Table 1, and the installation of the heat exchanger is shown in Figure 2. To install the heat exchangers, four 20-foot-deep bores were excavated. This excavation took less than 30 minutes per bore and required no grout to keep the bore from collapsing. This is very different than conventional vertical bore drilling, which typically requires a 200-foot-deep bore and grouting and a day to excavate each bore. Conventional installation also requires specific drilling equipment designed for this purpose. The LDSB heat exchanger had a helix design. The coil spacing was preserved by fabric ties and had a rigid tube to preserve the heat exchanger length. Drip irrigation tubes were added to each instrumented heat exchanger. After installation, the bores were backfilled with fine-grain sand, which helps to distribute moisture and preserve the desired heat-exchanging characteristics. Fine-grain sand was chosen over other backfill materials because it is readily available at major landscaping equipment retailers and is cheaper than custom backfill materials. It is therefore more likely that installers would use fine-grain sand in common GHE installations.

Figure 2: Installation of Ground Heat Exchanger into Bore

Source: University of California, Davis

Table 1: Ground Heat Exchanger Geometry

Parameters	Values
Helix pitch	0.2286 m (9 in.)
Helix diameter	0.5588 m (22 in.)
Helical pipe height	6.096 m (20 ft)
Depth of helical pipe top	0.762 m (2.5 ft)
Nominal pipe diameter	3/4 in. (nominal size)
Bore diameter	0.6096 m (24 in.)
Tube material	High-density polyethylene (HDPE)
Backfill	Fine-grain sand
Heat transfer fluid	Water
Supply pipe	Straight pipe

Source: University of California, Davis

Table 2 lists the types of sensors used for the various monitoring and control points and their performance specifications. Sensor selection was based on functionality, accuracy, cost, reliability, and durability. Specific model numbers are listed as examples; similar models by other manufacturers may have been used. Signal ranges for temperature sensors correspond approximately to listed spans. The rationale and requirement for each measurement and control point was as follows:

- Field Measurements
    - Ground loop flow rate for each monitored test bore
    - Ground loop supply and return temperatures for each monitored test bore
    - Ground moisture content at three depths for two test bores. Locations at the center and every 3.33 feet in between
    - Ground temperatures at three to five depths for two test bores. Locations at the center of the bore, the edge of the bore, and every 3.33 feet in between the two bores
    - Ground temperatures at three to five depths for far-field location
    - Ground moisture content at three depths for far-field location
- Control Points
    - Water flow on/off control to individual test bore
    - Water flow on/off control to irrigation supply
    - Water flow rate to ground loop supply
    - Ground loop supply temperature

Table 2: General Sensor Specifications

Measurement	Sensor	Accuracy	Range	Signal
Soil Temperature	Surface Mounted Type T Thermocouple	±1°F (0.6°C) or 0.4% of reading	–454°F (–270°C) to 750°F (399°C)	40 µV/°C
Water Temperature	RTD Pipe Plug Probe	±(0.15+.002*T) or 100±0.06*Ω	Max Temp 450°F (230°C)	100 Ω/°C
Flow Rate	Omega FTB4600	1.5%	0.15–13 gpm	Pulse
Soil Moisture	Hydra Probe SDI-12	±0.01 WFV	0–100% WFV	SDI-12
Thermocouple Input	NI-9213	<0.45°F (0.25°C)	Determined by TC	—*
Analog Output	NI-9265	±0.1%	0-4mA (output)	—*

***Connected to CompactDAQ through backplane**

Source: University of California, Davis

Heating and Cooling Control

Figure 3 shows the way that the load to each bore was controlled. The lab could produce a heating and a cooling load by use of a water heater and a chiller. For the hot side, the water heater was fed with a domestic water supply through a city water hookup. From the Domestic Supply on the leftmost side of Figure 4, water flowed through a fill assembly that mixed supply water with recirculated water from the bottom of the hot water storage tank and sent it to the tankless water heater assembly. Hot water was then pumped through an air separator before returning to the hot tank. The tank was used to stabilize temperatures so that fluctuations from the tankless water heater, such as from the beginning of burner cycles would be smoothed out. Hot water was then pumped to the supply manifold for the bores from the top of the hot tank.

For the cold side, water was fed directly into a chilled water holding tank through a fill assembly. Water from the top of the holding tank was pumped to the chiller, and chilled water was fed to the bottom of the chilled water tank. The water used for each test flowed through the bores and was then returned to the system through the return manifold, which returned water to the appropriate tank depending on the kind of test being run. Not pictured in Figure 3 are the hot and chilled water bleeds.

Controlling the temperature of the inlet water to the bores was crucial for controlling the load to each bore. Proprietary laboratory modelling software was used to provide a constant load or a cycling on/off load with a consistent input rate for the bores. This was done by measuring the outlet temperature of water from the bore and back-calculating what the inlet temperature would need to be at the test's flow rate for the desired load.

Figure 3: Ground Heat Exchanger Load Control Scheme

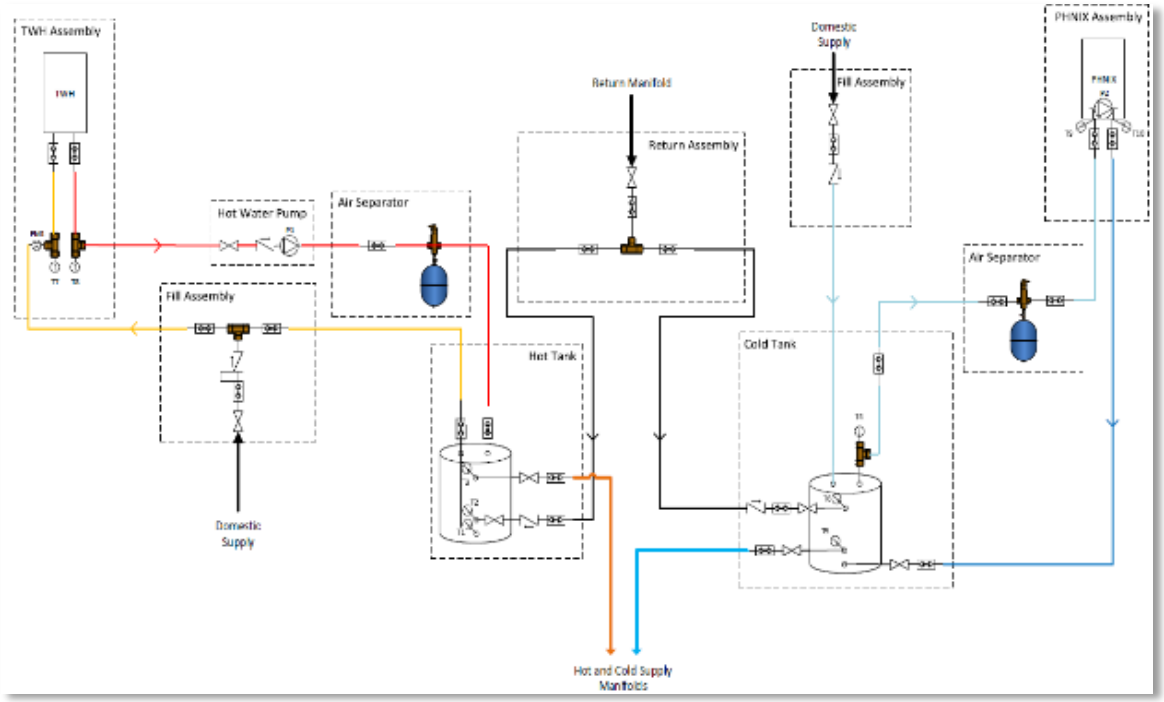

Source: University of California, Davis

Test Matrix

The lab completed tests to determine the capacity of a single bore. This was done by running a constant load through a bore for many hours and observing the outlet temperature. The test was set to be arrested if the outlet temperature stabilized or if it reached a high temperature limit of 120˚F. This test was repeated at increasing load magnitudes up to a maximum load of 1200 watts (W) per bore, which corresponds to an input rate around three tons per bore. This capacity is critical because it was previously determined that to be cost effective for residential applications, the heat exchanger would need to be able to handle this level of load. The single bore tests also provided a detailed understanding of the surrounding soil temperatures. The single bore tests were performed both in the short term of a few hours, which represented a single heating or cooling event, and for intermittent loads over the course of a few days, which was intended to measure the performance of a bore in a more realistic loading scenario. These tests were also important to further validate the CaRM-He model used for simulating heat exchanger performance. The single heat event test validated the simplest use case of the model, and the intermittent load tests required the model to match the performance of the GHEs during each heat exchange event and to predict the behavior of the surrounding soil including the soil saturation limits.

Array tests were also performed both with single heat events and intermittent loads, where multiple bores were operated at the same time. These tests were important to the model because they required the model to accurately predict the boundary conditions between each bore in terms of how bores exchanged heat with each other. These tests were done with three adjacent GHEs in a row, and tests are currently being done for three GHEs forming a right angle.

One of the tests was performed with a dry bore, but most tests were performed with irrigation control allowing for the center depth center bore moisture level to be at or above 20 percent. This was because it was determined that bore performance greatly suffered with the dry bore. The irrigation was done with a perforated pipe installed vertically in the bore, which allowed irrigation water distribution at different depths. Data was also taken during a no-load event but during a rain event to measure how soil parameters relaxed and how soil moisture content changed with rain.

The soil thermal properties are a key component of the model validation. Samples of the soil were taken on the site of the laboratory test bores by collecting soil from the drilling process. The samples were collected at different depths and reconstituted by pressing into a form with the representative force of soil above the sample depth. A thermal conductivity probe was used to measure conductivity in soil samples at the various depths.

These tests will provide a preliminary study into the potential to develop a controller that increases heat pump COP by adjusting water flow rate through the GHEs yielding more favorable water temperatures at the heat pump. Tests were performed studying how changes in flow rate affect the temperature of water returning to the heat pump and how changes in flow rate affect the rate of heat transfer from the GHEs to the ground. Table 3 shows the test matrix.

Table 3: Original Test Matrix

Run Date	Duration (hour)	Load (W)	gpm	Description	Objective
10/15/2019	1	0	0	No flow	Verify sensor operation
10/15/2019	3	300	1	Continuous flow for 3 hours	Obtain data on temperature response
10/17/2019	3	300	1	Continuous flow for 3 hours	Temperature difference between far-field and core is 9°F (5°C)
10/28/2019	3	300	1	Continuous flow for 3 hours	Re-run to ensure relaxed soil condition
10/16/2019	3	600	1	Continuous flow for 3 hours	Increase load from 300 to 600 W
10/17/2019	3	900	1	Continuous flow for 3 hours	Increase load from 600 to 900 W
10/30/2019	3	1200	1	Continuous flow for 3 hours	Increase Load from 900 to 1200 W
11/7/2019	4	1200	1	1 hour of baseline data, 3 hours of 1200W, 1 gpm.	Re-run to ensure relaxed soil condition

Run Date	Duration (hour)	Load (W)	gpm	Description	Objective
10/21/2019	3	600	1.2	600W 1.2 gpm	Test impact of increased flow rate
10/22/2019	3	600	0.8	600W 0.8 gpm	Test impact of reduced flow rate
11/12/2019	47	1200	1	1200W, 1 gpm. Intermittent every 4 hours for 20 hours	Simulate actual load on single bore
11/15/2019	71.5	1200	1	1200W total on 3 bores in a row	Simulate constant load on multiple bores
11/20/2019	24	1200	1	Constant 1200W per bore on 3 bores in a row	Simulate constant load on multiple bores
1/10/2020	24	1000	1	6 hours increment: flow no load, 500W per bore, 1000W per bore, flow no load	3 bores in a row
1/15/2020	24	1200	1	6 hours increment: flow no load, 600W per bore, 1200W per bore, flow no load	3 bores in a row
1/21/2020	24	1200	1	6 hours increment: flow no load, 600W per bore, 1200W per bore, flow no load	L-shaped bore orientation

Source: University of California, Davis

Computational Model Development

A survey of modeling approaches for GHEs was performed to select the most appropriate approach. Figure 4 presents a variety of different heat exchanger geometries that exist for GHEs. The modelling approaches in literature for GHEs can be divided into three categories: (1) models based on analytical solution, (2) numerical models, and (3) a combination of analytical and numerical approaches.

Several models have been developed previously for simulating the heat exchange process between a heat exchanger and the ground. These solutions were developed for various GHE geometries and using a range of methods. A distinct advantage that analytical models offer is their computational efficiency (Yavuzturk and Spitler 1999). They can work well for GHEs comprised of straight pipes with simple geometries. However, for more complicated geometries like slinky (Figure 4.C) or helical (Figure 4.D), several approximations must be made.

Figure 4: Illustration of Ground Heat Exchanger Configurations

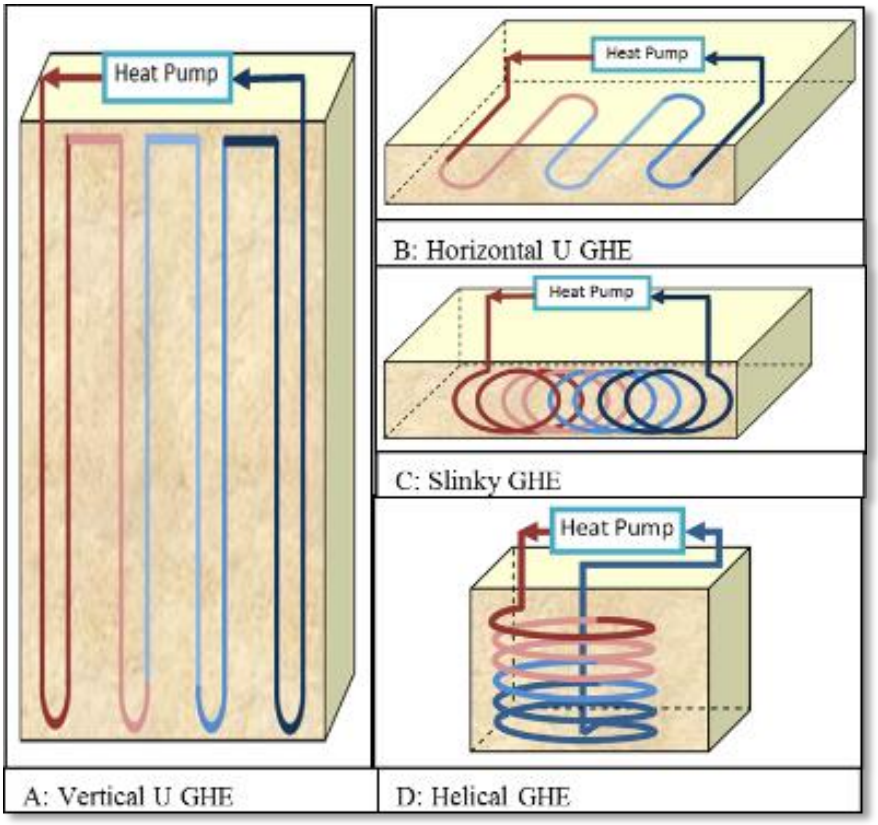

(A) Vertical, (B) Horizontal, (C) Slinky, (D) Helical GHEs

Source: University of California, Davis

Zarrella et al. (2009) developed a Capacitance Resistance Model (CaRM) to predict the performance of vertical GHEs. A modified version of this model for helical GHE (CaRM-He) was later developed by the same group of researchers (Zarrella et al. 2013). The modified CaRM-He model was the primary model used in this project to run parametric simulations of the helical GHE. This CaRM-He model was initially verified with results from a commercial computations fluid dynamics (CFD) solver. The greatest advantage that CFD models offer is the ability to account for complex geometries and various underlying heat transfer mechanisms and give spatially resolved results. A limitation, however, is the reliance on extensive computational resources. This also limits the method to short time duration modelling, as extensive simulation time is required for modelling longer time-scale events.

The objective was to develop a reliable modelling tool to characterize the thermal behavior of a LDSB helical GHE. As a balance among computational resources and fidelity and accuracy of the simulations, an approach that consisted of verifying the CaRM-He model with CFD simulations was undertaken. Field data from Honda Smart Home were used to provide a consistent set of soil properties and realistic load profile for both CFD and CaRM-He simulations. As a result of this process, it was found that the CaRM-He model did not consider all the heat transfer flows inside the bore. Consequently, the CaRM-He model was improved.

Once the revised CaRM-He model was validated with detailed soil profiles from CFD and less detailed experimental data from lab experiments, this model was used for further parametric

and non-dimensional soil resistance (g-function) estimations. The g-functions were further used in building level modeling using the EnergyPlus platform.

The next two sections describe the CaRM-HE and CFD models. Field data used for comparison of CFD and CaRM-He is discussed next, followed by a comparison of the prediction of return water temperatures and soil profiles. A revision to the CaRM-He model is discussed and then, use of the CaRM model to develop a g-function.

CaRM-He Tool

The CaRM-He (Zarrella et al. 2013) simulates the transient thermal behavior of shallow helical bore hole heat exchangers. This model used the electrical analogy to solve the transient heat conduction into the ground and bore hole heat exchanger. The original CaRM-He approach is reported in detail in Zarella et al. (2013). Figure 5 outlines the general scheme considered in the model. The domain was divided in three main zones: surface, bore hole, and deep zones (Figure 5). Each zone was then broken into discrete in thermal nodes for which the heat balance equations were written. The surface and deep zones had discrete nodes only in the z-direction (depth) while the bore hole zone also included discrete nodes in the radial direction. Figure 6 shows the modelling approach used inside the bore. The core within the bore was modelled as a single thermal node that exchanged heat from the helical pipe and the straight pipe. Furthermore, the helical pipe also exchanged heat with the bore wall through the backfill.

Figure 5: Model Schematic

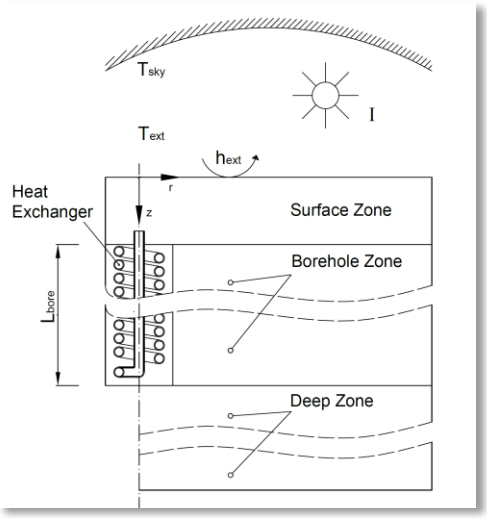

Source: University of California, Davis

Figure 6: Bore Hole Model

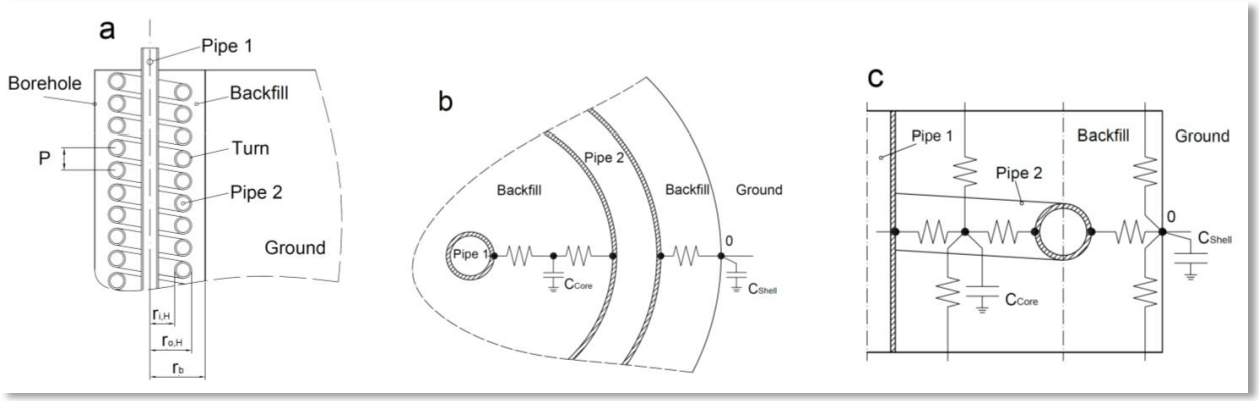

Modelling approach inside the bore; (a) general scheme, (b) capacitance-resistance scheme in horizontal section, (c) capacitance-resistance scheme in vertical section.

Source: University of California, Davis

CFD model

The CFD model is based on a more spatially resolved discretization as compared with CaRM-He. The domain was divided into large number control volumes several orders of magnitude larger than the CaRM-He tool. The CFD model also provided a basis for analyzing complex phenomenon associated with the heat transfer, such as viscous effects at the fluid and pipe interface. Correspondingly, the simulation time for CFD is much longer than for the CaRM-He tool. For example, for 15 hours of GHE operation, the simulation time required by CFD using the fine mesh (details of mesh given in Table 4) was about 30 hours and 15 hours with a coarse mesh on a workstation with a 24 core, 3.0 GHz Intel Xeon processor. The time required by CaRM-He for the same modeling period was less than three minutes.

The CFD simulations were carried out using ANSYS version 17.2 Fluent. The complete helical and central straight pipe geometry was created in SolidWorks®. This geometry was embedded in a cylindrical region with radius equal to 2.286 meters to represent the surrounding ground. The mesh quality parameters are provided in Table 4; additional parameters used in the CFD simulations are given in Table 5.

Table 4: Mesh Parameters for Grid Independence Study

Parameters	Coarse	Fine
Number of nodes	5,460,864	7,982,134
Number of elements	25,832,655	41,055,627
Average mesh skewness	0.259	0.233

Source: University of California, Davis

Table 5: Computations Fluid Dynamics Model Parameters

Parameters	Values
Elements	3D tetrahedral and hexahedral elements
Solver	3D unsteady
Numerical scheme	Semi-implicit method for pressure-linked equations (SIMPLE)
Viscous model (water)	Realizable k-ε, standard wall function
Transient formulation	First order implicit
Discretization scheme	Second order upwind

Source: University of California, Davis

To establish grid independence, a dataset of 15 hours from the Honda Smart Home field study was used on two different meshes whose parameters are shown in Table 4 (Najib et al. 2019). Figure 7 shows the mass flow rate and inlet and exit temperatures to the GHE from the dataset. Measured inlet fluid temperature was used as an input for the model and the simulated outlet fluid temperature was then compared to the corresponding measured value. The root-mean-square deviation (RMSD) of the outlet fluid temperature predicted by the simulation that used the coarse and the fine mesh was 0.14°F (0.08°C). As a reference for comparison of the RMSD value, the average temperature difference between the inlet and outlet is 7.24°F (4.02°C). Thus, the RMSD in the outlet fluid temperature between the fine and coarse mesh is less than 2 percent of the average inlet and outlet fluid temperature difference.

Figure 7: Field Data from Honda Smart Home Helical Ground Heat Exchanger

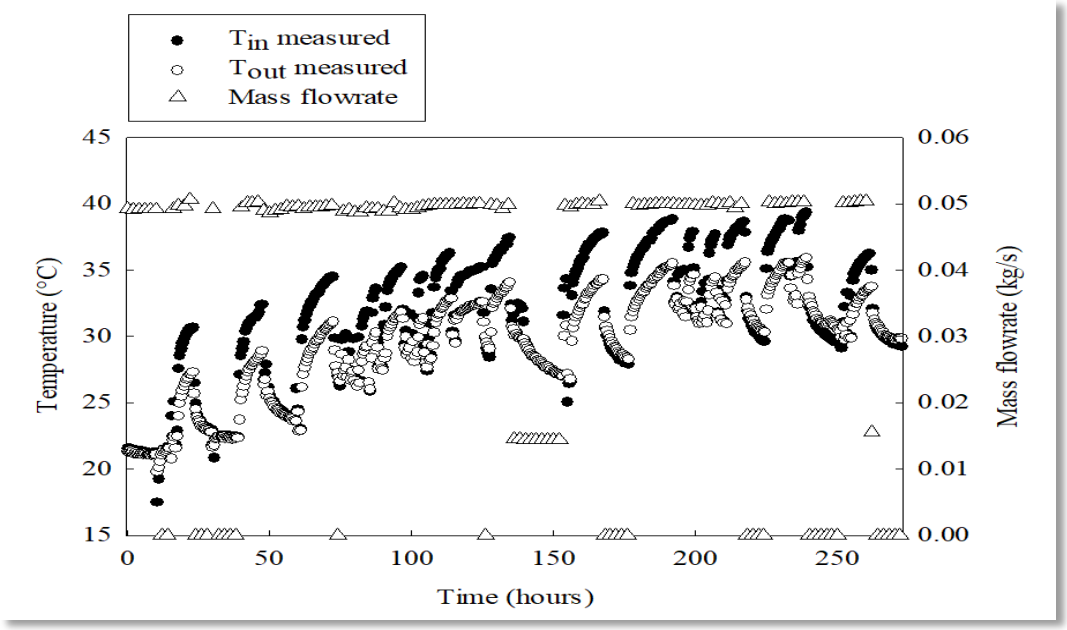

Field data for helical GHE for June 13, 2017 from 0 to 273 hours: outlet fluid temperature, inlet fluid temperature (primary axis), and mass flow rate (secondary axis) plotted against time.

Source: University of California, Davis

Figure 8 shows the ground temperature profiles from the simulations using the fine and coarse mesh at different time instances. As can be seen, both meshes predict similar ground profile temperatures. More details about analysis are reported in published work by the group (Najib et al. 2019).

Figure 8: Ground Temperature Profiles from Computations Fluid Dyamics Simulations with Fine and Coarse Mesh

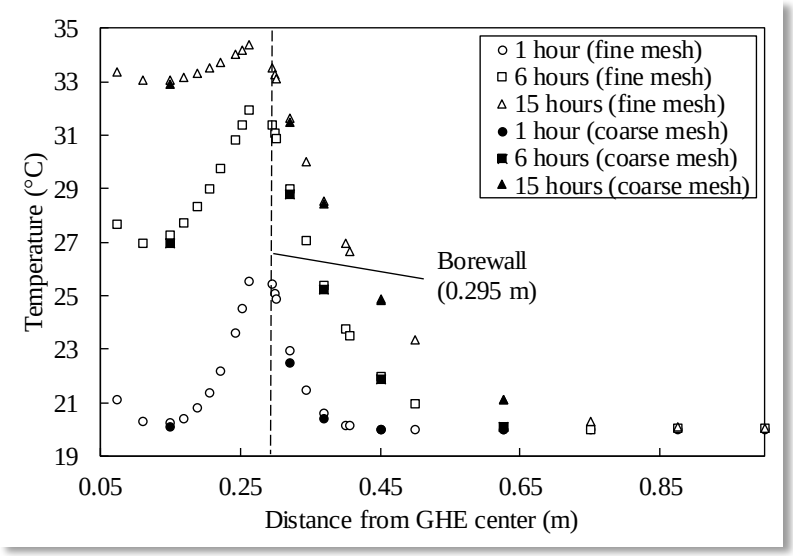

Ground temperature profiles showing agreement between fine mesh and coarse mesh simulations of GHE.

Source: University of California, Davis

Boundary Conditions

The boundary conditions and input parameters used in numerical simulations (both CFD and CaRM-He) are summarized in Table 6 and illustrated in Figure 9.

Table 6: Common Parameters Used in Computations Fluid Dynamics and CaRM-He Models

Parameters	Values
Inlet temperature	Inlet temperature from field data
Mass flow rate	0.0497 kg s^{-1}
Time step	60 s
Undisturbed ground temperature	68°F (20°C)
Specific surface convective thermal resistance	0.34 m^2 K W^{-1}
Far-field radius	2.286 m
Far-field depth (below GHE bottom)	3 m
Bore hole radius (outer helical pipe + clearance)	0.295 m
Thermal conductivity of pipe (High-density polyethylene)	0.47 W m^{-1} K^{-1}

Source: University of California, Davis

Although CaRM-He can model a combination of convection from ambient air, incident solar insolation, and radiation emitted to the sky at the ground surface, the impact of the latter two effects on outlet fluid temperature in the short-term was found to be negligible for the 11 days' duration (RMSE less than 0.18°F (0.1°C) for the time steps when flow was switched on). Consequently, only convection heat transfer was considered at the top surface as a boundary condition. The CFD and CaRM-He simulations were carried out with identical boundary conditions.

Figure 9: Boundary Conditions for Models

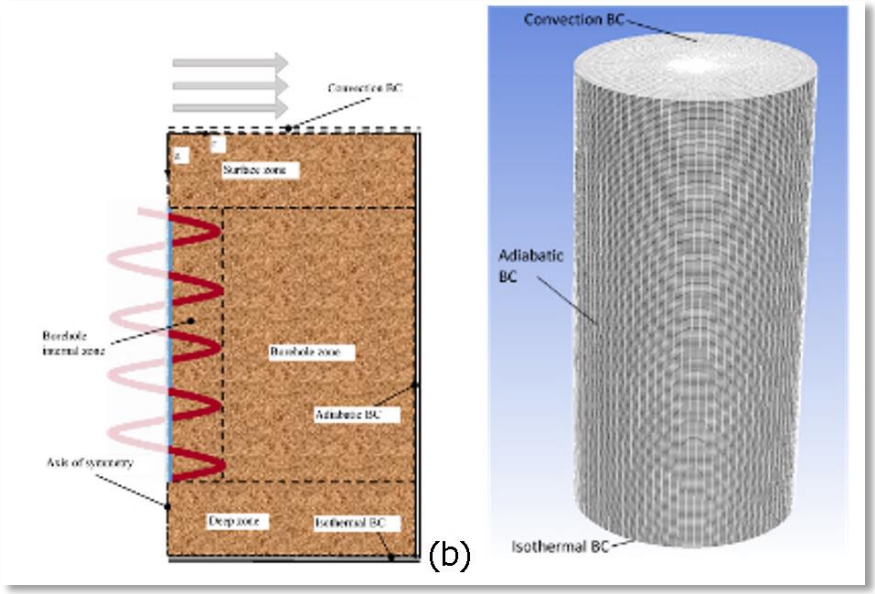

Boundary conditions in (a) CaRM-He and (b) CFD models.

Source: University of California, Davis

Numerical simulations require ground thermal properties as input, specifically the values of the thermal conductivity and specific heat capacity. Since the site was in operation, it was not possible to obtain ground property measurements in-situ. To estimate the soil properties at the field site, prior experimental research conducted on Yolo silt loam by Wierenga et al. (1969) in Davis, California, was used (Table 7). Ground properties are highly dependent on moisture (de Vries and Wijk 1966). Since the backfill at the test site is also native ground, the properties of the backfill were likely the same as those of the ground. The type of ground used for modeling was based on estimates from information available at various resources including the UC Davis soil resource lab (O'Green 2018). High-density polyethylene (HDPE) pipe material thermal properties were obtained from manufacturer specifications (INEOS 2017).

Since the moisture content in ground was not known a priori, the experimental data of the GHE operation shown in Figure 7 were used to infer the equivalent thermal properties of the ground via CaRM-He tool using an inverse approach. The measured inlet fluid temperature and mass flow rate were used as input to the tool. The soil moisture level was varied to evaluate properties using the Yolo silt loam property relations from (Wierenga et al. 1969). These properties were changed in the CaRM-He tool until the difference between the measured and simulated outlet fluid temperature resulted in the closest match with data.

Table 7: Ground Properties for Yolo Silt Loam Based on Moisture

Ground Moisture (volumetric basis)	Ground Moisture (mass basis)	Thermal Conduc-tivity ($Wm^{-1}K^{-1}$)	Density (kgm^{-3})	Specific Heat Capacity, ($Jkg^{-1}K^{-1}$)	RMSD Outlet Temperature Overall (˚C)	RMSD outlet temperature ON period (˚C)
Dry ground	0%	0.29	1250	886	1.60	1.33
10% moisture	8%	0.75	1230	1155	1.28	0.52
20% moisture	17%	1.07	1208	1435	1.41	0.57
30% moisture	26%	1.23	1186	1727	1.20	0.94

Source: (Wierenga et al., 1969)

The root-mean-square-deviations (RMSD) between the predicted and measured outlet fluid temperatures for dry, 10 percent moisture, 20 percent moisture, and 30 percent moisture soil properties are shown in Table 7. Two different sets of values of RMSD are shown in Table 7: one corresponding to the entire duration of the data and the second estimated only when the GHE was rejecting heat to the ground (denoted as the "ON" period). In general, for all moisture levels and for the period when the GHE was operational, the difference between the predicted and measured outlet temperature was lower. The RMSD with heat rejection to the ground were 1.33˚C, 0.52˚C, 0.57˚C, and 0.94˚C for dry, 10 percent moisture, 20 percent moisture, and 30 percent moisture, respectively. The dry ground properties tended to cause the model to over-predict the temperature (due to low thermal conductivity). On the other hand, use of properties based on 30 percent moisture resulted in a lower predicted temperature than the measured value. Properties based on a 10 percent moisture provided the best match, especially during the period when the flow was switched on. As a result, the soil properties of 10 percent moisture were used for subsequent validation simulations.

After calibrating the CaRM-He model to ground properties from the field data, the same properties were used in the CFD simulation. Results of outlet fluid temperature from the GHE, as well as more detailed evolution of soil temperature profiles, were compared between the CaRM-He and CFD simulations. The RMSD of the outlet fluid temperature predictions between CaRM-He and CFD was 3.26°F (1.81°C). A comparison of soil temperature profiles near the bore wall between CaRM-He and CFD after 1 hour, 21 hours, 120 hours, and 144 hours of start of simulation is depicted in Figure 10:. In CaRM-He, the core refers to the backfill between the helical and straight pipes. However, for calculation of thermal resistances, the thermal capacitance of the backfill was lumped midway between the helical and straight pipe. This location is also shown on Figure 10.

Figure 10: Ground Temperature Profile from CaRM-He Original and Computations Fluid Dynamics

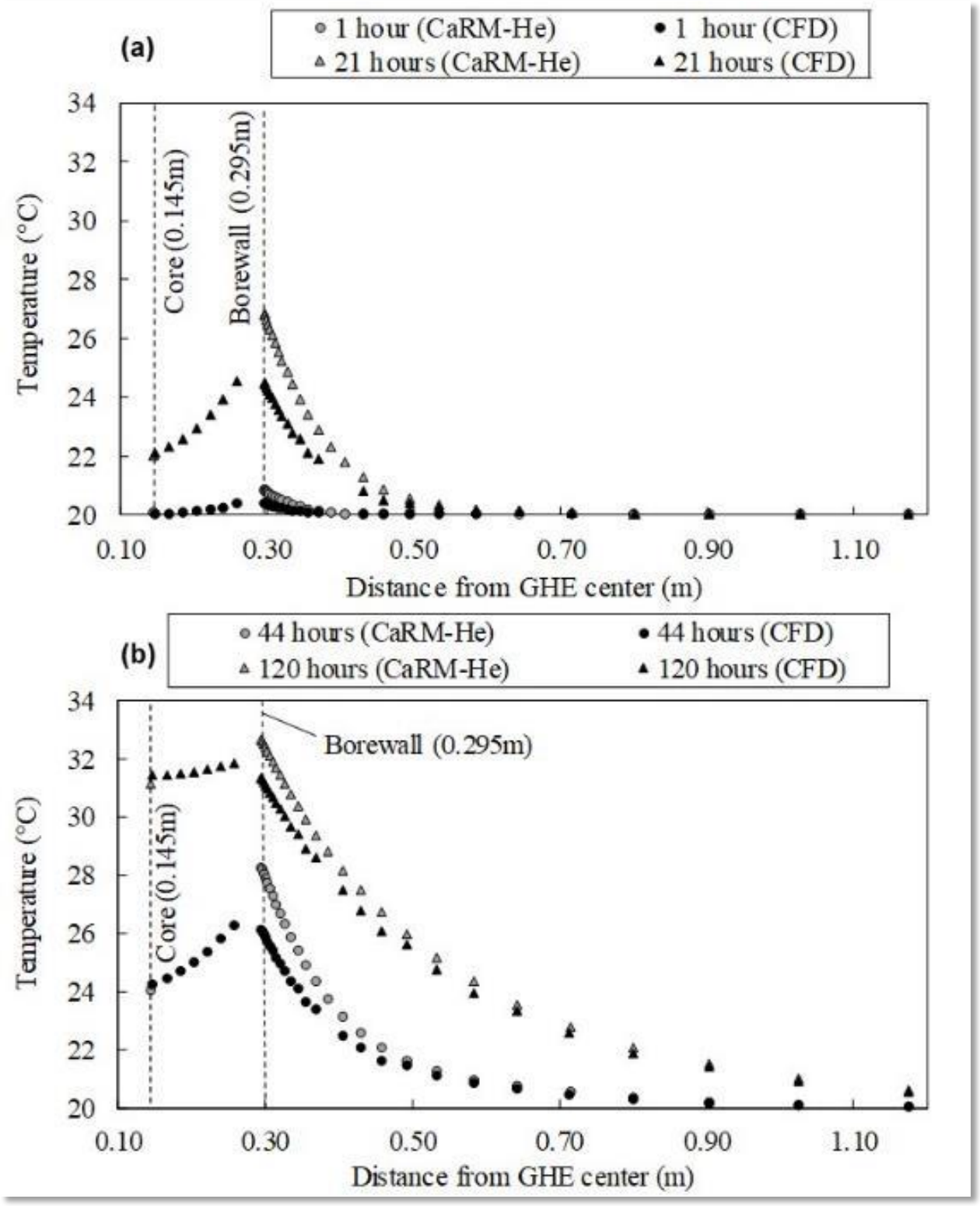

Ground temperature profile comparing results from CaRM-He original and CFD (a) 1 hour and 21 hours after start of simulation, (b) 44 hours and 120 hours after start of simulation.

Source: University of California, Davis

The selected time instances in the plot correspond to periods of heat rejection to the ground (Figure 7). Profiles for near-bore wall temperature within the bore and outside the bore are shown for CFD. For CaRM-He, since there is only one node in the core, a single area-average core temperature was calculated in this region as shown in Figure 6. Figure 10: shows that after 21 hours the bore wall temperature predicted by CaRM-He model is 2˚C higher than that predicted by CFD. It should also be noted that although the core temperature predicted by CaRM-He model matches the CFD predicted temperature at radius 0.145m, the temperature calculated by CaRM-He is an average for the entire core. The average core temperature predicted by CFD is 0.6˚C higher than that predicted by CaRM-He. The slope of the profile indicates that in CaRM-He more heat was dissipating outward from the bore hole wall, while the average core temperature was lower than that in the CFD results. It should be noted that with increase in time of heat rejection (for example, after 120 hours), the slopes of the temperature profile predicted by CaRM-He became similar to that predicted by CFD. This suggests that once the core is saturated, both models predict soil temperatures reasonably well.

In summary, although the outlet fluid temperature from CaRM-He and CFD models matched relatively well, CaRM-He predicts a higher heat rejection rate outward than into the core as compared with CFD. The differences in the results described led to a revision in the CaRM-He model. The changes made to the model, along with the ground temperature profile before and after the modifications, are discussed and compared in the subsequent sections.

Modifications to the CaRM-He Model (CaRM-He v2)

Considering the discrepancy in the heat flow near the bore wall outlined in the previous section, the CaRM-He model was improved to consider the real geometry of the helical GHE and better simulate its thermal performance, especially in the short term. The improvements pertained to modelling of the core section within the bore; whereas, the modelling of the surrounding ground outside the bore was unchanged.

In the original CaRM-He model there was no direct thermal communication between the bore wall and the core; each of these regions independently communicated with the helical pipe. In reality, these two regions were in direct contact with each other in between the pitch of the helical pipe. Hence, there is a need for an improved model to represent this interaction. Figure 11 shows the new modelling approach within the bore. As can be seen, in the new approach the thermal capacitance of the backfill is lumped in three thermal nodes: the core, the shell, and the bore hole wall. In the core node as in the original model, the thermal capacitance of the backfill between the helical pipe and the straight pipe was lumped. On the side of the helical pipe facing the bore wall, to better represent the transient thermal behavior, the thermal capacitance of the backfill between the helical pipe and the bore hole wall was lumped in two thermal nodes: the shell and in the bore hole wall nodes.

Figure 11: Approach of the New CaRM-He V2

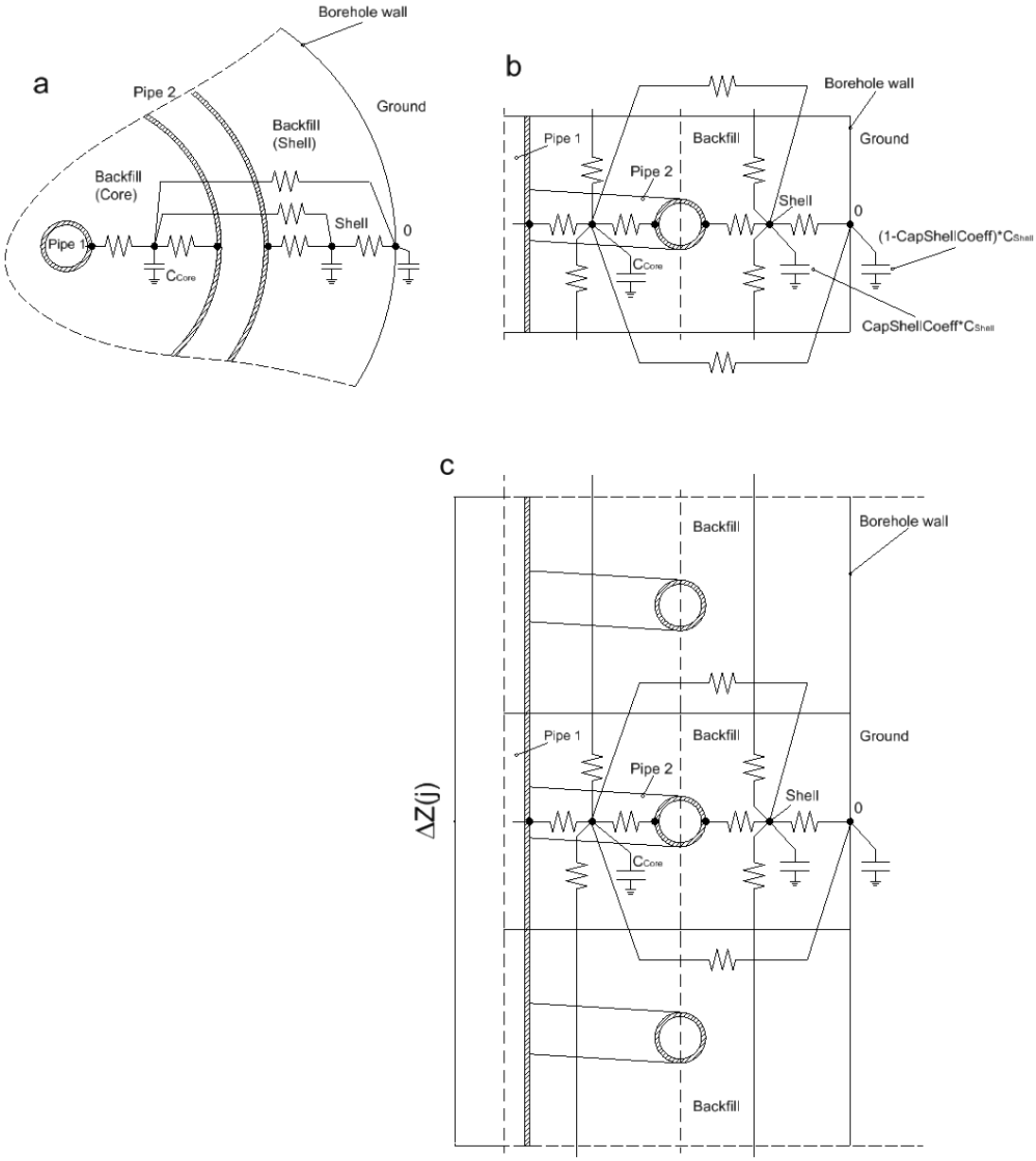

Schematic showing additional nodes added in CaRM-He v2: (a) capacitance-resistance scheme in horizontal section, (b) and (c) capacitance-resistance scheme in vertical section.

Source: Angelo Zarrella, University of Padova Italy

To incorporate heat communication between the bore wall and the core, as well as the shell and the core, parallel thermal resistances between the core and the shell thermal nodes and between the core and the bore hole wall thermal nodes were used. These additional resistances account for the heat transfer that took place between the core inside the helical pipe and the shell and bore wall regions in the pitch direction where the helical pipe is not present (Figure 11.c). This modification will be important in proper prediction of short-term thermal performance or transient operating modes of the GHE. Details of the revised CaRM-He model are described in a journal publication (Najib et al. 2019).

For the core thermal node, the heat balance was modified considering the effect of the thermal short-circuit with both the shell and bore wall thermal nodes via the backfill present between the turns of the helical shaped pipe. Considering a layer of thickness $\Delta z(j)$ in depth, this effect can be modeled by means of $(1 + \frac{\Delta z(j)}{Pitch})$ number of conduction cylindrical thermal resistances coupled in parallel between the corresponding thermal nodes. In addition, the heat transfer with the helical pipe (Pipe 2 in Figure 11.c) was modified to consider the actual thermal exchange surface of the helical shaped pipe due to the presence of spaces between the turns of the helix.

G-Function Development

General Equation for Long-Term G-function

The g-function is a non-dimensional temperature response factor proposed by Eskilson and Claesson (1988). The general long-term g-function is calculated using the equations found in Appendix B. G-functions are used to describe the temperature response of a bore field based on the thermal loads applied, and significantly reduces computation time relative to numerical or analytical solutions for the temperature response.

Short Term g-functions

According to Eskilson (1988), the longtime step g-function given by Equation 1 in Appendix B is valid for times in the range of $5r_b^2/\alpha < t < t_s$. According to Yavuzturk and Spitler (1999), for the short time step, the g-function equation becomes Equation 3 in Appendix B, where the variable R'_{total} (total resistance per unit length, KmW^{-1}) is the resistance from fluid to the bore hole wall. The equation for vertical GHEs also includes this additional term and can be found in Equation 4 of Appendix D.

In contrast to numerical models based on analytical solutions (i.e., line source which can be used to simplify a deep bore system by assuming it behaves like an infinite line heat source/sink), CaRM already accounts for the internal resistances when calculating the bore hole temperature. Thus, for generating g-functions from bore hole wall temperatures calculated by CaRM, R_{total} can be set to zero and Equation 1 and Equation 2 in Appendix B can be used for both short time step and long time step g-functions.

It should be noted that the g-functions for vertical GHEs described thus far are all based on bore hole wall temperature, T_b. Upon estimation of T_b, the typical approach is to use the T_b based g-function and the total resistance, R_{total} to back-calculate the mean fluid temperature for a given load profile.

Modification in g-function Formula for Shallow Helical GHEs

Following the typical procedure, a constant (that is, not changing with time) heat transfer rate is used to generate the g-function, which is then plotted against non-dimensionalized time t/t_s.

However, unlike the vertical GHEs, for helical GHE case, it was found that using the mean fluid temperature directly to calculate the g-function enables one to calculate the mean fluid temperature to a greater accuracy compared to the calculation that uses a g-function that is based on mean bore wall temperature. This is because it eliminates the inaccuracies associated with the calculation of the resistance between the bore wall and the fluid.

The CaRM output includes the inlet and outlet temperature, which makes calculating the mean fluid temperature quite straightforward. Thus, the revised g-function equation for the helical GHE becomes Equation 5 in Appendix B, where T_{mf} is the mean fluid temperature given as in Equation 6 in Appendix B.

Correspondingly, the mean fluid temperature T_{mf} can be back-calculated directly from the g-function given in Equation 5 in Appendix B, without using the total resistance, R'_{total}.

Effect of Surface Boundary Condition

An important aspect in the performance of a GHE is the surface condition. The effect of annual variation in the undisturbed ground temperature was incorporated in the final results by using the principle of superposition. The effect of annual variation on the undisturbed ground temperature and the heat transfer from the top surface was not accounted for while generating the g-functions. The same approach was used by Xiong et al. (2015) when generating g-functions for horizontal and vertical slinky GHEs. Mathematically, this approach can be expressed by Equation 7 in Appendix D, which was adopted from Xiong et al. (2015):

Xiong et al. (2015) assert that a simple one-dimensional numerical model can be used to calculate the undisturbed ground temperature. Furthermore, the researchers explained that a coarse-grid three-dimensional model was available in EnergyPlus and was thus used to estimate the undisturbed ground temperatures for their work. A method or model that provides computational efficiency as well as reasonable accuracy would be needed. Figure 12 shows a schematic of the superposition approach.

When calculating Mean Fluid Temperature or Cases $T_{amb} \neq T_g$= 59°F (15°C):, analytical equations for a semi-infinite medium with surface convection were used as the analytical model (Incropera et al. 2011).

Figure 12: Scheme Showing the Superposition Method

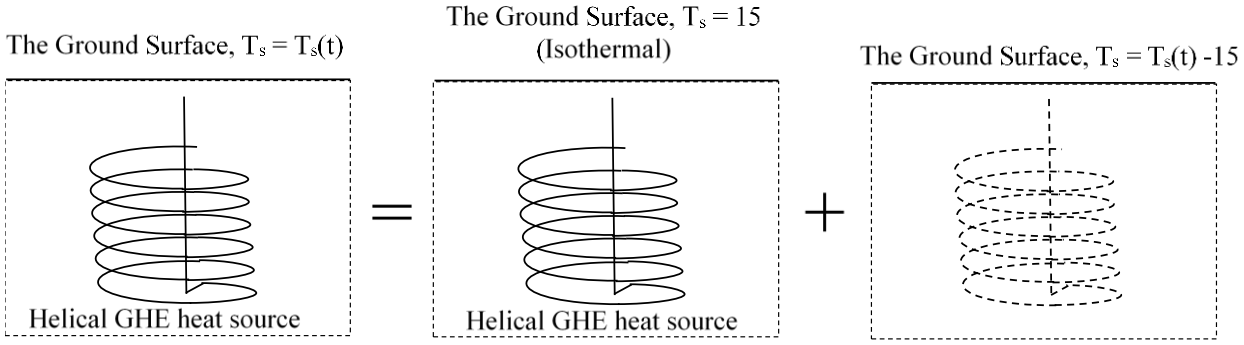

Source: Xiong et al. (2015)

Initialization

Another aspect pertaining to GHE modeling is the initial ground temperature.

Kusuda and Achenback (1965) proposed equations that allow curve fitting a sinusoidal equation to represent the ambient temperature data using the method of least squares. They also presented Equation 8 found in Appendix D for which the temperature at any depth in the ground can be calculated (Kusuda and Achenback 1965).

The CaRM model includes a provision to initialize the soil temperature based on the Kusuda and Achenback (1965) method. Consequently, after team discussions, it was decided that data from California climate zone 12 would be used with this method to initialize g-function simulations.

Using the method of least squares (Kusuda and Achenback 1965), data from climate zone 12 was used to calculate, T_m = 59.47°F (15.26°C). This was rounded to the nearest °C to get 59°F (15°C). The amplitude is A_T = 13.61°F (7.56°C) ≈ 13.7°F (7.6°C) (rounded to the nearest 0.1°C). t_{shift}= 18.9 days ≈ 19 days (which means the minimum temperature would occur on Jan 19). Figure 13 shows the ambient hourly temperature from California climate zone 12 and calculated using the Kusuda and Achenback method when depth = 0 m (Kusuda and Achenback, 1965).

Figure 13: Ambient Hourly Temperature Comparison

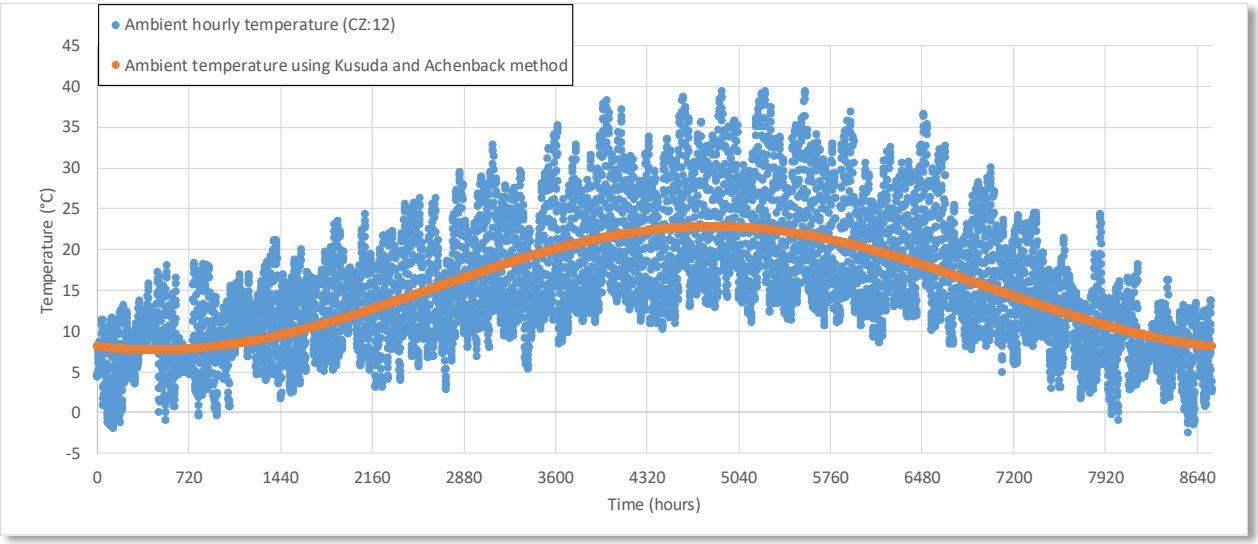

Ambient hourly temperature (A) from California climate zone 12 (B) calculated using the Kusuda and Achenback (1965) method at surface level (depth, Z=0 m).

Source: University of California, Davis

The undisturbed ground temperature was set equal to the mean air temperature (that is, T_g = T_m = 59°F [15°C]). These parameters were used as the input parameters in CaRM to generate the g-function. As expected, the ground was cold in the beginning of the simulation. However, this caused the mean fluid temperatures (T_{mf}) to be lower than the undisturbed ground temperature (T_g) 59°F (15°C), which caused the term $T_{mf} - T_g$ in Equation 5 and thus the g-function to be negative as shown in Figure 14.

Figure 14: G-Function Generated Using Parameters from Kusuda and Achenback (1965) Method

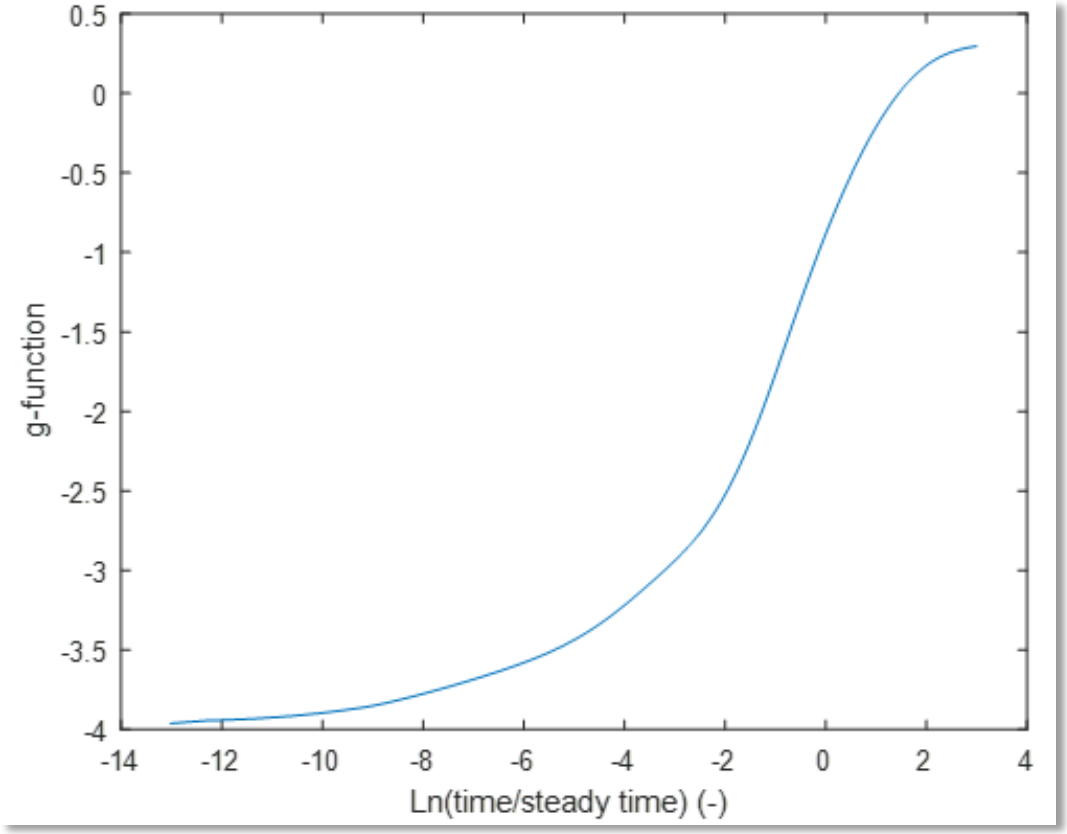

Source: University of California, Davis

To avoid the negative g-function, the initialization method was changed. A constant and uniform undisturbed ground temperature was used for all subsequent simulations. Mathematically, this meant that:

$$T_g = T_m = 15$$

$$A_t = 0$$

$$t_{shift} = 0$$

It was found that this approach was consistent with previous research (Xiong et al. 2015) focused on generating g-functions in which the method of superposition was used to incorporate the effect of the initial ground temperatures as well as the surface boundary condition.

Temporal Discretization

To generate g-functions that span a range of time starting from ln(t/ts) = -13 to ln(t/ts) = 3, the time step needed to be 10 seconds and the total duration needs to be 2.86 years. With a 10-second time step, this led to 10,000 steps repeated 900 times (that is, 9 million points). The CaRM-HE simulation took more than 29 hours with almost 3 hours required for post-processing.

Given the time required, separate long-term and short-term simulations were used. For the GHE geometry and soil property used, Table 8 shows the parameters used for generating the g-functions. Steady state time was found to be 51.9 days in this case.

Table 8: Temporal Parameters for G-Functions

Parameter	Short-Term	Long-Term
Start = time step	10 s ln (10 s/t_s) = -13.01	3600 s = 1 hour ln (1 hour/t_s) = -7.13
End	172,800 s = 48 hours ln (48 hours /t_s) = -3.26	3.15×10^8 s = 10 years ln (10 years /t_s) = 4.25
Number of time steps	17,280	8760
Number of repetitions	1	10

Source: University of California, Davis

To validate the approach, the settings allow an overlap between the long-term and short-term g-functions from time of 1 hour to 48 hours (or ln (t/t_s) from –7.13 to –3.26). The total number of points are 17,280+87,600 = 104,880.

System and Site-Specific Inputs

Site-specific inputs were needed for the simulations and are outlined in Table B-1 in Appendix B.

G-function for Multiple Bores

The g-functions depend on the number and the configuration of the GHEs. For the results shared here, a row of nine GHEs was considered. According to the CaRM modeling method (Zarrella and Carli 2013) the GHEs can be divided into six types based on the boundary condition being either isothermal or adiabatic. Type 1 to type 4 are shown in Figure 15. The red lines indicate adiabatic sides. A GHE that has isothermal boundaries on all four sides is called type 0 and is not shown in the figure.

Figure 15: Ground Heat Exchanger Boundary Conditions, Type 1 to Type 4 Used in CaRM

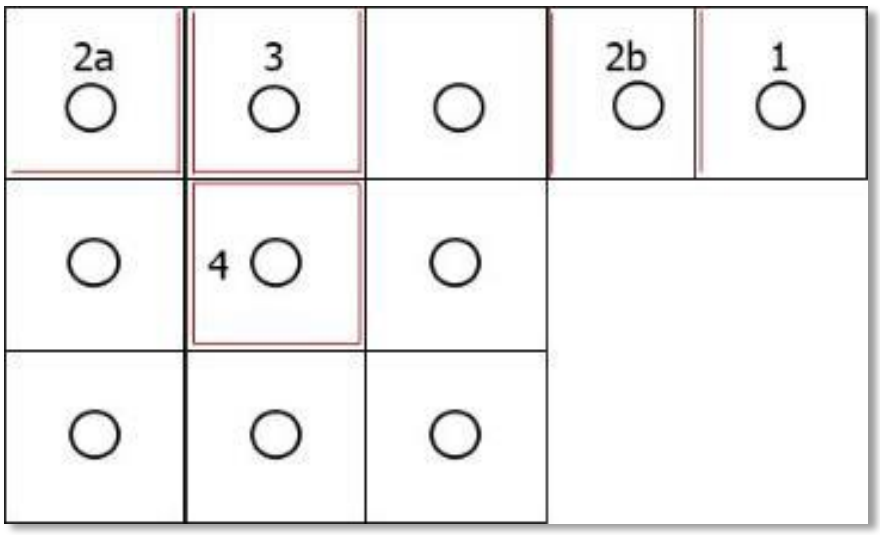

GHE boundary conditions, type 1 to type 4 used in CaRM. The red lines indicate adiabatic boundary. Figure adapted from (Zarrella and Carli 2013).

Source: University of California, Davis

To better understand this approach, consider a row of nine GHEs. The two GHEs at the end have only one adiabatic boundary (type 1), whereas the seven GHEs in between have two adjacent adiabatic boundaries (type 2b) as shown in Figure 16.

Figure 16: Nine Ground Heat Exchangers Row Used for Simulation

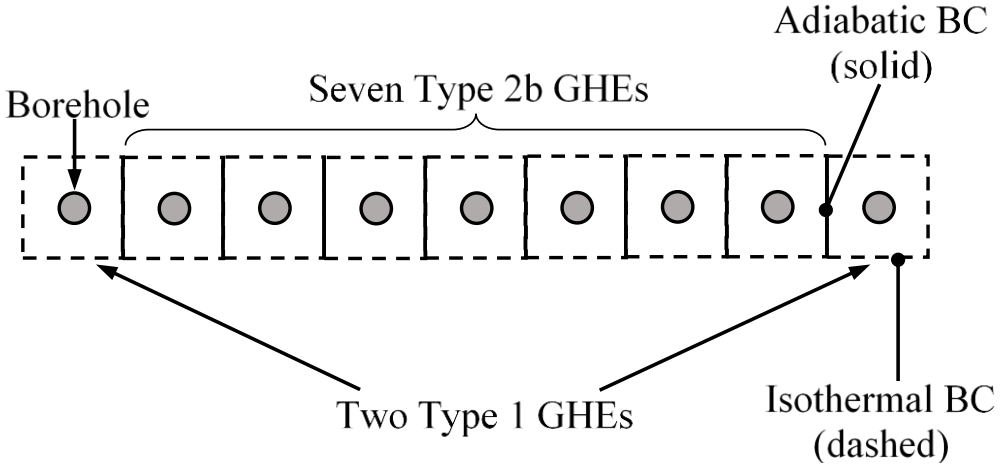

Nine GHE rows used for simulation. Boundary conditions are also shown.

Source: University of California, Davis

It can be shown mathematically that the combined g-function for all nine GHEs can be obtained by taking the number weighted average of the g-function of the individual GHEs (that is, type 1 and type 2b). This is shown in Equation 9 of Appendix B.

Validation Results

The following results validate the use of G-functions developed for individual bores with unique boundary conditions to generate G-functions for different bore field configurations. This allows

a limited set of G-functions to be used to for common bore field configurations without the need to generate new G-functions for each configuration.

G-function for $T_{amb} = T_g = 59°F$ (15°C):

Figure 17 shows the long-term and short-term g-functions for a single type 1 and type 2b with $T_{amb}=T_g=59°F$ (15°C).

Figure 17: Long-Term and Short-Term G-Functions for Types 1 and 2b with $T_{amb}=T_g=59°F$ (15°C)

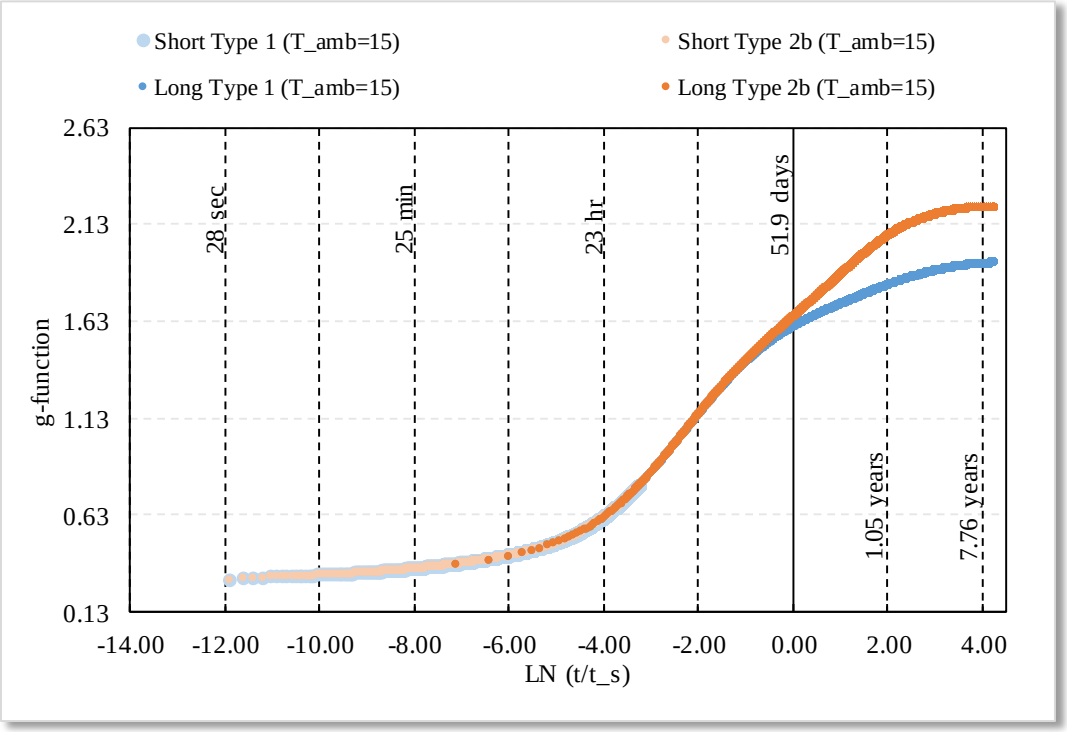

Source: University of California, Davis

Figure 17 shows the short-term g-functions for type 1 and type 2b are identical. The g-functions for both types are very similar for the first 52 days. Beyond this, the type 1 (which has one adiabatic and three isothermal boundaries) exhibits a lower resistance to heat flow than the type 2b (which has two adiabatic and two isothermal boundaries). The difference increases with the passage of time and is maximum at the end of the simulation (after 10 years).

Figure 18 shows the long-term g-functions for type 1 and type 2b under different configurations and heat loads. The legend "1 each" designates a simulation in which there were six GHEs, one of each boundary condition type. A row of nine GHEs was also simulated under different loads. The results show that for type 1, the g-functions are identical for all cases and lie on top of each other. The same is true for type 2b. This means that regardless of configuration, the g-function for a given type of GHE (type 1, for example) will be the same. Referring back to the row of nine GHE example, this essentially means that the type 1 and type 2b g-functions generated for this case can be used for any other row configuration of GHE (for example, row of 16 GHEs or row of 5 GHEs).

Figure 18: Long-Term G-Functions for Types 1 and 2b Under Different Configurations and Loads

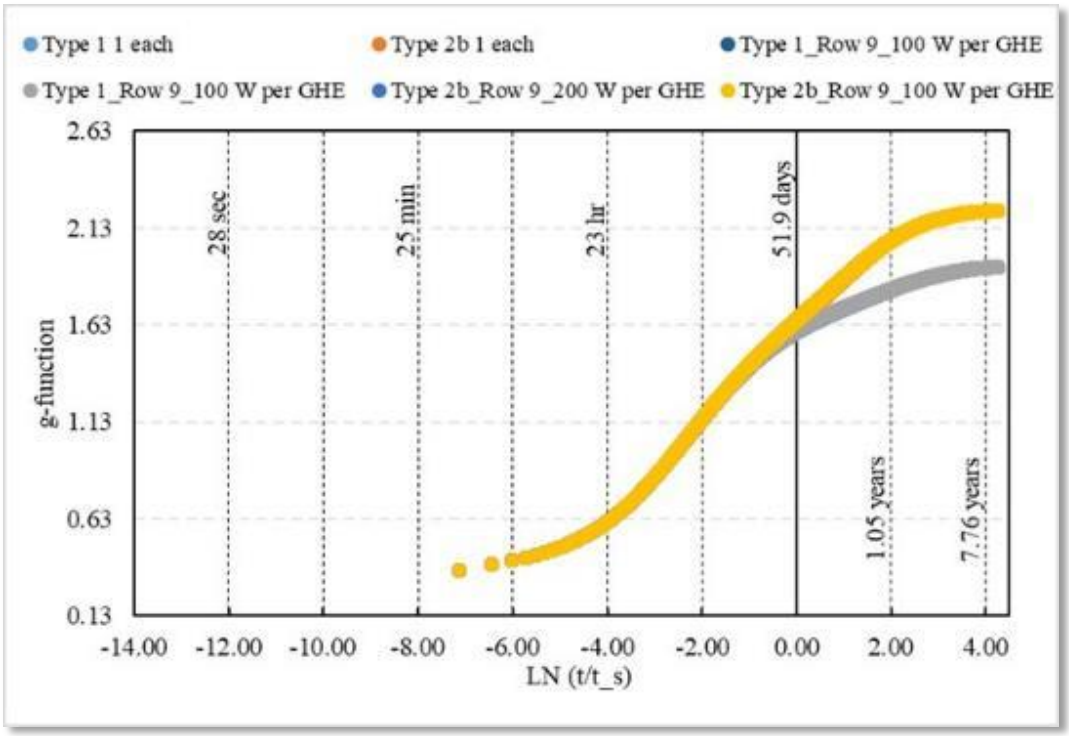

Source: University of California, Davis

Table 9 shows 21 points that define the g-functions for GHEs of all six types. They are divided into short- and long-term range based on the simulation time step. The formulae for calculations are the same in both ranges. The six g-functions in Table 9 can be used to construct the combined g-function for any configuration of GHEs.

Table 9: G-Functions at 21 Points for Ground Heat Exchangers of All Six Types

G-function range	ln(t/t_s) (t_s= 51.9 days)	g-function Type 0	g-function Type 1	g-function Type 2b	g-function Type 2a	g-function Type 3	g-function Type 4
Short	–5.3003	0.460	0.460	0.460	0.460	0.460	0.460
Short	–4.2013	0.581	0.581	0.581	0.581	0.581	0.581
Short	–3.5081	0.716	0.716	0.716	0.716	0.716	0.716
Long	–2.7455	0.918	0.918	0.918	0.918	0.918	0.919
Long	–2.3153	1.047	1.047	1.048	1.048	1.048	1.051
Long	–1.8964	1.174	1.174	1.176	1.175	1.177	1.184
Long	–1.4715	1.295	1.296	1.299	1.298	1.302	1.321
Long	–1.0521	1.400	1.403	1.410	1.407	1.418	1.462
Long	–0.6292	1.485	1.493	1.511	1.504	1.532	1.630
Long	–0.2088	1.550	1.566	1.603	1.589	1.649	1.849
Long	0.2127	1.600	1.626	1.694	1.664	1.778	2.137
Long	0.6343	1.638	1.676	1.785	1.732	1.917	2.481
Long	1.0556	1.670	1.720	1.877	1.797	2.062	2.824
Long	1.4768	1.699	1.762	1.969	1.859	2.198	3.098
Long	1.8980	1.728	1.803	2.049	1.917	2.308	3.280
Long	2.3192	1.756	1.840	2.112	1.965	2.386	3.395
Long	2.7404	1.781	1.871	2.157	2.001	2.438	3.470
Long	3.1615	1.803	1.896	2.187	2.028	2.472	3.521
Long	3.5827	1.821	1.914	2.206	2.046	2.493	3.552
Long	4.0039	1.833	1.925	2.216	2.056	2.504	3.567
Long	4.2532	1.837	1.928	2.218	2.059	2.506	3.570
Long	4.2532	1.837	1.928	2.218	2.059	2.506	3.570

Source: University of California, Davis

Table 10 shows the reconstruction of combined g-function for two cases: row of 9 GHEs and perimeter of 16 GHEs. The percentage difference is very small. However, the difference increases with time. This is because of the assumption of constant Q'.

The user can, therefore, select any GHE configuration based on building load, heat pump requirements, and resources available (land, financial capital, and other factors).

Table 10: G-functions for Row of 9 and 16 Ground Heat Exchangers

ln(t/t_s) (t_s= 51.9 days)	Row of 9 GHE (2 type 1 & 7 type 2b) Construc-tion from type 1 & type 2b	Row of 9 GHE (2 type 1 & 7 type 2b) Actual CaRM simu-lation	Row of 9 GHE (2 type 1 & 7 type 2b) % difference	Perimeter of 16 GHEs (4 type 2a & 16 type 2b) Construc-tion from type 2a & type 2b	Perimeter of 16 GHEs (4 type 2a & 16 type 2b) Actual CaRM simu-lation	Perimeter of 16 GHEs (4 type 2a & 16 type 2b) Percentage difference
–2.7455	0.918	0.918	0.01%	0.918	0.918	–0.01%
–2.3153	1.048	1.048	0.01%	1.048	1.048	–0.01%
–1.8964	1.175	1.176	0.03%	1.175	1.176	–0.03%
–1.4715	1.298	1.299	0.07%	1.299	1.300	–0.06%
–1.0521	1.408	1.410	0.14%	1.409	1.411	–0.12%
–0.6292	1.507	1.511	0.25%	1.509	1.512	–0.22%
–0.2088	1.595	1.601	0.36%	1.600	1.605	–0.32%
0.2127	1.679	1.685	0.40%	1.686	1.692	–0.36%
0.6343	1.760	1.766	0.33%	1.772	1.777	–0.31%
1.0556	1.842	1.845	0.15%	1.857	1.861	–0.18%
1.4768	1.923	1.922	–0.06%	1.941	1.942	–0.01%
1.8980	1.995	1.990	–0.23%	2.016	2.014	0.10%
2.3192	2.052	2.045	–0.32%	2.075	2.072	0.14%
2.7404	2.093	2.086	–0.34%	2.118	2.115	0.13%
3.1615	2.122	2.115	–0.33%	2.147	2.145	0.11%
3.5827	2.141	2.134	–0.32%	2.166	2.164	0.10%
4.0039	2.151	2.144	–0.32%	2.176	2.174	0.10%
4.2532	2.154	2.147	–0.32%	2.178	2.176	0.10%
4.2532	2.154	2.147	–0.32%	2.178	2.176	0.10%

G-functions for row of 9 GHEs and 16 GHEs from CaRM complete simulation and construction from individual GHE g-functions. Percentage difference is also shown.

Source: University of California, Davis

Mean Fluid Temperature or Cases $T_{amb} \neq T_g$= 59°F (15°C):

According to the approach proposed by Xiong et al. (2015), a simple one-dimensional analytical solution was used to estimate the ground undisturbed temperature. The analytical equation to calculate the temperature at any point in a semi-infinite medium with surface convection can be found in Incropera et al. (2011).

Figure 19 shows the mean fluid temperature against time in days. The blue curve shows the mean fluid temperature calculated using CaRM with T_{amb} = 72.7°F (22.6°C). The yellow curve

shows mean fluid temperature calculated using CaRM with T_{amb} = 59°F (15°C) to which a temperature rise term is added.

The temperature rise term is calculated as follows. Using an initial temperature of 59°F (15°C) and surface temperature of 72.7°F (22.6°C), the analytical equations are used to calculate the ground temperature at depths that correspond to helical GHE nodes in CaRM. The depths of these nodes are 1.48 m, 2.43 m, 3.38 m, 4.33 m, 5.28 m, and 6.23 m. An average of these temperatures is calculated. The initial temperature, 59°F (15°C), is then subtracted from the average temperature to obtain the temperature rise term. The process is carried out for all time steps.

Figure 19 shows that the simple model can predict the temperature rise to a reasonable level of accuracy. However, more sophisticated models such as those available in EnergyPlus can be explored further. It should also be noted that the undisturbed ground temperature is 59°F (15°C) in both cases, which is also the mean fluid temperature at time = 0 hours. This value is not shown on the graph (since $\ln(t/t_s)$ term becomes undefined for g-function graphs). At time = 1 hour, the mean fluid temperature for (CaRM 72.7°F [22.6°C]) is 60.19°F (15.66°C).

Figure 19: Mean Fluid Temperature Calculated at Different Ambient Conditions

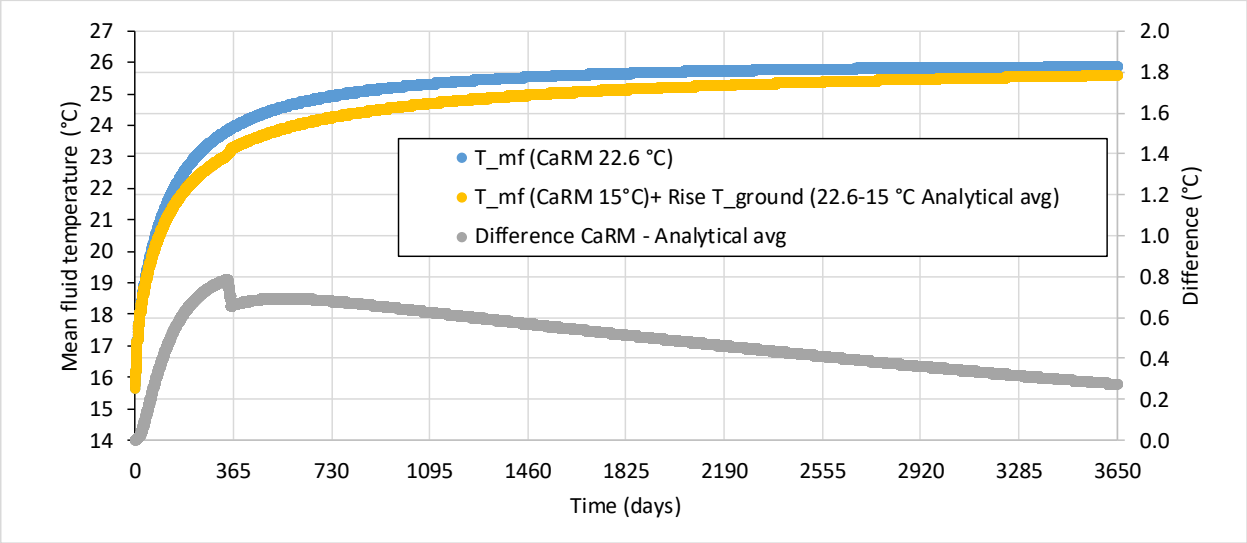

Mean fluid temperature calculated using (a) CaRM with T_{amb} = 72.7°F (22.6°C) (b) CaRM with T_{amb} = 59°F+ (15°C+). Temperature rise calculated using analytical model. The difference between the two is shown on the secondary axis.

Source: University of California, Davis

EnergyPlus Integration

The g-functions developed using the CaRM model were applied in EnergyPlus to simulate building energy consumption when using a ground-source heat pump coupled to the large-diameter shallow bore GHE. The simulations were performed on a prototypical detached single-family home located in various locations representative of California climate zones. The home has two stories with a total conditioned area of 2400 ft^2 (223 m^2) with window-to-wall ratio of 15 percent. Figure 20 shows a three-dimensional rendering of the two-story home model, and Table 11 summarizes the main features of the home model considered in EnergyPlus, a state-of-the art whole-building energy simulation tool used to perform the

analysis. The baseline heating and cooling system for the home consists of a direct expansion unitary air-to-air heat pump.

Figure 20: Rendering of Detached Home Model Used for EnergyPlus Modeling

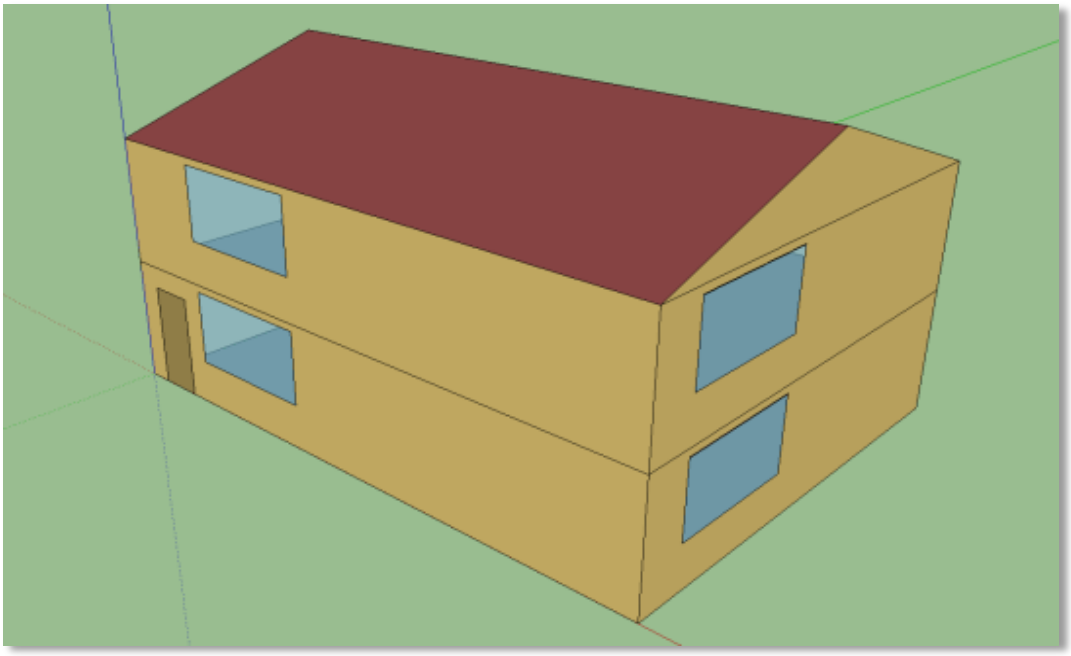

Source: University of California, Davis

Table 11: Basic Features of Detached Home Model Used for Simulation Analysis

Building Characteristic	Value
General Home Dimensions	
Conditioned floor area	2400 ft^2 (223 m^2)
Roof Area	1270 ft^2 (118 m^2)
Number of Stories	2
Window-to-Wall Ratio	0.15
Wall Area by Orientation	
North	569.2 ft^2 (52.9 m^2)
East	421.8 ft^2 (39.2 m^2)
South	569.2 ft^2 (52.9 m^2)
West	421.8 ft^2 (39.2 m^2)
Foundation Type	Slab-on-grade
Effective Air Leakage Area	
Living Space	1.813 ft^2 (0.1685 m^2)
Attic	0.398 ft^2 (0.037 m^2)
Air-to-Air Nominal System Efficiency*	**Carrier 25HBC542AP030****
COP Heating: 46.99°F (8.33°C) Outdoor DB, 70°F (21.11°C) Indoor DB	3.74
COP Cooling: 95°F (35°C) Outdoor DB, 66.99°F (19.44°C) Indoor WB	3.61
Water-to-Air Nominal System Efficiency*	**Carrier GB042***
COP Heating: 50°F (10°C) EWT, 50°F (10°C) Indoor DB, 50°F (10°C) Indoor WB	6.21
COP Cooling: 50°F (10°C) EWT, 50°F (10°C) Indoor DB, 50°F (10°C) Indoor WB	7.10

***Nominal system efficiency for EnergyPlus based on rated conditions shown for each COP value (DB=drybulb temperature, WB=wetbulb temperature, and EWT=entering water temperature).**

****performance curves based on manufacturer data tables**

Source: University of California, Davis

California Climate Zones

The simulation analysis for the energy performance of the shallow GCHP is carried out for 16 locations to represent the California climate zones as depicted by the map of Figure 21. The annual heating and cooling degree days for the selected 16 Californian locations are summarized in Table 12. California includes a wide spectrum of climatic conditions ranging from cold (Arcata and Bishop) to hot (Brawley) weather. However, most zones in California exhibit mild climates with cooling and heating thermal needs, with some dominance of cooling requirements especially for buildings with significant internal loads.

Figure 21: Map of 16 California Climate Zones

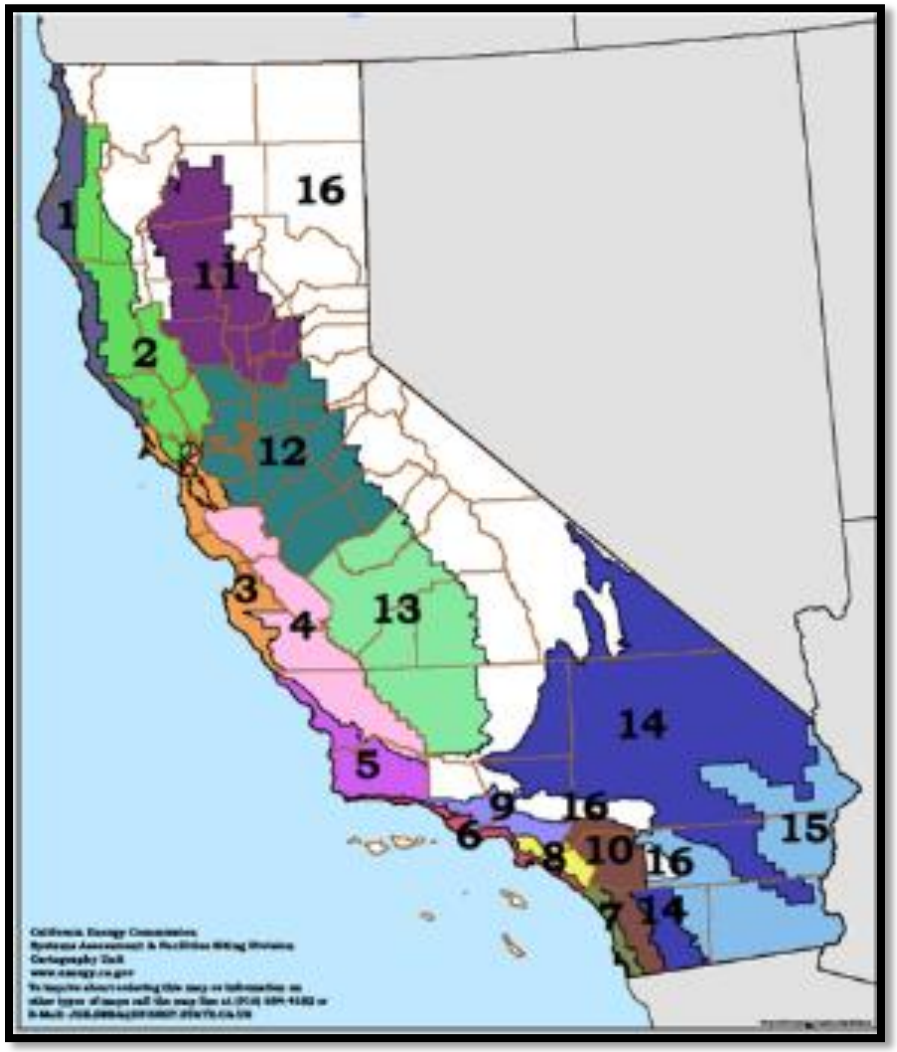

Source: University of California, Davis

Table 12: Summary of Annual Heating and Cooling Degree Days

Climate Zone (CZ) Reference City	Heating Degree Days (65°F [18°C])	Cooling Degree Days (80°F [27°C])
CZ1 (Arcata)	4496	0
CZ2 (Napa)	2844	456
CZ3 (San Francisco)	3042	108
CZ4 (San Jose)	2335	574
CZ5 (Santa Maria)	2844	456
CZ6 (Los Angeles International Airport)	1458	727
CZ7 (San Diego)	1256	984
CZ8 (Long Beach)	1430	1201
CZ9 (Los Angeles Civic Center)	1154	1537
CZ10 (Riverside)	1678	1456
CZ11 (Red Bluff)	2688	1904
CZ12 (Stockton)	2702	1470
CZ13 (Fresno)	2702	1470
CZ14 (Barstow)	2581	4239
CZ15 (Brawley)	1106	6565
CZ16 (Bishop)	4313	1037

Summary of annual heating and cooling degree days for 16 locations representative of California climate zones based on 65°F (18°C) for heating and 80°F (26.67°C) for cooling.

Source:
https://www.pge.com/includes/docs/pdfs/about/edusafety/training/pec/toolbox/arch/climate/california_climate_zones_01-16.pdf

CHAPTER 3:
Project Results

Lab Testing Results

Results from Single Bore Testing

One of the primary goals of the single bore testing was to determine whether a single bore could achieve a nominal capacity of 1200W. The first test run (Figure 22) was intended to check whether the bores could absorb 1200W effectively. However, the control for the irrigation system failed, so the moisture in the bore fell below the intended 20 percent critical level. The first test therefore was a dry bore test. The top and 10' depth moisture levels were 2 percent and 3 percent, respectively. As shown in Figure 23, the return temperature did not increase appreciably during the hour duration of the test, which indicates that the ground was able to absorb most of the heat even with the absence of adequate moisture. Testing was arrested after about 45 minutes so that researchers could address the irrigation problem.

Figure 22: Test at 1200W with a Dry Bore

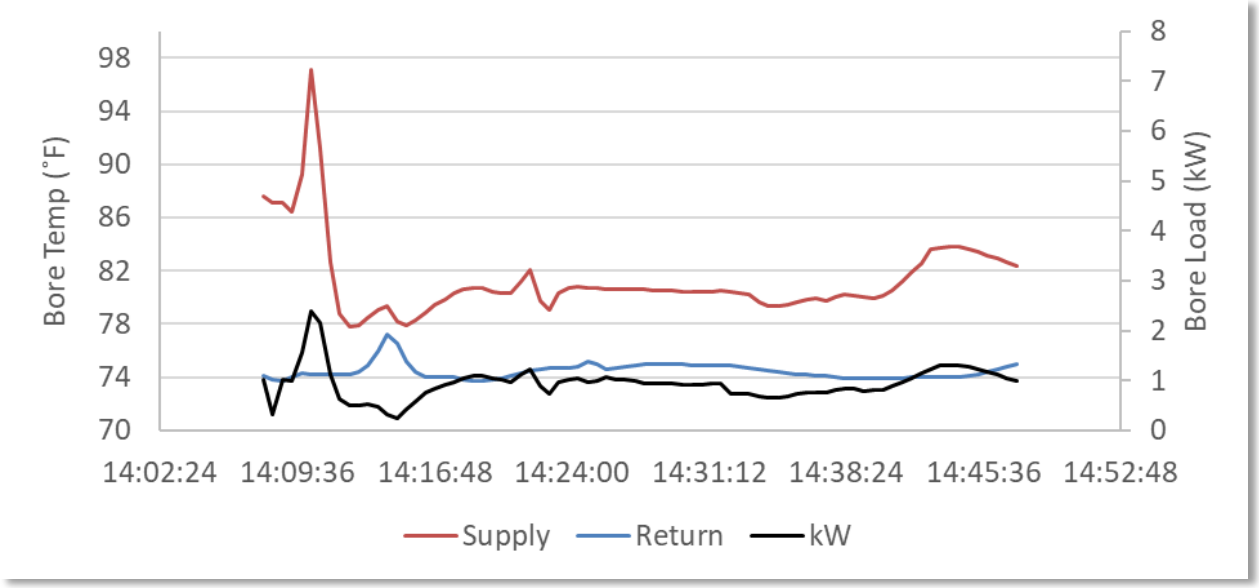

Source: University of California, Davis

The second test (Figure 23) was to determine whether the single bore with adequate irrigation could handle a 300W load, or a quarter of the desired capacity, for a simulated three-hour heating event. This test was also a chance to ensure that the irrigation system in the bore worked adequately. The surface moisture sensor was around 8 percent, but the average moisture level in the bore was 22 percent and therefore deemed adequate for the test. When the pump for the test was first turned on at 9:55 a.m., the first slug of water through the bore was colder than the return temperature. This is the volume of water in the pipe between the hot tank and the bore inlet, and the beginnings of all these tests have a fluctuation before the system can stabilize. The outlet temperature of the bore rose slightly over three hours, but appeared to level off at around 70°F. This is an indication that the bore could easily handle this

load. Testing was arrested after a few hours, and the soil could relax for a few days before the next test was run.

Figure 23: Single Bore Test at 300W and 1 gpm

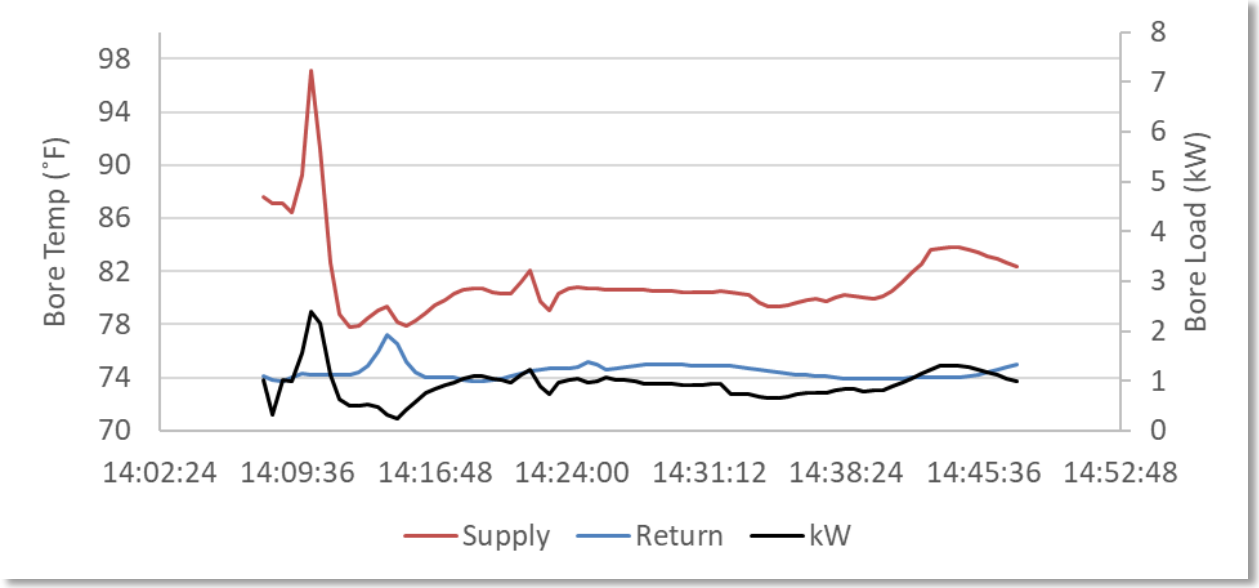

Source: University of California, Davis

The next test (Figure 24) was virtually the same as the previous test, except the load was doubled to 600W. Testing was arrested after three hours because the bore outlet temperature had stabilized. During this test, there were a few small fluctuations in the bore inlet temperature, which led to similar fluctuations in the bore's load. These were due to some minor issues with the water heater control that were later resolved. Regardless, the result of this test was that 600W was less than the capacity of the bore.

Figure 24: Single Bore Test at 600W and 1 gpm

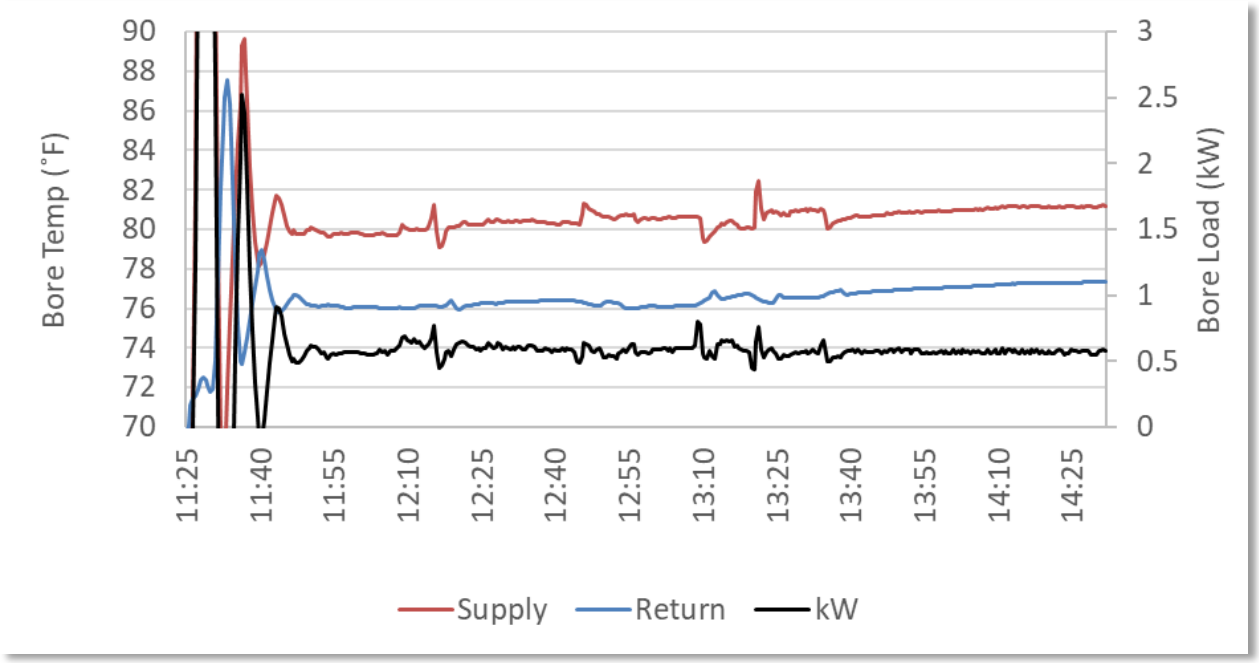

Source: University of California, Davis

The next test (Figure 25) was similar to the first two, but with a 900W load. The soil temperatures for this test were generally higher than the first two, so the return temperature started out around 80˚F. The soil temperature had a slight upward trend for the few hours before the test began, and this was regarded as a natural/weather-based phenomenon.

Figure 25: Single Bore Test at 900W and 1 gpm

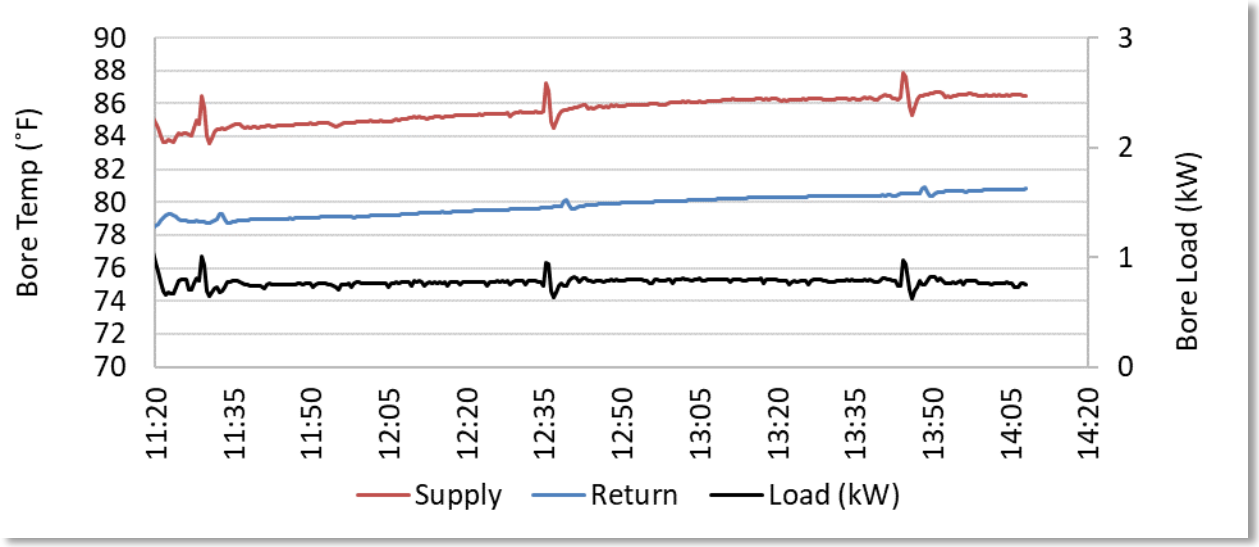

Source: University of California, Davis

The final single load test (Figure 26) was run for a longer period of time, about 18 hours. The flow rate had some fluctuations in the evening, which caused too low a load, but after correction, the test was completed overnight. Because the outlet temperature stayed virtually the same throughout the test, the bore absorbed the whole load, and it was confirmed that a single bore has a capacity of 1200W.

Figure 26: Single Bore Test at 1200W and 1 gpm

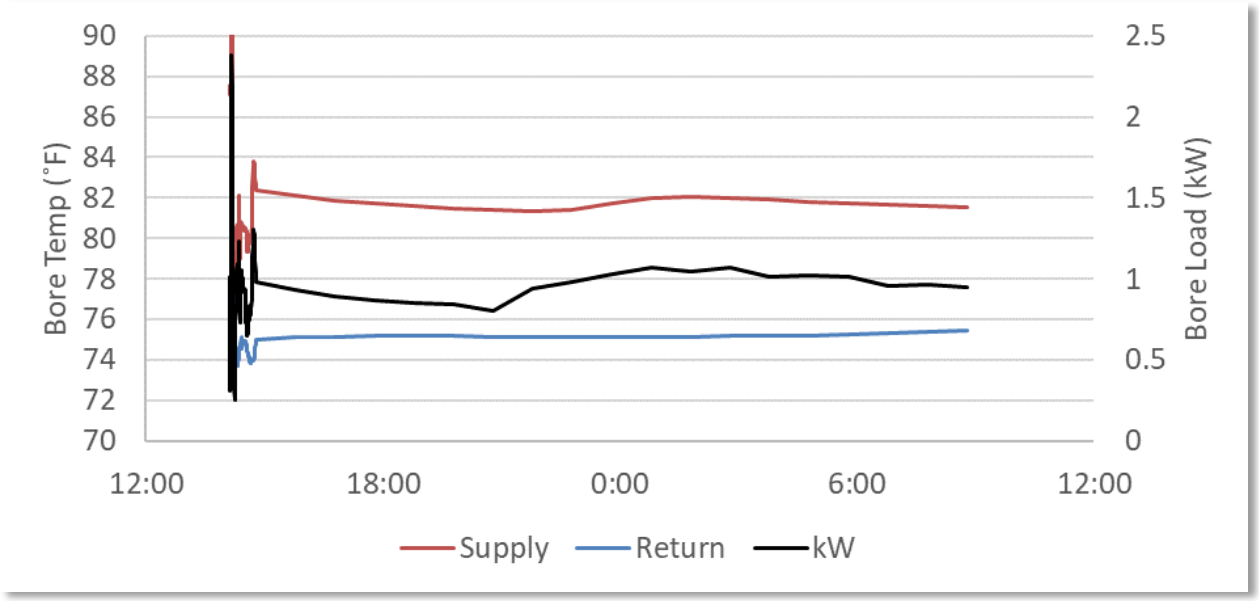

Source: University of California, Davis

Next, the effect of the flow rate through the bore was examined. It was presumed that lower flow rates would increase the temperature difference between supply and return water, which would affect heat pump performance. Figure 27 shows a test run at 600W at 1.2 gpm and Figure 28 shows a test run at 0.8 gpm. The average temperature difference of the test at 0.8 gpm is clearly a few degrees higher (about 5°F [2.8°C] as opposed to about 3°F [1.7°C]), which confirms that more heat can be rejected to the ground per unit water at lower flow rates.

Figure 27: Single Bore Test at 600W and 1.2 gpm

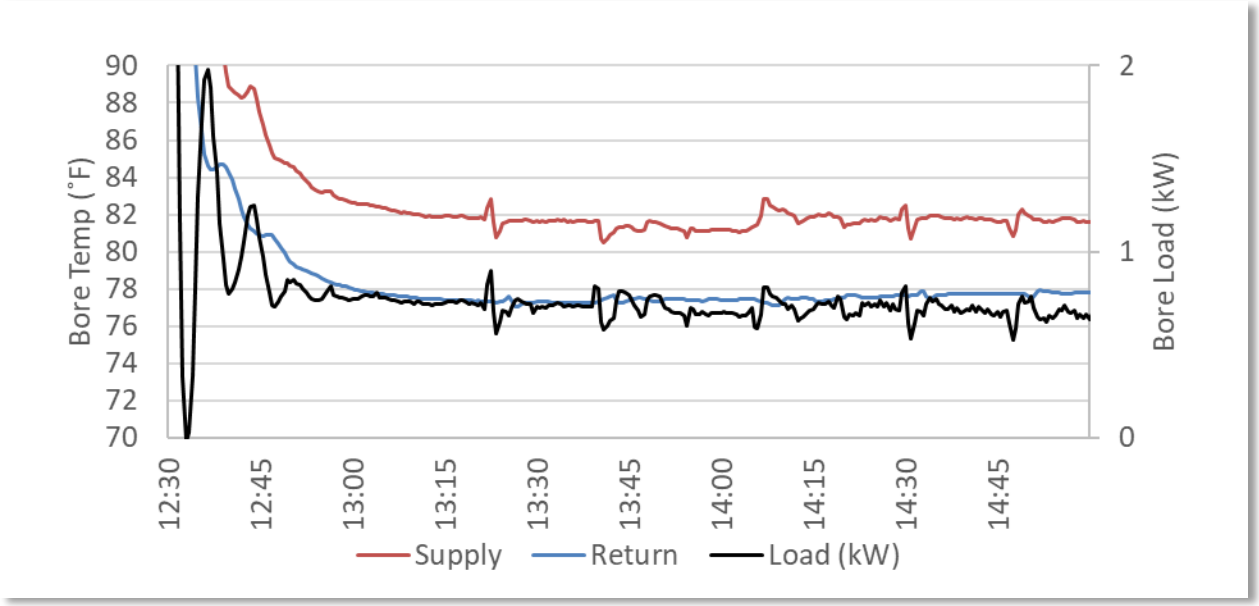

Source: University of California, Davis

Figure 28: Single Bore Test at 600W and 0.8 gpm

Source: University of California, Davis

Figure 29 shows a long-term constant load test where 1200W was rejected to the ground for multiple days. After about 9 a.m. on the third day of testing, the flow became unsteady because

there was an obstruction in the hot water line, but for the period before this, heat was successfully rejected to the ground for multiple days. The brief spikes in delivery temperature during the first half of the figure did not appreciably affect the test's outcome. The spikes occurred when the water level in the tank was low and the water heater cycled on, causing an overheating in the tank to which the controls struggled to react. Nevertheless, the bores were able to dissipate the load as the temperature difference did not get appreciably different between them until the flow became unsteady and the load spiked consistently.

Figure 29: Single Bore Test at 1200W, 1 gpm Constant Load Long Term

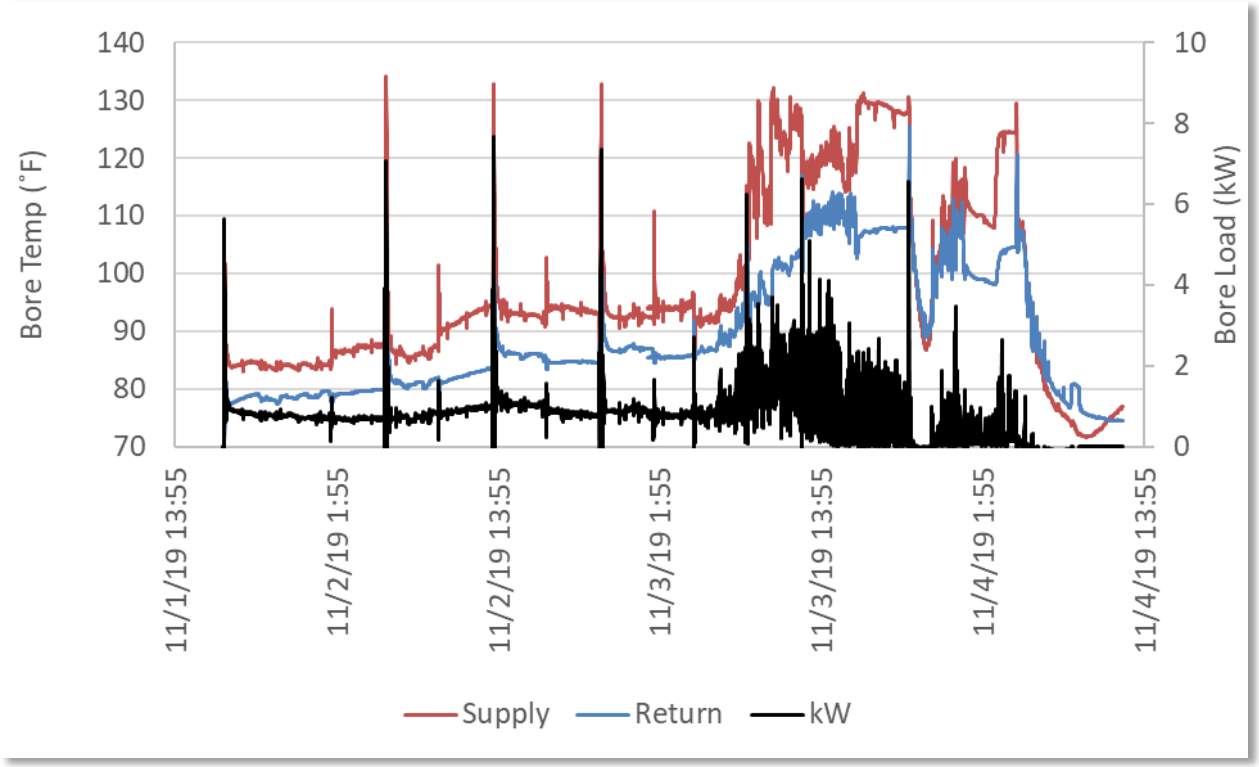

Source: University of California, Davis

The last single bore test was performed at 1200W with an intermittent, four-hours-on/four-hours-off, loading pattern over the course of a few days (Figure 30). This provided an opportunity for researchers to observe the bores between loading events and to see if a single bore could handle a quasi-realistic loading pattern with downtime between loading events to simulate the operation of a real heat pump. During the heating events, the bore reacted as expected. While the bore was not being loaded, the inlet and outlet temperatures of the bore closely followed the outdoor ambient temperature because the temperature sensors were buried close to the surface of the bore, which reacted more readily to surface conditions than the temperature sensors at lower depths.

Figure 30: Single Bore 1200w Intermittent Load Test

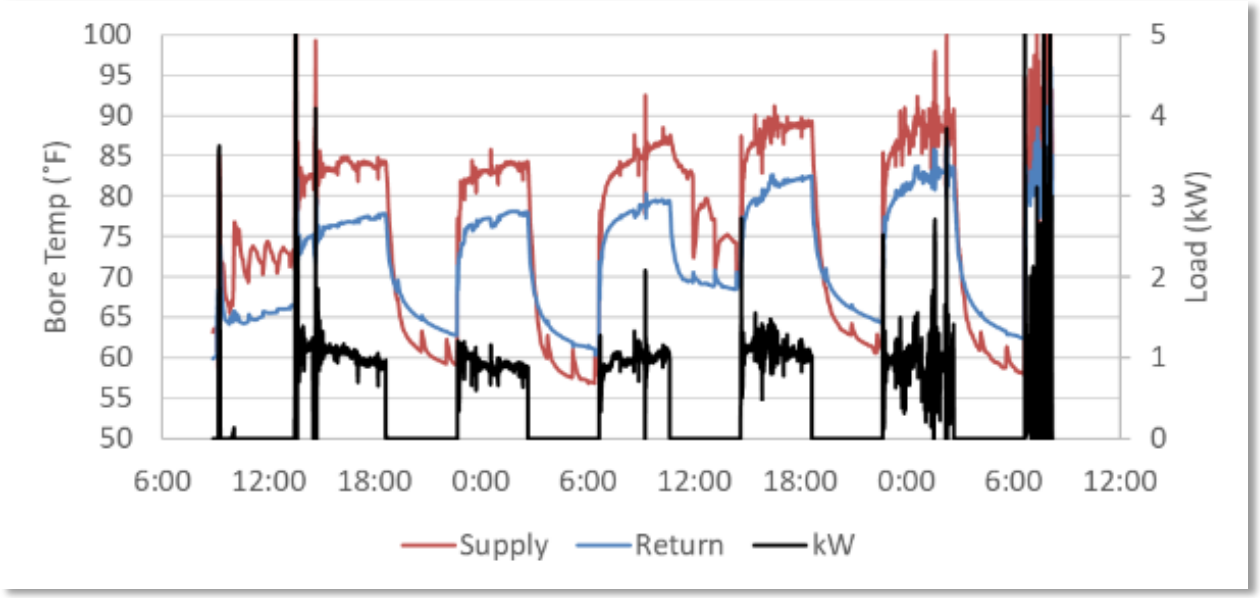

Source: University of California, Davis

Results from Multiple Bore Testing

The only multiple bore test that was run was a test on three bores in a line. The bores were plumbed in parallel and an illustration of the bore arrangement is shown in Figure 1. This compared the performance of three bores running at 1 gpm at roughly 1200W per bore for a measured total of 3516W. The moisture and temperature between the bores (that is, on the helix at either side of the center bore) were also recorded and analyzed. The temperature of each bore rose at roughly the same rate until testing was completed after a period of almost 24 hours. The loads were not exactly the same due to minor differences in flow rate to each bore and differences in the installed conditions of the bores. In Figure 31, the light blue and green lines are the supply temperatures, and the purple, bright red, and yellow lines are the return temperatures, which explain the disparity in the load applied. The outlet temperatures of each bore were observed to rise significantly over the course of the test.

Figure 31: Bore Performance in Multiple Bore Testing at 1200W per Bore

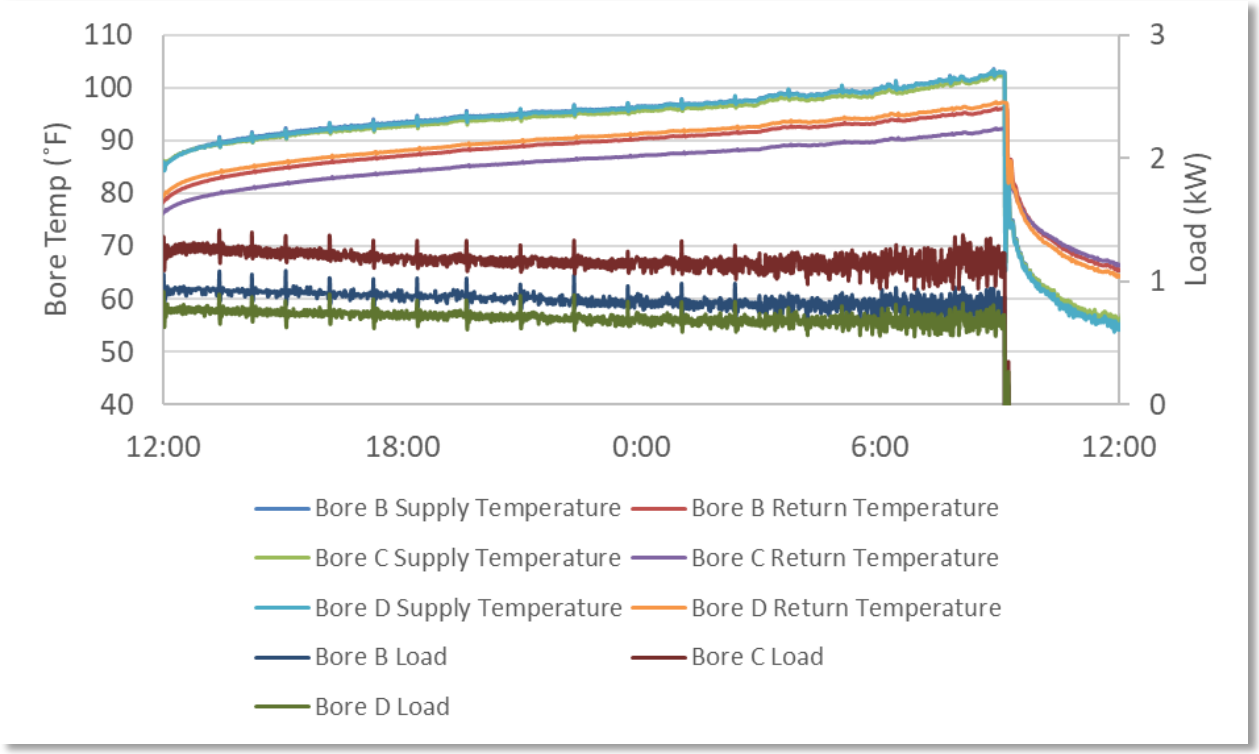

Source: University of California, Davis

Model Validation

The CaRM-HE v2 model was validated using a combination of efforts. First, existing field data from the Honda Smart Home were used to calibrate the model with estimates of the soil properties. Detailed CFD simulations using the same geometry, load conditions, and soil properties were then used to validate the CaRM-HE v2 model results. A second validation was performed using results from the laboratory testing where soil properties were measured from samples taken at the site.

Model Calibration with Existing Field Data and Validation with Detailed CFD Model

To validate the new CaRM-He v2 model, simulations were performed using the same geometry and conditions from the Honda Smart Home with properties that were used for the CaRM-He and CFD simulations. Figure 32 shows the difference between outlet fluid temperature (temperature of water exiting the ground loop) predicted by CaRM-He, CaRM-He v2, CFD, and the measured outlet fluid temperature as a function of time. The fluid outlet temperature was predicted every minute; however, for clarity one of every 30 temperature differences is shown in the graph.

Between 11 to 15.5 hours, the flow rate was off; however, the ambient temperature was much higher than the ground temperature. Since the CFD model included the pipes in the surface zone, during this period the outlet fluid temperature predicted by CFD rose rapidly due to heat transfer from the ambient.

Figure 32: Modeled Temperature Predictions Compared to Measured Data

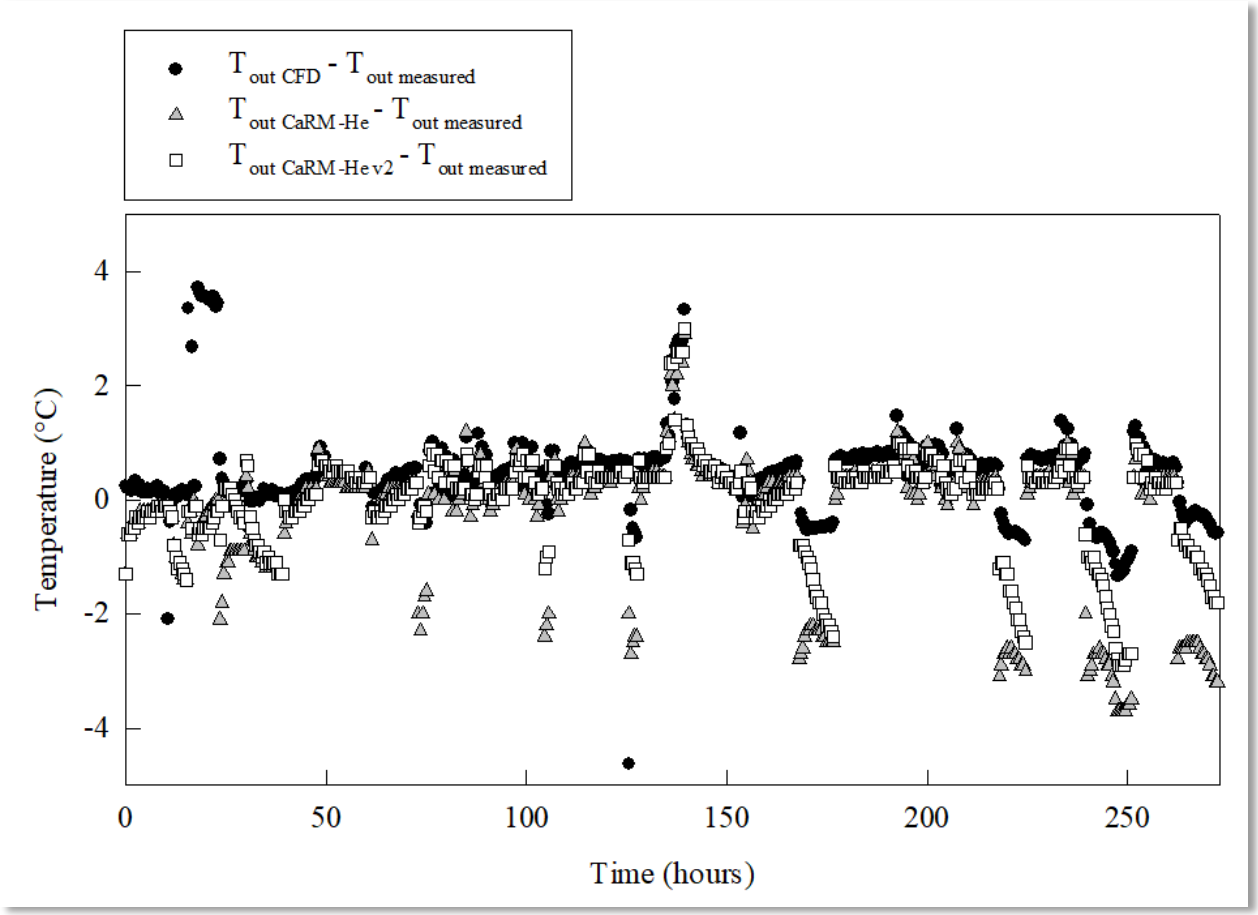

Difference between outlet fluid temperature predicted by CaRM-He, CaRM-He v2, CFD, and the measured outlet fluid temperature.

Source: University of California, Davis

The RMSD values between the predicted and measured outlet fluid temperature for CaRM-He and CaRM-He v2 were approximately the same (respectively 0.94°F [0.52°C] and 0.99°F [0.55°C]) when the flow was switched on. When the entire period is considered, the RMSD value between the measured outlet fluid temperature and that predicted by the new version was lower than that of the initial version (2.3°F [1.28°C] for CaRM-He and 1.55°F [0.86°C] for CaRM-He v2). As reference, the RMSD between the CFD result and measured outlet fluid temperature for the overall 273 hours' period was 1.39°F (0.77˚C).

Figure 33 shows the ground temperature from CaRM-He, CaRM v2, and CFD simulations at 1 hours and 21 hours after the start of simulations at different distances from the axis of the GHE. All three models predict that the maximum temperature occurs at the bore hole wall. However, the temperature of the bore hole wall predicted by CaRM-He was higher than that predicted by CaRM-He v2 and CFD. The difference was less initially. After one hour, the bore wall temperatures were 20.8˚C, 20.6˚C, and 20.4˚C from CaRM-He, CaRM-He v2, and CFD, respectively. However, after 21 hours the difference was higher, and the bore hole wall temperatures were 26.8˚C, 25.8˚C, and 24.5˚C from CaRM-He, CaRM-He v2, and CFD, respectively. Hence after the modifications to the bore hole part of the model, the CaRM-He v2 results were closer to CFD results. Another observation in Figure 33 is that the core

temperature predicted by CaRM-He v2 is higher than both CaRM-He and CFD. This is somewhat misleading since that temperature in both the original and improved CaRM-He model represents the temperature of the entire core. As we can see from the CFD model results, there is a core temperature profile that increases as it approaches the bore wall. Therefore, the core temperature predicted by CaRM-He v2 more closely matches the average core temperature predicted by CFD and provides improved predictions over CaRM-He.

Figure 33: Short-Term Ground Temperature Profile from Models

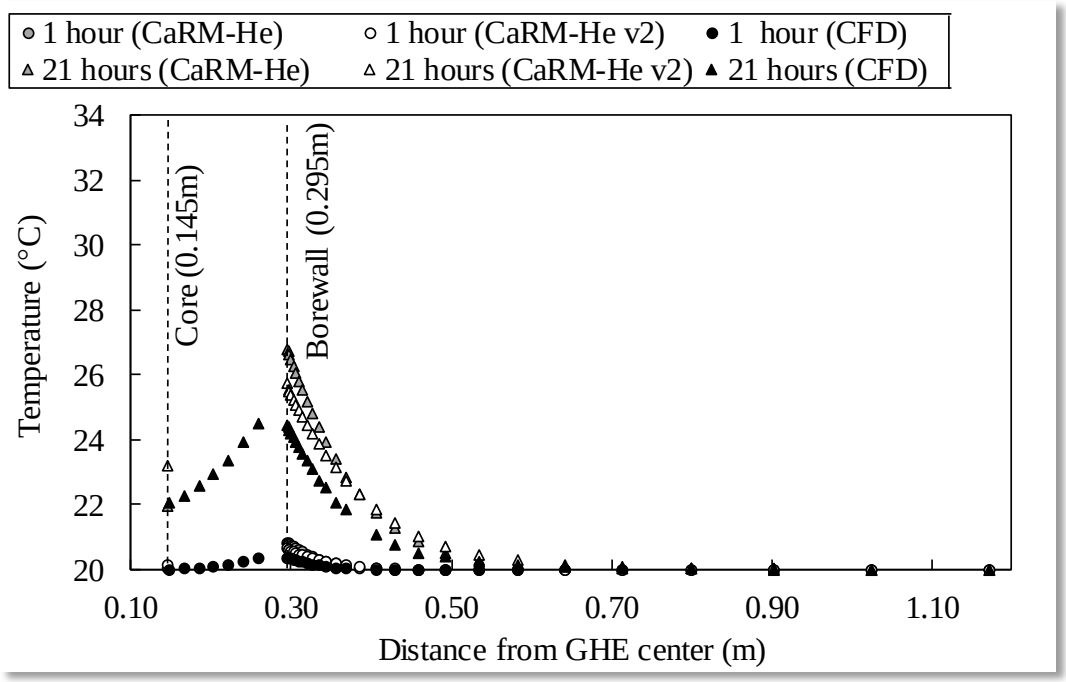

Ground temperature profile from CaRM-He, CaRM-He v2, and CFD after 1 hour and 21 hours after start of simulation.

Source: University of California, Davis

Figure 34 shows the ground temperature from CaRM-He, CaRM-He v2, and CFD at 44 hours, 120 hours, and 184 hours after the start of simulations at different distances from the axis of the GHE. As was seen before, CaRM-He predicted bore hole wall temperature was higher than that of CFD and CaRM-He v2. However, as time progressed, the temperature gradient predicted by the three models became similar. This indicates the heat conducted outward from the bore hole wall was similar for all three models in the long-term due to saturation of the soil in the core.

Figure 34: Long-Term Ground Temperature Profile from Models

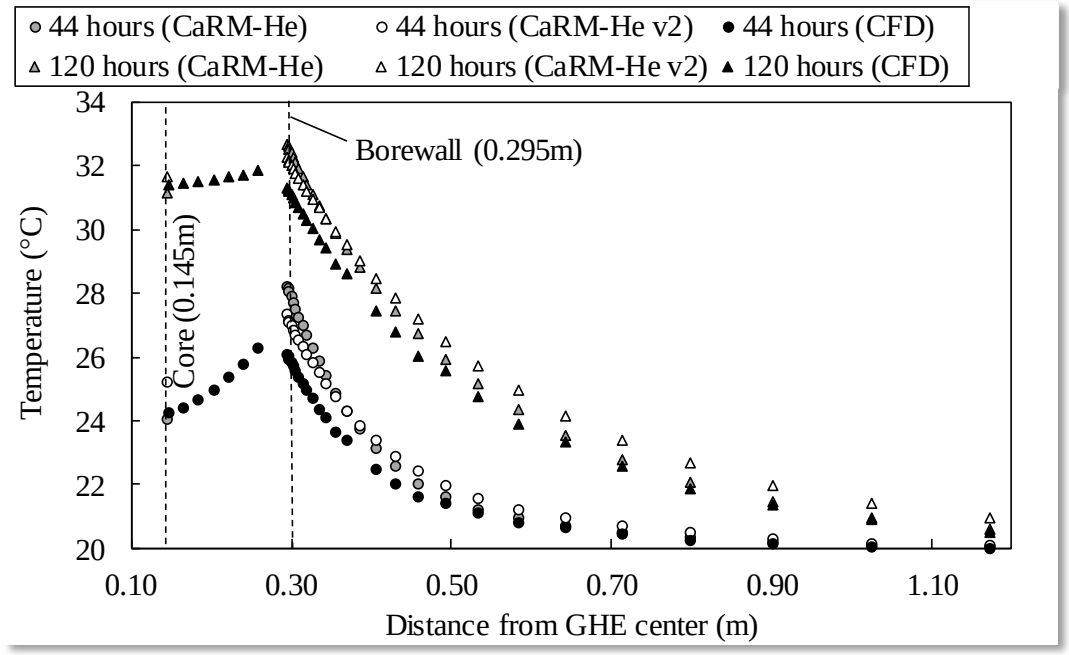

Ground temperature profile from CaRM-He, CaRM-He v2, and CFD after 44 hours and 120 hours after start of simulation.

Source: University of California, Davis

As described in the preceding sections, the CaRM-He model (original and revised versions) can discretize the ground into a number of elements along the depth. The temperatures averaged over the depth were calculated for each model. It was found that core temperatures from CaRM-He v2 matched the CFD results better compared to the original CaRM-He. The RMSD between CaRM-He v2 and CFD was 0.29˚C; whereas, the RMSD between CaRM-He and CFD was 0.39˚C. This indicates an improvement of 27 percent in prediction of the core temperature.

The depth average bore wall temperature predicted by each model was also calculated. The predicted bore wall temperature from CaRM-He v2 matched the CFD results better compared to the original CaRM-He. The RMSD for CaRM-He v2 and CFD was 0.75˚C; whereas, the RMSD between the original CaRM-He and CFD was 1.16˚C. This indicates an improvement of 35 percent in prediction of the bore wall temperature. Accurate calculation of the bore wall temperature is essential to calculate dimensionless parameters called g-functions that provide an efficient method of estimating the GHE performance. Thus an improvement in the CaRM-He model's capability to predict the soil temperature profiles is a major advancement.

A detailed comparison of the soil temperatures at different locations predicted by the models with respect to depth and time is now presented. Figure 35 shows the contour maps of core temperatures from CaRM-He v2 (Figure 35.a) and CFD (Figure 35.b) with depth on the y-axis and time on the x-axis. The measured inlet fluid temperature was superimposed over the contour maps to help to correlate the response of soil temperature to heat being rejected in the GHE. The temperature difference between CFD and CaRM-He v2 predicted results is plotted in Figure 35.c. The maximum negative and positive differences between CFD and CaRM-He v2 predicted core temperatures were -0.87 and 5˚C, respectively. It can be seen in

Figure 35.c that the temperature difference was within -0.87 to 1°C (that is, within ±3 percent of the temperature predicted by CFD) for most of the domain, except for some locations at the top and the bottom for a few hours. These brief periods of mismatch mostly occurred after a period of heat transfer to the ground followed by the flow being turned off. The dissipation of this heat built up in the ground at the surface and bottom zones was modelled in 3D in CFD. In CaRM-He the heat transfer in the surface and bottom zones was modelled in 1D. This could be a possible reason for the slight mismatch.

Figure 35: Core Temperatures Predicted by Models

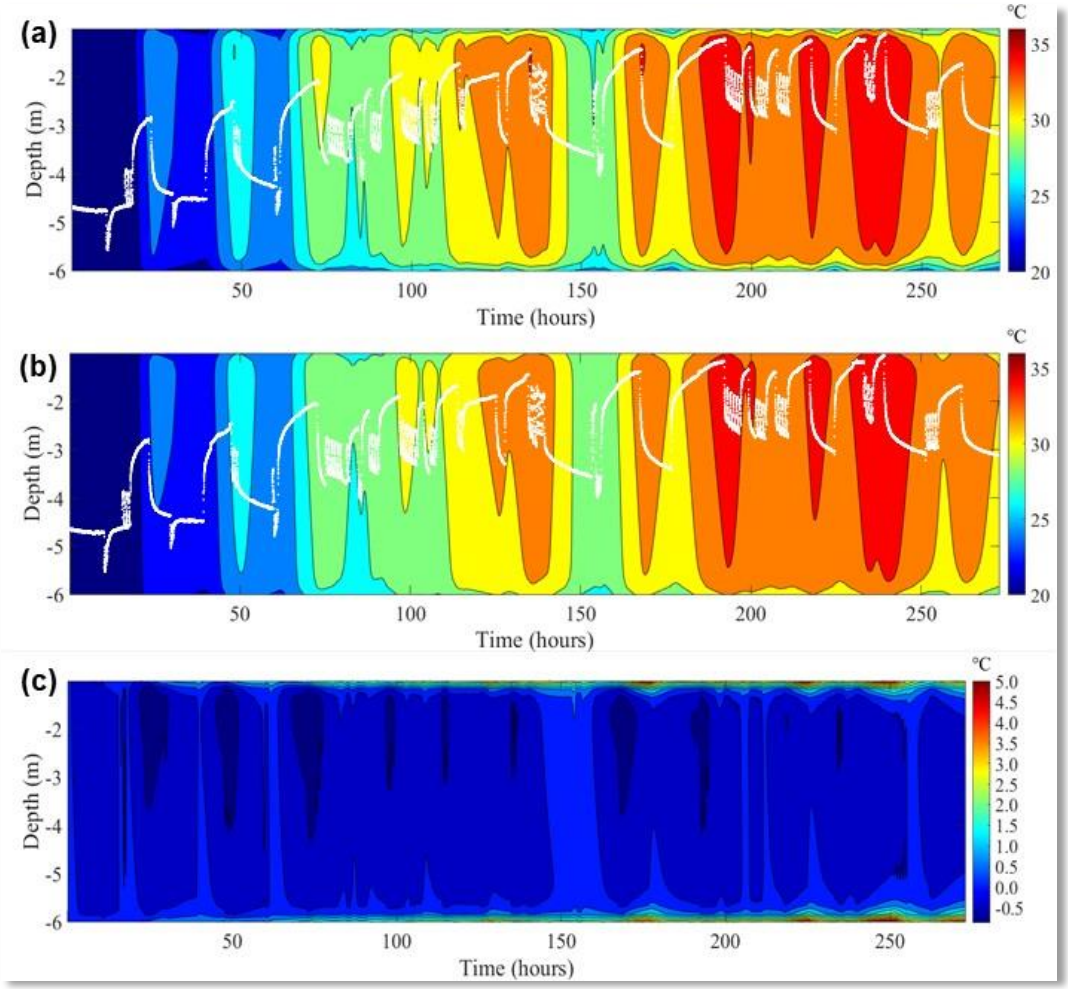

Core temperatures predicted by (a) CaRM-He v2 (color map) with depth on the y-axis and time on the x-axis, (b) CFD. The measured fluid inlet temperature was also plotted over the contour maps to help understand how it affected the ground temperature. (c) Temperature difference between CFD and CaRM-He v2 (T_{CFD}-$T_{CaRM\text{-}He\ v2}$).

Source: University of California, Davis

Similarly, Figure 36 shows the bore wall temperatures from measured data, CaRM-He v2 (Figure 36.a) and CFD (Figure 36.b) with depth on the y-axis and time on the x-axis. Figure 36.c shows the temperature difference between CFD and CaRM-He v2 predicted results. The maximum negative and positive temperature differences between CFD and CaRM-He v2 predicted bore wall temperatures was -2.18 and 4°C. It can be seen in Figure 36.c that the temperature difference was within -2.18 to 0°C (that is, within ±7 percent of the temperature

predicted by CFD) for most of the domain, except for some locations at the top and the bottom for a few hours.

Figure 36: Bore wall Temperatures Predicted by Models

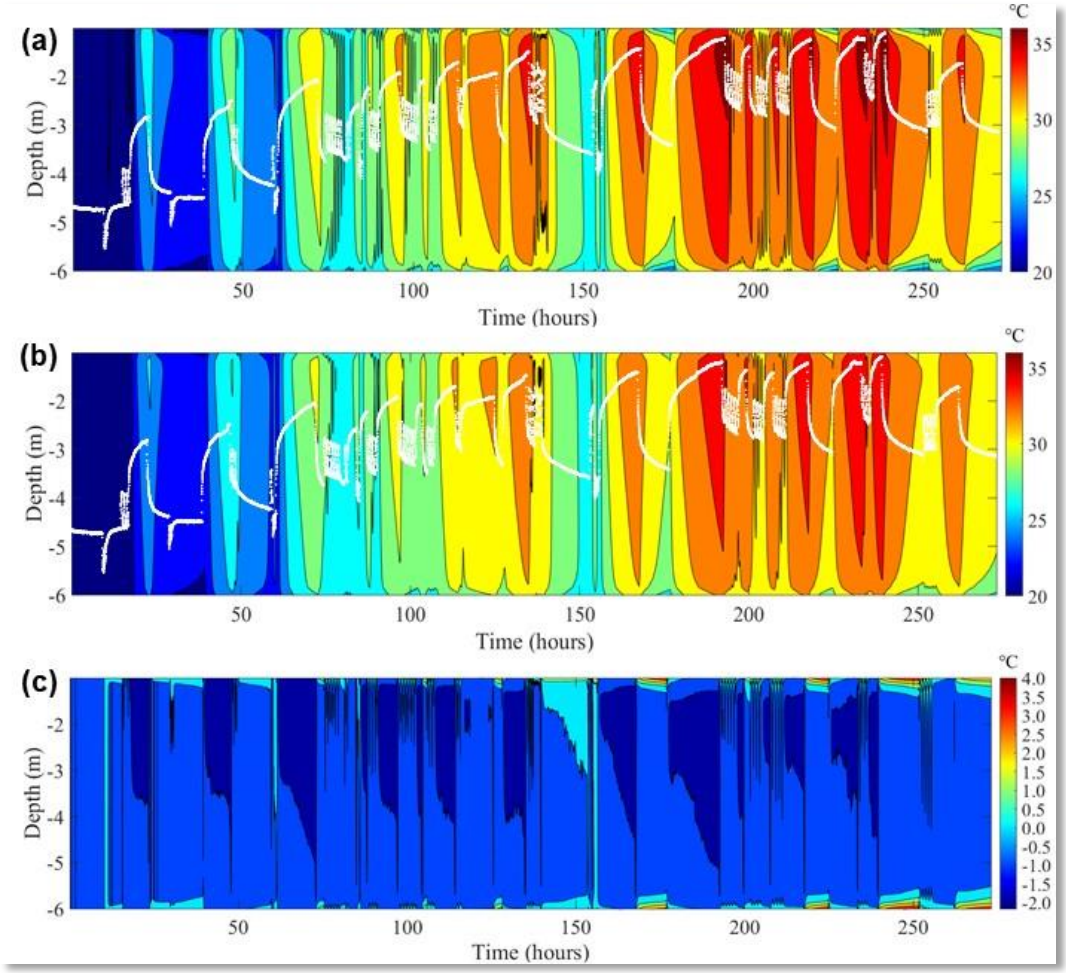

Bore wall temperatures predicted by (a) CaRM-He v2 (color map) with depth on the y-axis and time on the x-axis, (b) CFD. The measured fluid inlet temperature was also plotted over the contour maps to help understand how it affected the ground temperature. (c) Temperature difference between CFD and CaRM-He v2 (T_{CFD}-$T_{CaRM\text{-}He\ v2}$).

Source: University of California, Davis

In summary, the revised CaRM model is better able to model the heat transfer inside the bore hole. The resultant revised model simulation for the same field data indicated a closer match with CFD results for the core and bore wall temperatures. The RMSD between the new CaRM and CFD was 0.29˚C for the average core temperature and 0.75˚C for the bore wall temperature. This revised CaRM tool can hence be used for long-term simulations of GHE performance, while also obtaining a temperature map at different depths and distances from axis of bore hole. Finally, the new tool can be used to develop g-functions for helical ground heat exchangers to be integrated in building simulation software to carry out rapidly integrated computer simulations.

Model Validation with Laboratory Data

Soil Property Measurement Results

One excavated soil sample was sent to UC Davis Analytical Lab for compositional analysis. The analysis included percentage volume of solid fraction of sand (14 percent), silt (48 percent) and clay (37 percent). Total organic carbon percentage was also measured (0.61 percent). Soil sample mass was measured using a mass balance, and along with the soil volume was used to estimate density. Using the density and soil composition, the soil specific heat capacity was calculated at different moisture levels as a weighted average of the constituents. A similar approach was adopted for fine sand used to backfill the bores.

Soil sample thermal conductivity was measured using a Thermtest probe (TLS-100) with an accuracy of 5 percent in accordance with ASTM D5334 (2014). Moisture at two locations within the 3-inch (76.2 mm) diameter and 8.9-inch-long (226 mm) soil sample was also recorded to obtain data of thermal conductivity as a function of moisture content. A similar approach was adopted for obtaining thermal conductivity of fine sand used to backfill the bores. The only differences were that due to the free-flowing nature of sand, the measurements were carried out in a glass beaker and using a single moisture probe.

Figure 37 (a) and (b) shows the variation in thermal conductivity of soil and sand, respectively, as a function of percentage of volumetric moisture content. The error associated with sensor bias errors are also shown. Note that thermal conductivity scale for soil was highly magnified, which makes the error bars appear large. The soil thermal conductivity increases slightly (0.05 $Wm^{-1}K^{-1}$ or 4.2 percent) with increase in moisture from about 25 percent to 42 percent. In contrast, the increase is much more dramatic in sand thermal conductivity, which increases by more than a factor of 4.5 as moisture increases from 4.3 percent to 35.5 percent. This trend indicates that it might be more important to irrigate the core than the bore-field area to improve the performance of the GHE.

Figure 37: Soil Thermal Conductivity Testing

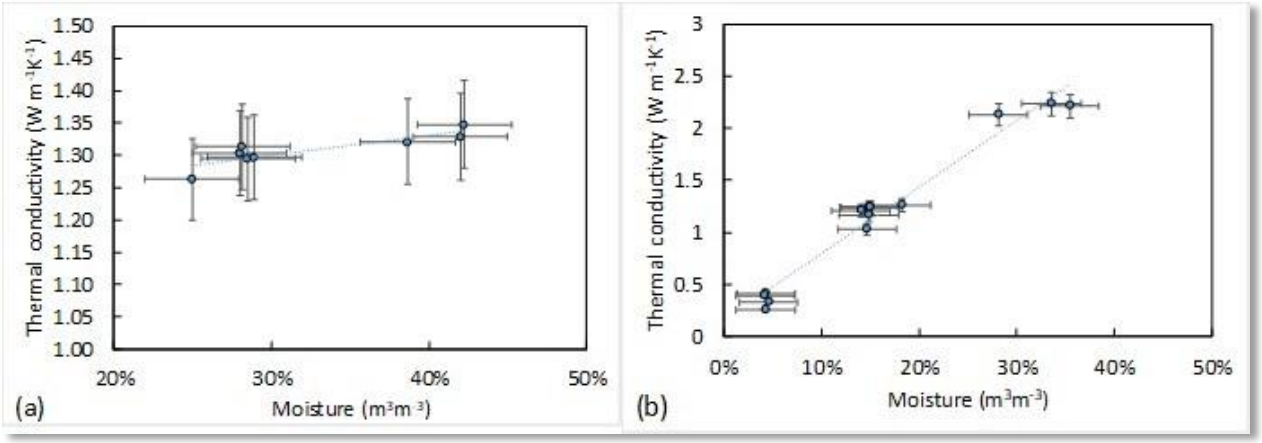

Soil thermal conductivity variation with changes in moisture in (a) soil (b) sand.

Source: University of California, Davis

Single Bore Test Data and Validation

Figure 38 shows the measured inlet and outlet temperature from the single bore cyclic test. The ambient air temperature and the far-field temperature nearest to the surface (depth of

2.5 ft) are also shown for reference. The mass flow rate is shown on a secondary axis. The test was not the first performed at the site, and therefore the soil was not at undisturbed ground temperature. Figure 38 also shows outlet temperature predicted by CaRM when flow was ON.

Figure 38: Measured and Modeled Inlet and Outlet Temperature for Single Bore with Cyclic Loading

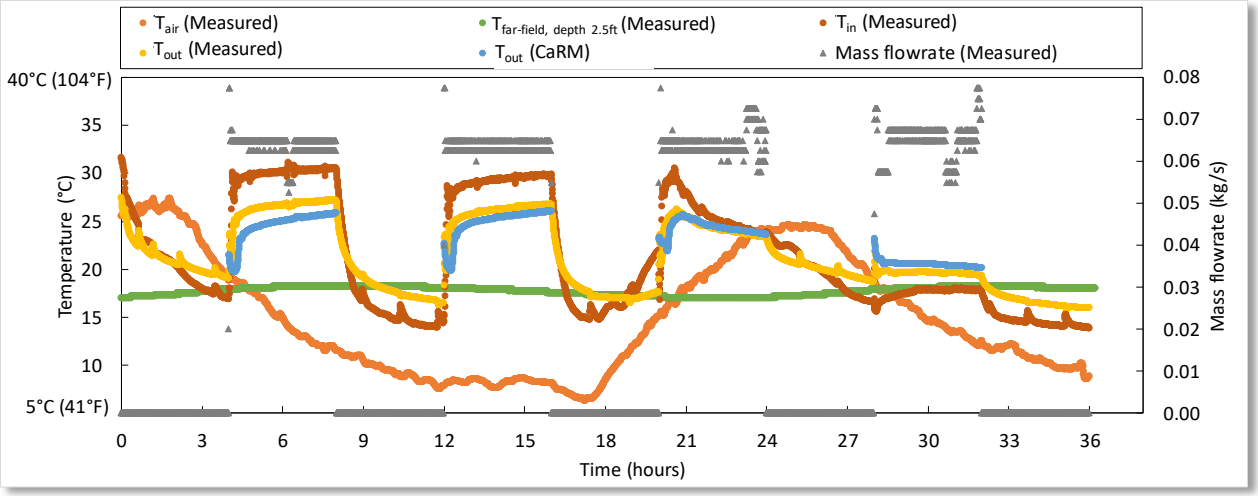

Inlet and outlet temperatures measured for the single bore cyclic test. The ambient air temperature and the far-field temperature nearest to the surface (depth of 2.5 ft) are also shown for reference. The mass flow rate is shown on a secondary axis. Outlet temperature predicted by CaRM during the ON period is shown for comparison.

Source: University of California, Davis

When the flow was OFF the measured outlet temperature was influenced more by the environmental conditions; therefore, it does not truly represent the temperature of the water inside the GHE. This is to be expected as the outlet section of the pipe is buried in the ground near the surface without insulation. There were considerable fluctuations in the mass flow rate at some time periods. The average mass flow rate (during the ON period) was 0.0643 kg s^{-1}, which was the constant value used as an input in CaRM during the ON period.

The moisture levels measured during the test varied spatially, especially in the depth. The average core, surface, bore hole surrounding, and deep zone moisture were 26 percent, 11 percent, 42 percent, and 46 percent, respectively. The measured zone moisture at each time step was used as an input in the model. Figure 38 shows the measured and predicted outlet temperatures match overall. Since the test did not start at the undisturbed ground temperature, there was some difference when the flow was turned on the first time (four to eight hours). The results matched well after the twelfth hour. The root mean square difference (RMSD) for this period was 1.85°F (1.03°C). The overall RMSD was 2.41°F (1.34°C). Possible cause for the rising trend of the outlet predicted by CaRM could be variation and inaccuracies in measurement of the thermal conductivity.

Figure 39 shows the measured depth average bore hole wall temperature along with that obtained from CaRM results. Except for the first four hours, the results matched well. The RMSD for the 4 to 36-hour period was 0.49°F (0.27°C), while the overall RMSD was 2.00°F (1.11°C). Tests under other loads and longer time durations are underway.

Figure 39: Measured and Modeled Bore hole Wall Temperature

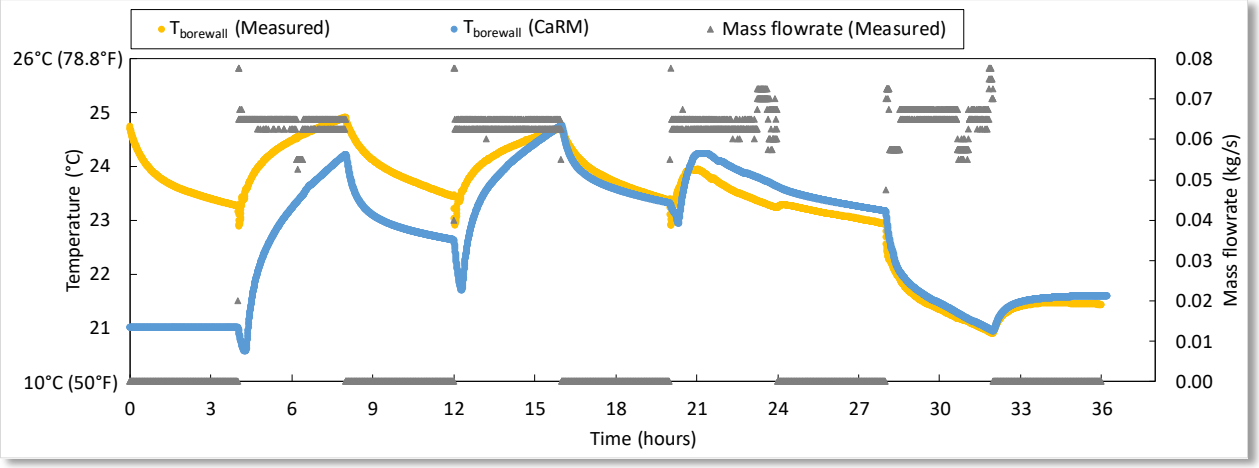

The measured depth average bore hole wall temperature and CaRM predicted depth average bore hole wall temperature. Mass flow rate is also shown for reference.

Source: University of California, Davis

Multiple Bore Test Data and Validation

Figure 40 shows the measured combined inlet and combined outlet temperature from the multiple bore continuous load test. The ambient air temperature is also shown for reference. The mass flow rate is shown on the secondary axis. The time average load for the duration of the test, for all three bores, was 2759-W. The time average combined mass flow rate was 0.176 kg s^{-1}, which was the constant value used as an input in CaRM. The average moisture at core, surface, bore hole surrounding, and deep zone moisture was 25 percent, 11 percent, 42 percent, and 46 percent, respectively, similar to the single bore test. Figure 40 also shows combined outlet temperature predicted by CaRM, which matched well with the measured value. The RMSD between the simulation results and measurements was 1.71°F (0.95°C).

Figure 41 shows the measured depth average bore hole wall temperature for Bore 2/D along with that obtained from CaRM results. The results matched well; however, an offset is present. The overall RMSD was 1.21°F (0.67°C). Testing in other configurations (corner) and loads is in progress. Soil experiments are also underway to investigate the soil thermal conductivity over a wider range of moisture.

Figure 40: Measured and Modeled Inlet and Outlet Temperature for Multiple Bore with Constant Loading

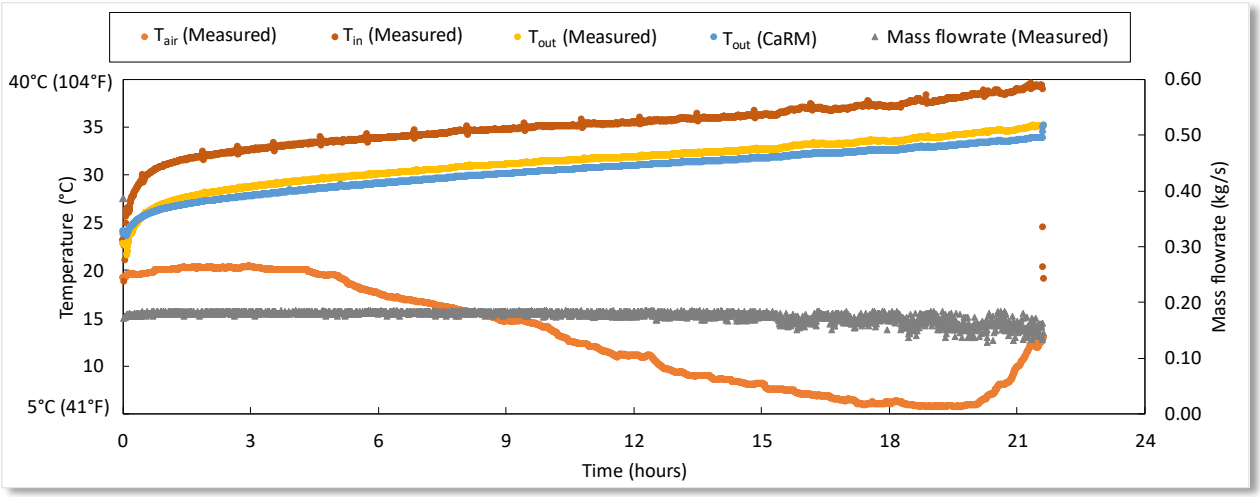

The combined inlet and outlet temperatures measured for the multiple bore continuous load test. The ambient air temperature is also shown for reference. The mass flow rate is shown on a secondary axis.

Source: University of California, Davis

Figure 41: Measured and Modeled Bore hole Wall Temperature for Multiple Bore with Constant Loading

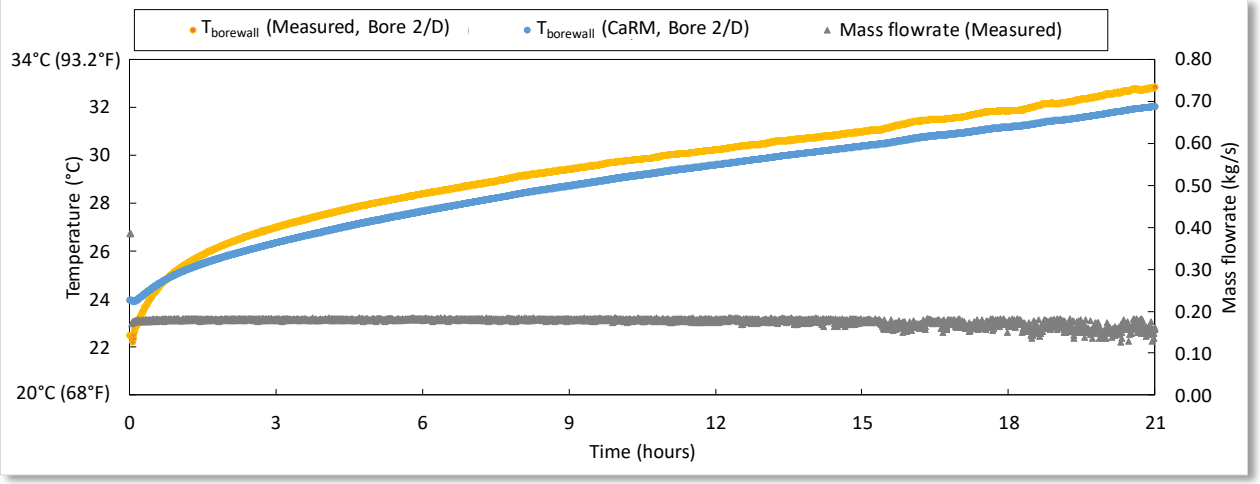

The measured depth average bore hole wall temperature of Bore 2/D and CaRM predicted depth average bore hole wall temperature. Mass flow rate are also shown for reference.

Source: University of California, Davis

In summary, the CaRM-He v2 model was validated against lab test data. Using a multiple bore test site, temperature and moisture data were collected for intermittent and continuous tests. In addition to field data of the performance of the GHE, experiments were performed to measure soil thermal conductivity at different moisture levels. Moisture had a considerable effect on the conductivity of sand, while its effect was minimal on the soil conductivity from 25 to 42 percent moisture content. The model predicted outlet fluid and bore hole wall temperature well when compared with the experimental data. The root mean square deviation between model and lab bore hole wall temperatures was 1.21°F (0.67°C).

Ground Heat Exchanger Parametric Analysis

A parametric analysis was performed using the validated CaRM model to understand the implications of changing a range of GHE geometrical variables including bore hole spacing, number of GHEs, bore hole depth, bore hole arrangement, and soil properties. A modified version of the CaRM model that includes a water-to-air heat pump was used for the analysis. The building load for the analysis was determined from a 2,700 sq. ft. home in California climate zones 10 (Riverside) and 12 (Sacramento). The California Building Energy Code Compliance for Residential buildings (CBECC-Res) energy simulation tool was used to calculate the cooling and heating load of a detached, single-family, two story home for each of the three California climate zones. The total conditioned area was 2,700 ft^2 (250.8 m^2), not including an attached garage. The house construction is based on the 2013 California Residential Alternative Calculation Method (ACM) Reference Manual prototype houses. Table 13 lists the main characteristics of the home model.

Table 13: Basic Characteristics of Home Model Used

Building Characteristic	Value
General building dimensions	
– Conditioned floor area	250.8 m^2 (2700 ft^2)
– Roof area	134.7 m^2 (1450 ft^2)
– Number of stories	2
– Window-to-wall ratio	0.20
Wall area by orientation	
– North	672.5 ft^2 (62.5 m^2)
– East	672.5 ft^2 (62.5 m^2)
– South	672.5 ft^2 (62.5 m^2)
– West	672.5 ft^2 (62.5 m^2)
Foundation type	Slab-on-grade
Effective air leakage area	
– Living space	5 ACH @ 50Pa
– Attic	N/A (Ventilated)

Source: University of California, Davis

Figure 42 shows the ambient air, dry bulb temperature for climate zone (CZ) 12 (Sacramento) used in the building and CaRM models. The line represents a least square curve fit of the outdoor air temperature.

Figure 42: Ambient Air, Dry Bulb Temperature for Climate Zone 12 and Periodic Temperature Curve Fitted to Data

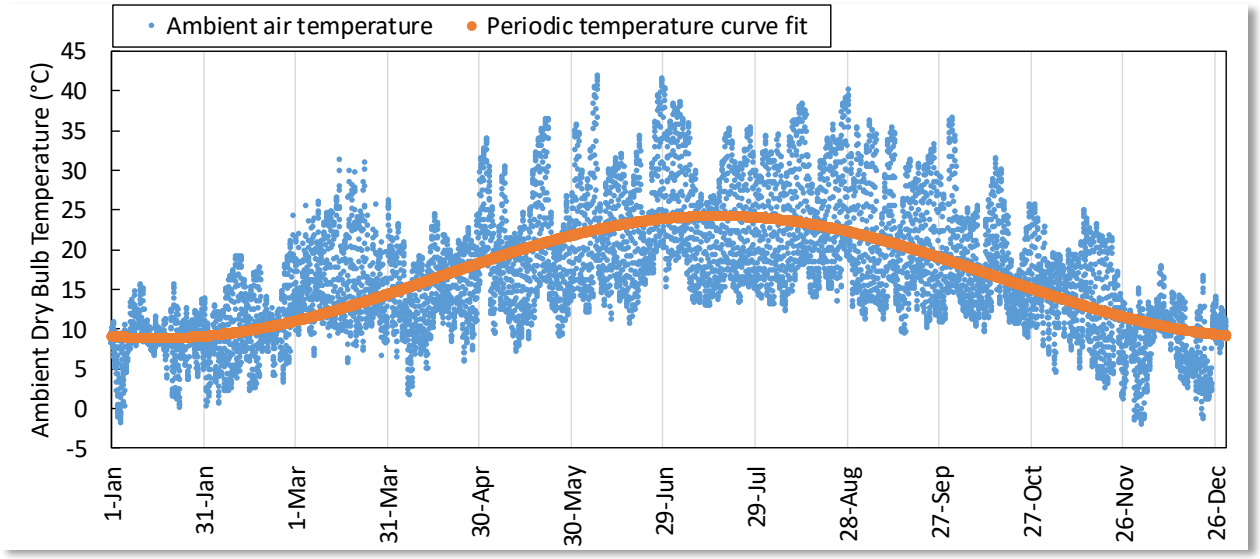

Source: University of California, Davis

Figure 43(a) shows the hourly building load profile resulting from the CBECC-Res simulation for a typical year in CZ12 Sacramento. The summer (cooling) load is shown as positive (that is, heat removed from the building is positive). Figure 43(b) shows the cumulative summer (cooling) and winter (heating) load for CZ12 Sacramento for one year in kilowatt-hours (kWh). It can be seen that the load is winter dominant (67 percent of overall building load). It should also be noted that there are 502 hours of the year when cooling is required and 1605 hours when heating is required.

Figure 43: Hourly and Cumulative Seasonal Load Profiles for Model Home in Climate Zone 12

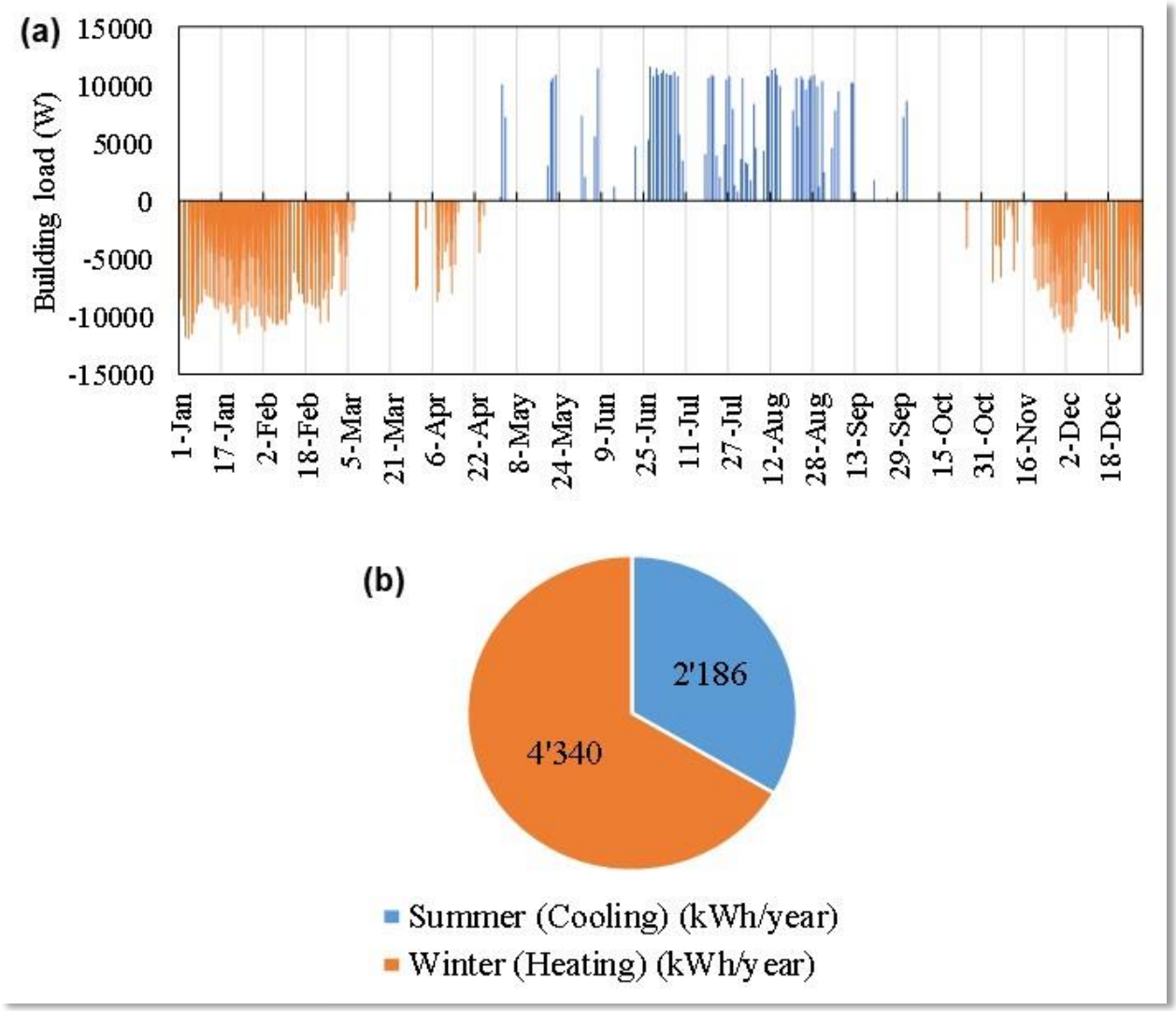

(a) Hourly building load profile for a typical year in CZ12 Sacramento that was used as an input for CaRM-HP model. The summer (cooling) load is shown as positive.

(b) Cumulative summer (cooling) and winter (heating) load for CZ12 Sacramento for one year in kWh.

Source: University of California, Davis

Figure 44 shows the ambient air, dry bulb temperature for CZ10 Riverside used in the building and CaRM models. The line represents a least square curve fit of the outdoor air temperature. In comparison to climate zone 12 (Figure 42) it is seen that the winter temperatures are higher in this climate zone.

Figure 44: Ambient Air, Dry Bulb Temperature for Climate Zone 10 and Periodic Temperature Curve Fitted to Data

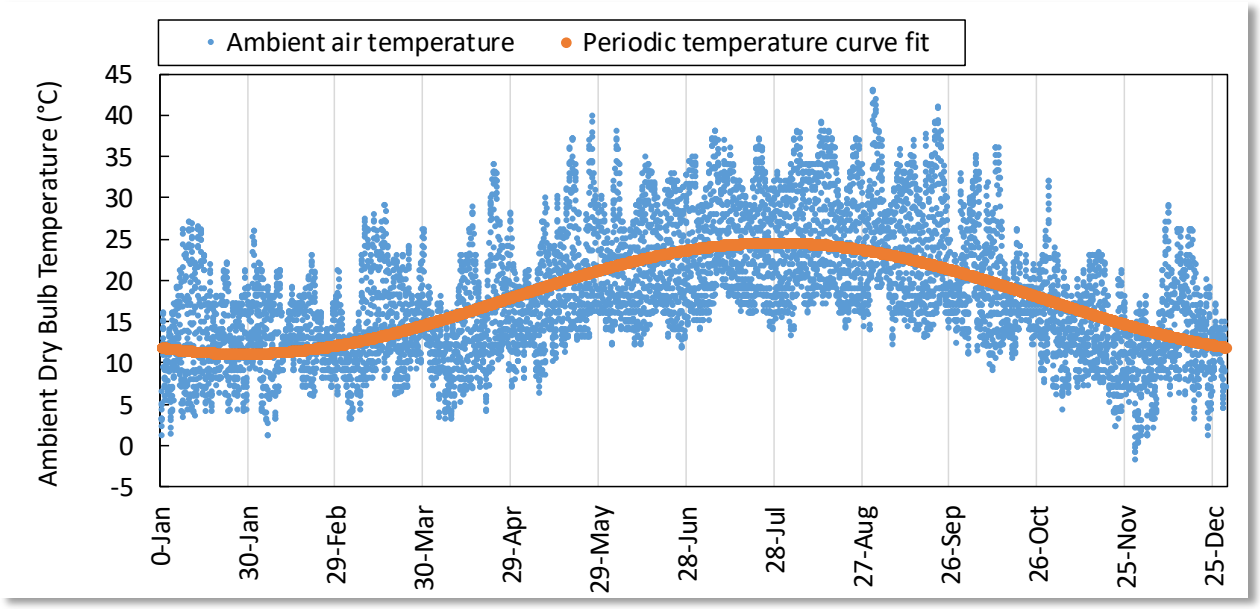

Source: University of California, Davis

Figure 45(a) shows the hourly building load profile resulting from the CBECC-Res simulation for a typical year in CZ10 Riverside. The cumulative summer (cooling) and winter (heating) load for CZ10 Riverside for a typical year is also shown in Figure 45(b). It can be seen that the summer load forms a larger portion of the overall building load (56 percent of overall building load). There are 811 hours of the year when cooling is required and 909 hours when heating is required. This means that the cooling load is less frequent but higher in magnitude than the winter load.

Figure 45: Hourly and Cumulative Seasonal Load Profiles for Model Home in Climate Zone 10

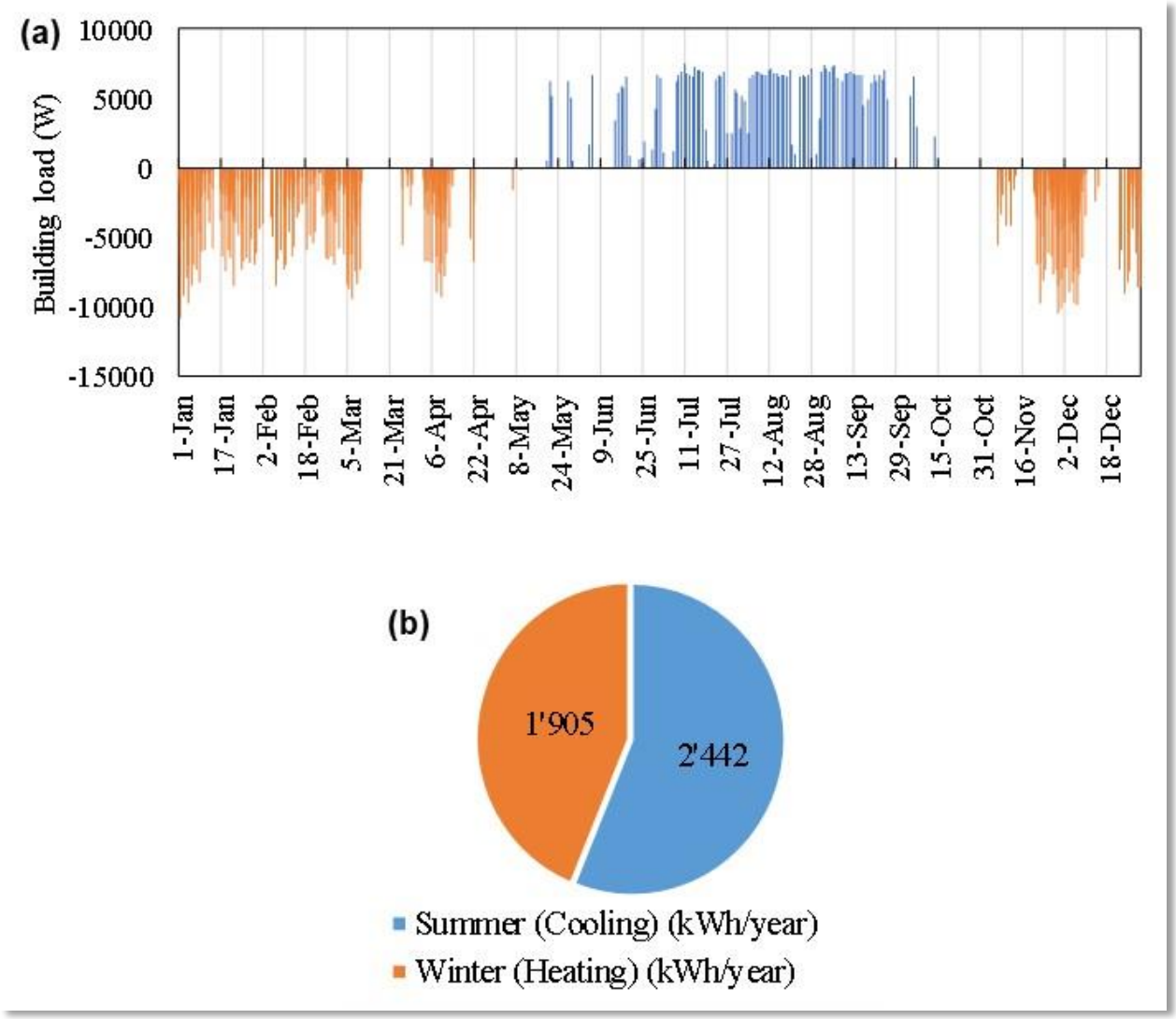

(a) Hourly building load profile for a typical year in Riverside. The summer (cooling) load is shown as positive.

(b) Cumulative summer (cooling) and winter (heating) load for Riverside for one year in kWh.

Source: University of California, Davis

Based on the load profiles in both climate zones, heating and cooling were provided by a 3.5-ton water-to-water heat pump. Manufacturer specifications were used to determine performance curves for cooling or heating capacity and electric power consumption as a function of source side inlet temperature. For calculating the electricity consumed by the GHE system, the power consumed by the circulation pump was also considered. The pressure drop across the GHE was calculated using analytical expressions for pipe flow, whereas the pressure loss across the heat pump was obtained from manufacturer specification. The pump efficiency was assumed to be 50 percent.

As a benchmark for the GHE system performance, a 3.5-ton air-source heat pump from the same manufacturer was also used with the outdoor air temperature as the inlet source side

temperature. The flow rate of air on the load side was constant for both heat pumps at 1400 cubic feet per minute.

Table 14 shows a listing of the varied parameters in the analysis. A reference case was chosen for each climate zone and a perturbation in parameters performed on this reference case. Since the summer and winter loads are different for both climate zones, the number of GHEs in the reference case were different as well. For climate zone (CZ) 12, the reference case had eight GHEs; whereas, for CZ10, the reference case had five GHEs.

Table 14: Parametric Variables Used in Simulations

GHE Parameters	Reference	Variable Min.	Variable Max.
1) Spacing	3.5 m	2 m	5 m
2) Number of GHEs	-	-	-
CZ12 Sacramento	8	6	10
CZ10 Riverside	5	3	7
3) Bore hole diameter	0.610 m (24 in.)	0.406 m (16 in.)	0.914 m (36 in.)
Pipe length (one GHE)	73.8 m	48.4 m	112.0 m
Spacing	3.5 m	2.33 m	5.25 m
Far-field radius	10 m	7 m	15 m
Number of GHEs	-	-	-
CZ12 Sacramento	8	12	5
CZ10 Riverside	5	8	3
Cost of one GHE	$ 308	$ 243	$ 417
4) Arrangement	L-shaped	Grid	—
5) GHE height	6.10 m (20 ft)	3.96 m (13 ft)	—
Pipe length (one GHE)	73.8 m	48.0 m	
Number of GHEs	-	-	-
CZ12 Sacramento	8	12	
CZ10 Riverside	5	9	
Cost of one GHE	$ 308	$ 215	
Bore hole depth	6.71 m (22 ft)	4.57 m (15 ft)	
6) Soil type (moisture)	Heavy clay (15%)	Heavy clay (15%)	Light Sand (15%)
Backfill	Fine sand; Backfill properties [1]	Native soil	Native soil
Thermal conductivity	2.08 W m^{-1} K^{-1}	1.64 W m^{-1} K^{-1}	1.56 W m^{-1} K^{-1}
Specific heat capacity	1359 J kg^{-1} K^{-1}	1559 J kg^{-1} K^{-1}	1559 J kg^{-1} K^{-1}
Density	1350 kg m^{-3}	1784 kg m^{-3}	1239 kg m^{-3}

1 based on soil property measurements from testing (Figure 37).

Source: University of California, Davis

For most cases (spacing, number of GHEs, arrangement, and soil type), only one parameter was changed while the other parameters were kept same as the reference. As an example, for CZ12 Sacramento, when the number of GHEs was changed from 8 GHEs to 6 GHEs or 10 GHEs, the spacing was kept at 3.5 m (that is, the same as the reference).

However, when bore hole diameter and bore hole depth were changed, the number of GHEs also changed. This was done so the total bore hole area (of all GHEs in a simulation) could be kept approximately the same as the reference case. Furthermore, the cost of one GHE also changed as the bore hole diameter or bore hole depth changed as shown in the table. As expected, the pipe length of the GHE also changed. Figure 46 shows the layout of the GHEs used in the parametric study for CZ12 Sacramento. The plot area was kept fixed at 100 feet x 60 feet and the home was centrally located on this land. Soil variation had no effect on the layout of the GHEs and is therefore not shown in the figure.

Figure 46: Land Area Considerations Based on Bore hole Configuration

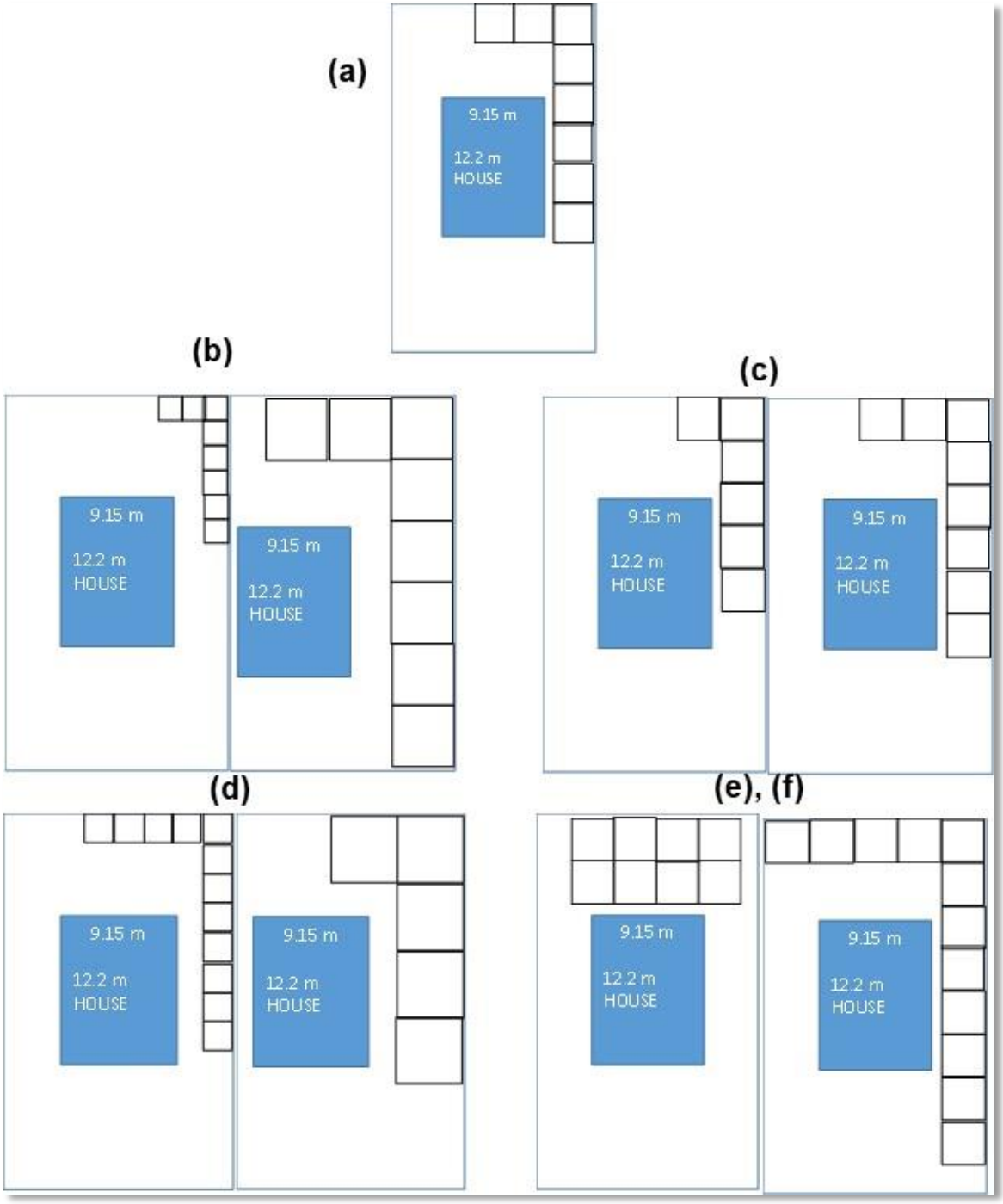

(a) Reference design layout. Eight GHEs with 3.5 m spacing. Bore hole diameter and depth is 0.610 m (24 in.) and 6.71m (22 ft) respectively.
(b) Spacing variation layouts (i) 2 m, (ii) 5 m.
(c) Number of GHEs variation layouts (i) 6 GHEs, (ii) 10 GHEs.
(d) Diameter of bore hole variation layouts (i) 0.406 m (16 in.) (ii) 0.914 m (36 in.)
(e) Grid arrangement layout, (f) bore hole depth 4.57 m (15 ft)

Source: University of California, Davis

Results from the parametric simulations for CZ12 Sacramento are shown in Figure 47. Figure 47(a) shows the total installation cost for different GHE systems from variations listed in Table 14. Changes in soil properties do not affect the total installation cost and are therefore not

shown separately. Figure 47(b) shows the five-year average annual electricity consumed for each GHE configuration. Also included is the performance of the benchmark air-source heat pump. Figure 47(c) shows the installed cost ($) per kWh saved annually.

Figure 47: Results from Parametric Study for Climate Zone 12

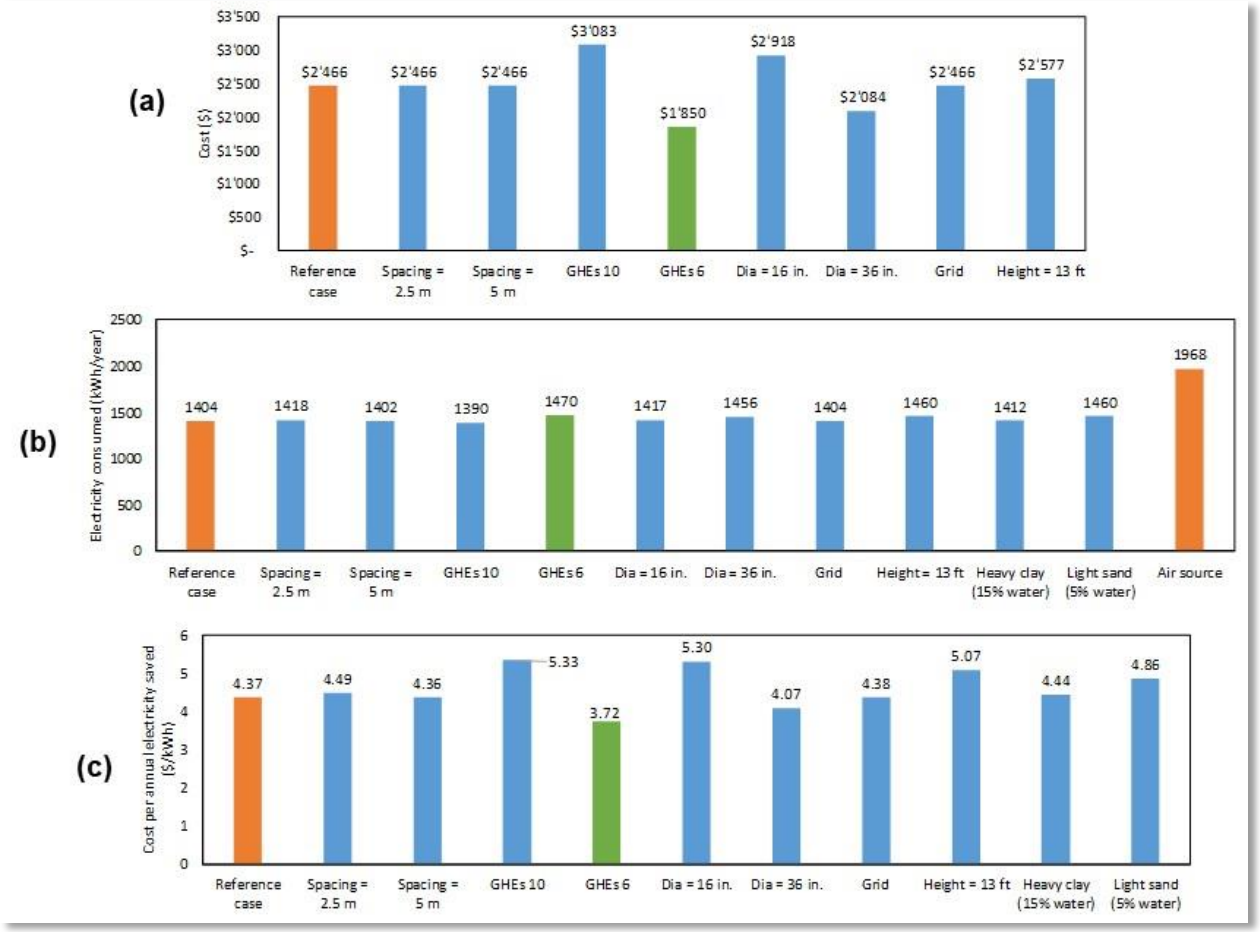

(a) Total installation cost ($) for all configurations (except soil property changes) for CZ12 Sacramento.
(b) Five-year average electricity consumed (kWh/year) for each case for CZ12 Sacramento. Air-source is also shown for reference.
(c) Installed cost per annual kWh saved compared to the air-source heat pump for CZ12 Sacramento.

Source: University of California, Davis

As seen in Figure 47(a), changing the spacing had no effect on the installation cost. Predictably, increasing the number of GHEs to 10 increased the total cost by 25 percent. Conversely, using six GHEs decreased the cost by 25 percent. As noted in Table 14, a 36-inch GHE costs $109 more than the reference 24-inch GHE. However, since the bore hole area was maintained the same in the parametric study, six 36-inch GHEs were equivalent in bore hole area to eight 24-inch GHEs used in the reference case. As a consequence, the overall cost of the system decreases by 15 percent. Similarly, using 12 16-inch GHEs increased the total cost by 18 percent relative to the reference. Since changing the arrangement to grid layout did not change the number of GHEs, the cost did not change. The figure also shows the cost for a GHE with a height of 13 feet. Although a single 13-foot GHE was $93 cheaper than the reference 20-foot GHE, the total cost of 12 13-foot GHEs is 5 percent larger than the reference case (8 20-foot GHEs).

Figure 47(b) shows the five-year average electricity consumed (kWh/year) using the different configurations for CZ12 Sacramento. The results indicate that decreasing the spacing from the reference case of 3.5m to 2m increases the electricity consumption by only 1 percent. The slight increase is because the GHEs are closer to each other relative to the reference, and the thermal mass of the ground available for heat rejection is lower. Increasing the spacing to 5m has no significant effect on the electricity consumption (it decreases by 0.1 percent). The parametric results of spacing indicate that a spacing of even 2m is sufficient for this climate zone.

The effect of changing the number of GHEs on electricity consumed is also shown in Figure 47(b). As expected, the electricity consumed decreases with an increase in the number of GHEs as there are more GHEs to dissipate the heat into the ground. Using 10 GHEs (instead of the reference case 8 GHEs) decreases the electricity consumed by 1 percent. Conversely, using six GHEs increases the electricity consumed by 5 percent. Using fewer large-diameter (36-inch) GHEs, increases the electricity consumed by 4 percent, while using 12 16-inch-diameter GHEs also increases the electricity consumed by 1 percent. This increase in electricity consumption is due to the decrease in the total bore hole area for 16-inch and 36-inch-diameter cases. While the total bore hole area was held nominally constant, it was slightly lower between the reference case and the 16-inch and 36-inch cases to maintain an integer number of bores. Changing the arrangement to grid has no effect on the GHE electricity consumed. Using 13-foot GHEs increases the electricity consumption by 4 percent.

The figure also shows that the soil properties affect the electricity consumption of the GHE system. In the reference case, the soil is heavy clay at 15 percent moisture, with sand at 30 percent moisture as the backfill. The electricity consumed increases by 1 percent when the soil and backfill both are composed of heavy clay at 15 percent moisture. This is because the thermal conductivity of heavy clay is 21 percent lower in comparison to sand, at 30 percent moisture. Similarly, when the soil is changed to light sand at 15 percent moisture, the electricity consumed increases by 4 percent. This is because the thermal conductivity of light sand is 5 percent lower than heavy clay. It is also likely that the performance of light soil could be affected by the lower thermal storage capacity (mass times specific heat) compared with the 15 percent moisture heavy clay soil.

Finally, the air-source system consumes 40 percent more electricity annually than the reference GHE system. It also consumes more electricity than any of the other ground-source configurations.

Figure 47(c) shows the installed cost relative to saved kWh (installed $/kWh saved) compared to the air-source GHE on an annual basis. The lower this cost, the more attractive is the GHE configuration. Based on this criterion, the line configuration with six GHEs is the optimum design for the CZ12 Sacramento for the simulated building load. The performance of this case is shown in detail in the subsequent section. The system saves 25 percent of the electricity that an air-source system consumes. In contrast, the 16-inch GHE has the highest cost per annual kWh saved.

Figure 48 shows the annual electricity consumed (kWh) in heating and cooling season for the optimal six GHE configuration in CZ12 Sacramento. It can be seen that there is a slight decrease (11 kWh) in the heating electricity consumed from year 1 to year 5. In contrast, the

cooling electricity slightly increases by 9 kWh from year 1 to year 5. The electricity consumed by the air-source system is also shown. The air-source heat pump consumes more electricity in cooling and heating season compared to the optimal GHE configuration.

Figure 48: Climate Zone 12 Annual Heating and Cooling Season Electricity Consumption

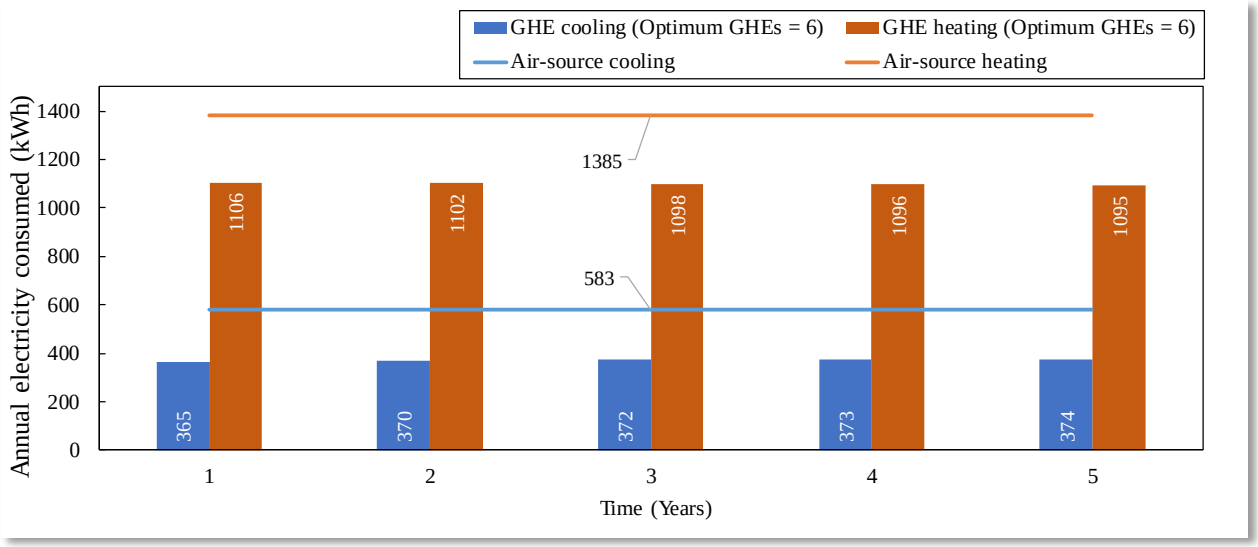

Optimum case for CZ12 Sacramento, number of GHEs = 6; rest of parameters are at baseline values in Table 14. Air-source annual electricity is shown for reference.

Source: University of California, Davis

Results from the parametric simulations for CZ10 Riverside are shown in Figure 49. Figure 49 (a) shows the total installation costs for different GHE systems in CZ10 Riverside. Whereas the cost of one GHE for each design (for example, for a given diameter and height) does not change based on climate, the reduced cost of installation for CZ10 Riverside relative to CZ12 Sacramento is due to the lower number of GHEs needed for this climate zone. Figure 49(b) shows the five-year average annual electricity consumed for each system (including the air-source heat pump). Figure 49(c) shows the installed cost ($) per kWh saved annually.

Figure 49(a) shows that increasing the number of GHEs to seven increases the total cost by 40 percent. Furthermore, using three GHEs decreases the cost by 40 percent. As listed in Table 14, for the 36-inch-diameter case, there are only three GHEs in place of eight 24-inch-diameter GHEs that were used in the reference case. The overall cost of the system decreases by 19 percent. However, if eight 16-inch-diameter GHEs are used, the total cost increases by 26 percent. Four GHEs are used when the arrangement is changed to grid layout. Therefore, the cost decreases proportionally to the change in the number of GHEs, that is, by 20 percent. As mentioned in the previous section, a single 13-foot GHE is $93 cheaper than the reference 20-foot GHE. However, the total cost of nine 13-foot GHEs is 25 percent higher than the reference case (five 20-foot GHEs).

Figure 49. Results from Parametric Study for CZ 10 (Riverside)

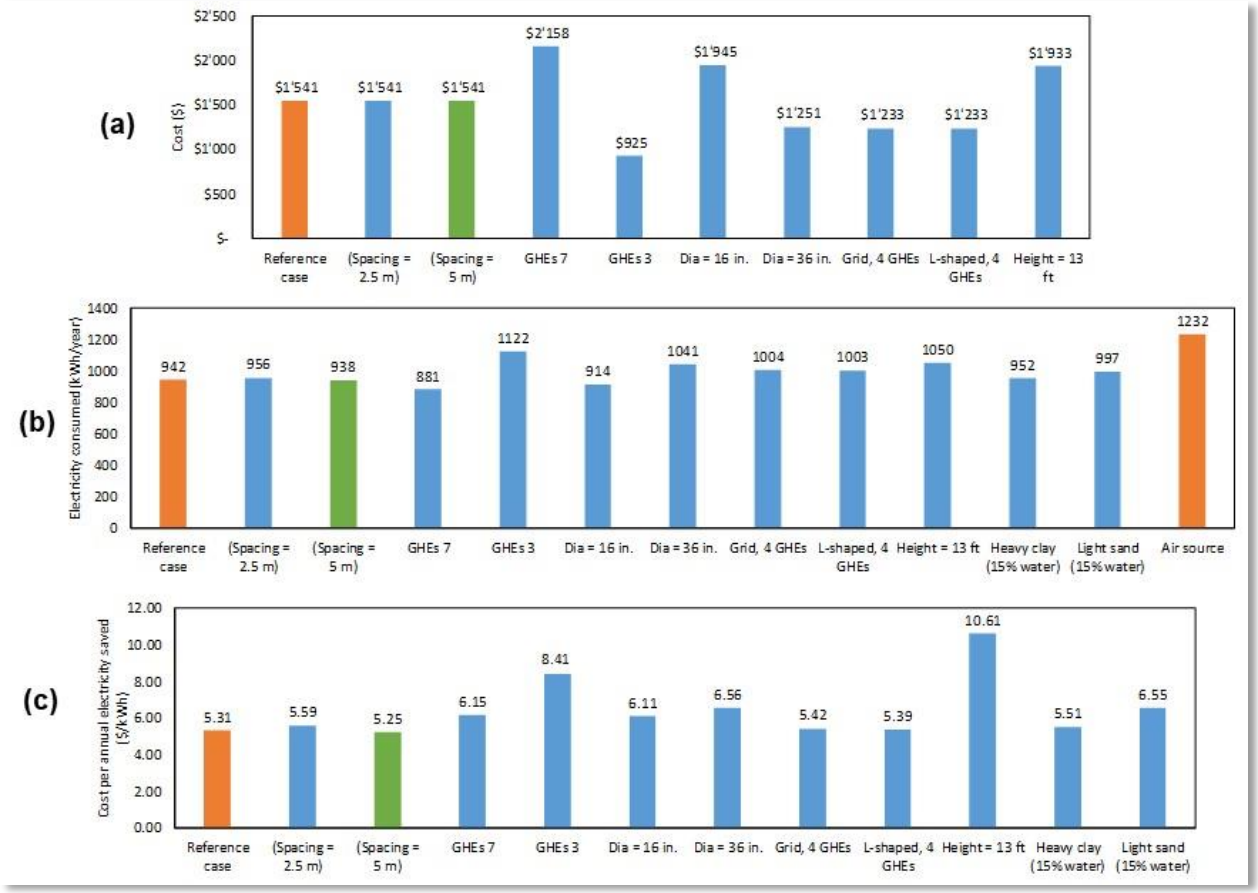

(a) Total installation cost ($) for all configurations (except soil property changes).
(b) Five-year average electricity consumed (kWh/year) for each case. Air-source is also shown for reference.
(c) Cost per annual kWh saved compared to the air-source heat pump.

Source: University of California, Davis

Figure 49(b) shows the five-year average electricity consumed (kWh/year) by all configurations for climate zone 10 (Riverside). The figure shows that decreasing the spacing to 2m increases the electricity consumption by 1.5 percent; whereas, increasing the spacing to 5m has no significant effect on the electricity consumption (it decreases by 0.4 percent). The electricity consumed decreases by 6 percent when seven GHEs are used (instead of the reference case five GHEs). Conversely, using three GHEs significantly increases the electricity consumed, by 19 percent. Using three large-diameter (36-inch) GHEs increases the electricity consumed by 11 percent. However, in contrast to the results for CZ12 Sacramento, in CZ10 Riverside, using eight 16-inch-diameter GHEs decreases the electricity consumed by 6 percent. Changing the arrangement to grid with four GHEs increases the electricity consumed by 6.7 percent. If the same number of GHEs (that is, four) are arranged in the L-shaped arrangement, the electricity consumption is almost identical to that of the grid arrangement (it decreases by 1 kWh/year in comparison to grid arrangement). Using 13-foot GHEs significantly increases the electricity consumption (by 11 percent). Similar to CZ12 Sacramento, in the reference case for CZ10 Riverside, the soil is heavy clay at 15 percent moisture with sand at 30 percent moisture as the backfill. The electricity consumed increases by 1 percent when the soil and backfill both are composed of heavy clay at 15 percent moisture. There is an even more

significant increase in the electricity consumption (5.8 percent) when the soil is changed to light sand at 15 percent moisture.

Finally, the air-source system consumes 31 percent more electricity than the reference GHE system. It also consumes more electricity than any of the other ground-source configurations.

Figure 49(c) shows that using a spacing of 5m between the GHEs is the optimum design for CZ10 Riverside. The performance of this case is shown in detail in the subsequent section. The system saves 24 percent of the electricity that an air-source system consumes. However, it should be noted that this design saves only 4 kWh/year more than the reference case, in which the spacing is 3.5m. In contrast, the 13-foot GHE has the highest cost per annual kWh saved.

Figure 50 shows the annual electricity consumed (kWh) in heating and cooling season for the GHE case with a spacing of 5m. It can be seen that there is a slight decrease (9 kWh) in the heating electricity consumed from year 1 to year 5. In contrast, the cooling electricity consumption slightly increases by 16 kWh from year 1 to year 5. The electricity consumed by the air-source system is also shown. The air-source heat pump consumes more electricity in both cooling and heating season.

Figure 50: Climate Zone 10 Annual Heating and Cooling Season Electricity Consumption

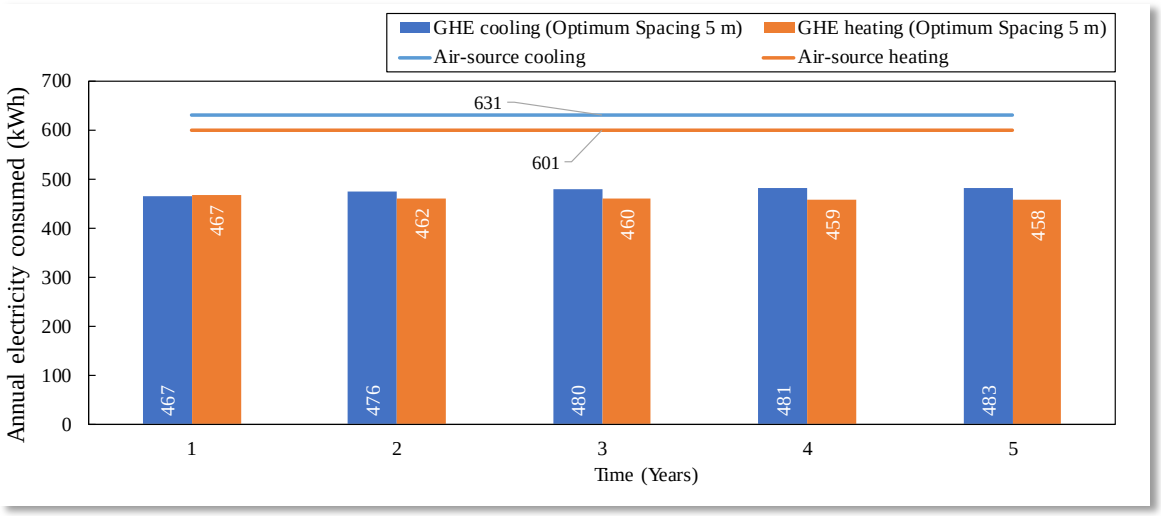

Optimum GHE case for CZ10 Riverside with spacing of 5m; rest of parameters are at baseline values in Table 14. Air-source annual electricity also shown for reference.

Source: University of California, Davis

The analysis of the two valley climate zones indicates that there is a larger benefit to installing GHE systems in regions where the electricity use is larger. While the cooling load of the building is relatively similar in CZ12 Sacramento and CZ10 Riverside, the heating load (winter) is about 2.3 times larger in CZ12 Sacramento. Despite the lower number of GHEs needed in CZ10 Riverside, the installed cost per kWh saved is greater in CZ 12 compared to CZ 10.

CHAPTER 4: Technology/Knowledge/Market Transfer Activities

The research team conducted stakeholder outreach throughout the project to disseminate project results. One outreach activity is a poster presentation on the project that the Western Cooling Efficiency Center includes in tours of its facility for visitors from throughout the world. As a result, the work, and the potential for LDSB technology reaches a broader audience than the one that would necessarily seek research related to ground-source heat pumps.

The research team produced several papers, including:

- "A revised capacitance and resistance model for large diameter shallow bore ground heat exchanger", Applied Thermal Engineering vol. 162 (2019)
- "Modeling and Parametric Study of Large Diameter Shallow Bore Helical Ground Heat Exchanger", ASHRAE Conference presentation (2019)
- "Field Tests of Large Diameter Shallow Bore Helical Ground Heat Exchanger with Simulated Heating Loads", ASHRAE Conference presentation (2020)

ASHRAE is the largest heating, ventilation, and air conditioning-related society in the world. ASHRAE and its members focus on building systems, energy efficiency, indoor air quality, refrigeration, and sustainability in buildings. The conference papers for ASHRAE exposed many experts to the work performed in this project.

Antash Najib, the graduate student researcher on this project, received multiple awards for his work, including the College of Fellows award from ASHRAE and the Kirk T. Mescher Award.

The project team also worked closely with Integrated Comfort Inc. (ICI), a manufacturer of the LDSB heat exchanger technology that provided detailed cost information used in the parametric analysis, to develop the design and installation guide found in APPENDIX C: Design and Installation Guide. ICI plans to use the modeling results from this project to market the technology in California.

Another impediment to technologies making a significant impact in the California housing market is whether they can be accurately simulated in the California code compliance software. EnergyPlus is used as the simulation engine for commercial buildings but residential building rely on the California Simulation Engine (CSE) through CBECC-Res. According to the 2019 Residential Alternative Calculation Method (ACM) Reference Manual, ground-source heat pumps are currently simulated as a minimum efficiency split-system equivalent to the standard design. This clearly does not capture the efficiency improvement potential of ground-source heat pumps and does not allow for designers to qualify for incentives for installing the technology. Discussions with the California Building Standards Office highlighted that future versions of the ACM will include improved performance maps which might accommodate ground-source heat pumps. A similar approach could be applied as used for variable capacity heat pumps (VCHPs) or "mini-splits" wherein a percentage improvement over minimum standard efficiencies could be used. Designs would have to meet specific eligibility criteria for

ground heat exchanger design. The problem with this method is that there is a much wider variation in ground-source heat pump performance than for VCHPs (COPs range from 3.1 to 5.6 and EERs from 13.8 to 42). The efficiency adjustments could be developed using the modeling approaches developed in this project along with a heat pump model, or EnergyPlus simulations.

CHAPTER 5:
Conclusions and Recommendations

Ground-source heat pumps have the potential to reduce heating and cooling energy use in California. Results from this project show significant energy reduction when using the LDSB-GSHP system compared to a standard air-source heat pump. Heating and cooling energy use was reduced in all California climate zones except climate zone 15. In many cases the LDSB-GSHP system reduced HVAC energy costs by more than $100 each year. Ground-source heat pump systems are less prone to large fluctuations in energy use due to the relatively stable ground temperature. This reduces overall peak power draw and flattens the energy use profile of the heat pump throughout the day and season.

Market adoption of these systems has been slow in California largely due to the lack of available tools for modeling performance and for developing system sizing parameters, as well as first cost and relatively long payback period. This project developed modeling tools specifically for the LDSB ground heat exchanger. The models were validated against data from both existing installations of LDSB-GSHP systems as well as laboratory testing of the LDSB heat exchanger. The numerical model developed was used to generate response factors (g-functions) that were ultimately incorporated into an EnergyPlus model for simulating energy performance in a prototype home. Incorporating these modeling tools into compliance software would be one way to reduce barriers to adoption by providing incentives for the LDSB-GSHP systems.

Using the CaRM-He model, parametric simulations were performed to assess the effect on heating and cooling energy use when varying design conditions including number of GHEs, soil thermal properties, bore hole arrangement including spacing and configuration, and cost. The simulations were performed in three California climate zones using building loads generated from CBECC-Res (2013) which is the compliance software used by the California Building Energy Efficiency Standards. The analysis of two valley climate zones indicated that the ground-source system outperformed the air-source system in all configurations tested. The parametric analysis found the optimal bore design based on installation cost and energy performance. Using the results, the research team was able to calculate the cost per kWh of electricity saved ($/kWh) as $4.35/kWh and $3.72/kWh for climate zones 10 and 12, respectively. This metric describes the trade-off between different bore field designs and system efficiency (e.g., more bores provide better efficiency but at a higher installations cost.) This metric also allows the GSHP technology to be compared to other technologies such as photovoltaic system to determine the better investment.

To evaluate the benefits to California ratepayers, the research team performed an analysis using EnergyPlus. The analysis considered the effect of using the large-diameter shallow bore GSHP on heating and cooling energy end uses for a prototypical single-family home located in each of the 16 California climate zones. Simulations of the technology show the reduction in energy use is significant for many California climate zones — roughly 20 percent heating and cooling energy savings for many climate zones and up to 27 percent in certain regions. Based

on a general cost of $0.20/kWh, annual cost savings for California ratepayers would be more than $100 for 9 of the 16 climate zones and more than $300 for climate zone 16.

In summary, LDSB-GSHPs have the potential to save money for California ratepayers and reduce the state's heating and cooling energy use, moving California closer to its long-term energy goals.

CHAPTER 6:
Benefits to Ratepayers

A comparison of total HVAC energy use between the air-source heat pump and the LDSB-GSHP showed lower energy consumption for the LDSB-GSHP in all climate zones except one. Specifically, simulations showed significant heating and cooling energy savings of roughly 20 percent in many California climate zones and up to 27 percent savings in certain other regions. Based on a general cost of $0.20 per kilowatt-hour, the energy savings translate to actual annual cost savings for California ratepayers of more than $100 for 9 of the 16 climate zones and more than $300 for residents of climate zone 16.

The GSHP systems also offer significant peak power draw reductions. The GSHP system uses significantly less power during very hot days. When outdoor temperatures approached 100°F (38°C), the GSHP system used nearly half the power of the ASHP system, due to the much lower heat rejection temperature of the GSHP system of 68°F (20°C). Reducing peak power draw decreases the strain on the electric grid and provides more stable and cost-efficient electric service, while also decreasing greenhouse gas emissions, providing cleaner air, and moving California closer to its long-term, statewide energy goals. APPENDIX D: Additional Advantages of GSHP Systems lists other advantages of GSHP systems not considered in this report, expressed by Dick Bourne. The implications of these advantages were not evaluated.

Analyzing Ratepayer Benefits

To evaluate the benefits to California ratepayers, the research team used EnergyPlus to perform an analysis that considered the effect of using the LDSB-GSHPs on heating and cooling energy end uses for a prototypical detached single-family home located in various locations representative of California climate zones. APPENDIX E: LDSB-GSHP Integration User Guide for EnergyPlus discusses in detail how the research team used EnergyPlus Because occupant behavior varies significantly from home to home, the research team developed an annual set of hypothetical daily load profiles for lights, equipment, and miscellaneous electric loads to simulate energy use for a typical home.

The total HVAC energy use was compared between the air-source heat pump and the LDSB-GSHP (Figure 51). The results show lower energy consumption for the LDSB-GSHP system in all climate zones except climate zone 15, which is the hottest climate zone with the largest cooling loads and minimal heating loads. This unbalanced load results in poorer performance for the LDSB-GSHP system. The climate zone with the largest savings was climate zone 16. While this climate zone is also unbalanced with much higher heating loads than cooling loads, the very low ambient temperatures result in poor performance from the air-source system. The LDSB-GSHP system does not experience the same temperature extremes when exchanging heat with the ground.

Figure 51: Annual Combined Heating and Cooling Energy Consumption for Both Baseline (ASHP) and Shallow GSHP Systems for All California Locations

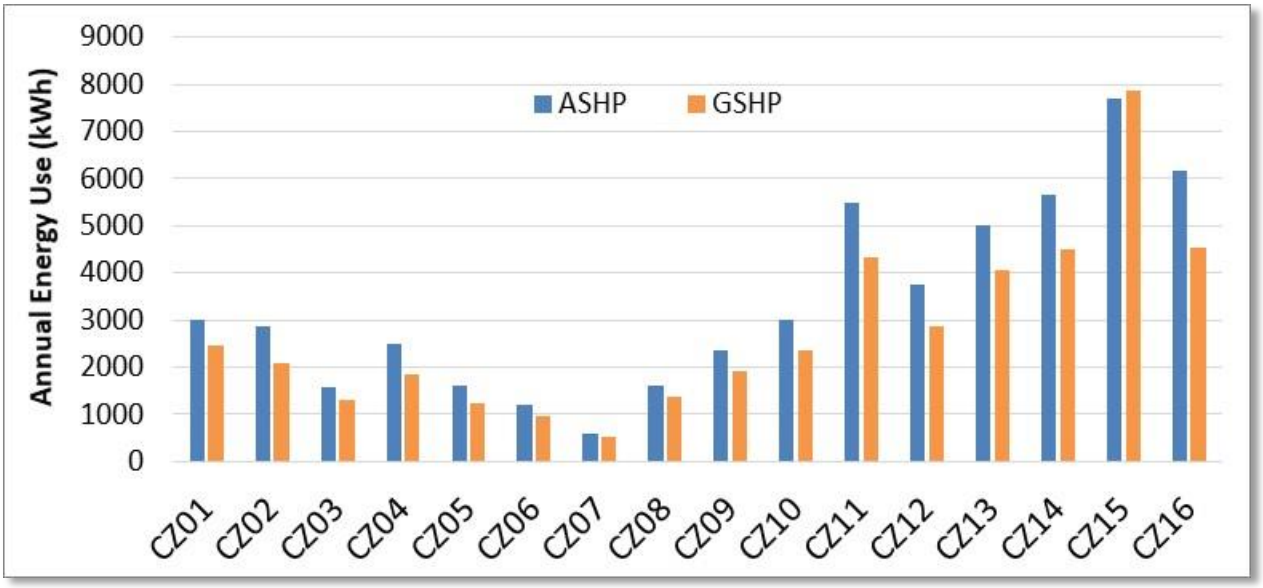

Source: University of California, Davis

LIST OF ACRONYMS

Term	Definition
ACM	alternative calculation method
CaRM	Capacitance and Resistance Model
CEC	California Energy Commission
CFD	computational fluid dynamics
Cfm	Cubic feet per minute
COP	coefficient of performance
CZ	climate zone
EER	energy efficiency ratio
EPIC	Electric Program Investment Charge
GHE	ground heat exchanger
gpm	Gallons per minute
GSHP	ground-source heat pump
HDPE	high density polyethylene
HSH	Honda Smart Home
HSPF	heating seasonal performance factor
HVAC	heating, ventilation, and air conditioning
LDSB	large diameter shallow bore
m	meter
RMSD	root mean square deviations
SEER	seasonal energy efficiency rating
W	watts
WCEC	Western Cooling Efficiency Center

REFERENCES

California Energy Commission, Geothermal Heat Pump and Ground Loop Technologies. Staff Paper. Building Standards Office Efficiency Division. 2014.

Davis Energy Group. Ground-Coupled Heat Pump Technology Assessment. PG&E Zero Net Energy Program, 2010.

de Vries, D.A., and W.R. Wijk. Thermal Properties of Soils. Physics of Plant Environment, Amsterdam, North Holland Publishing Company, 1966.

Eskilson, P., and J. Claesson, Simulation model for thermally interacting heat extraction bore holes, *Numerical Heat Transfer,* no. 13, pp. 149-165, 1988.

Hart, D.P., and R. Couvillion. Earth-Coupled Heat Transfer. National Water Well Association, Dublin, OH. 1986

Incropera, F.P., A.S. Lavine, T.L. Bergman, and D.P. Dewitt. Fundamentals of Heat and Mass Transfer, 7th Edition, Jefferson City: John Wiley & Sons, 2011.

KEMA, Inc. 2010. 2009 California Residential Appliance Saturation Study. California Energy Commission. Publication Number: CEC-200-2010-004

Kusuda, T., and P.R. Achenback. Earth temperatures and thermal diffusivity, ASHRAE Trans, vol. 1, no. 71, p. 61–74, 1965.

Najib A., A. Zarrella, V. Narayanan, P. Grant, C. Harrington, and R. Larson. Modeling and Parametric Study of Large Diameter Shallow Bore Helical Ground Source Heat Exchanger. American Society of Heating, Refrigerating and Air-Conditioning Engineers, Winter Conference 2019, Atlanta.

Najib A., A. Zarrella, V. Narayanan, P. Grant, and C. Harrington. A revised capacitance resistance model for large diameter shallow bore ground heat exchanger. Applied Thermal Engineering, no. 162, 2019.

O'Green, T. National Cooperative Soil Survey data. Soil Web, https://casoilresource.lawr.ucdavis.edu/gmap/. [Accessed 01 January 2018].

Typical Engineering Properties of High Density Polyethylene. INEOS Olefins & Polymers USA (www.ineos-op.com), League City, Texas, 2017.

Wierenga, P.J., D.R. Nielsen, and R.M. Hagan. Thermal Properties of a Soil Based Upon Field and Laboratory Measurements. Soil Science Society of America Journal, vol. 3, n. 33, p. 354, 1969. doi:10.2136/sssaj1969.03615995003300030009x

Xiong, Z., D.E. Fisher, and J.D. Spitler, Development and validation of a Slinky ground heat exchanger, Applied Energy, no. 141, pp. 57-69, 2015.

Yavuzturk, C., and J.D. Spitler, A Short Time Step Response Factor Model for Vertical. ASHRAE Transactions 1999;105(2):475-485.

Zarrella, A., M. De Carli, M. Tonon, and R. Zecchin. A computational capacity resistance model (CaRM) for vertical ground-coupled heat exchangers. Renewable Energy 2009; 1537–1550. https://doi.org/10.1016/j.renene.2009.11.034

Zarrella, A., and M. De Carli, Heat transfer analysis of short helical bore hole heat exchangers. Applied Energy 2013; 102:1477–1491. https://doi.org/10.1016/j.apenergy.2012.09.012

APPENDIX A:
Excerpts from California Energy Commission Documents and Other References

Since California's residential standards require SEER and HSPF as the descriptors for heat pump performance, the Energy Commission has had an interim methodology in place for many years which assigns equivalent SEER and HSPF ratings based on equipment EER and COP ratings, respectively. The interim methodology specifies that the SEER rating for a GHP system is equal to the ARI-330 77°F EER rating, and that the HSPF is calculated from the ARI-330 32°F COP, based on the following relationship: HSPF = 3.2 x COP – 2.4"

Note: Using this method the minimum HSPF would be 7.5 and minimum SEER would be 13.4. The current federal minimum efficiency for heat pumps is 8.2 HSPF and SEER is 14.0.

CEC-500-2014-060: *Assessment of California's Low Temperature Geothermal Resources (2012)*
This study used a variety of models to reach the following conclusions.

"The low temperature [geothermal] resource…has remained inadequately characterized and developed, especially the technology that can be used for heating and cooling homes."

"The results [of modeling] showed that significant reductions in energy and natural gas demand and emissions would occur with geothermal heat pumps in 15 of the 16 climate zones. The energy use savings and emissions reductions (between about 20 and 70 percent) indicated that deploying these highly efficient systems could dramatically reduce energy consumption and atmospheric emissions statewide."

CEC-400-2014-019*: Geothermal Heat Pump and Ground Loop Technologies (2014)*
"The first barrier discussed concerns system modeling to show compliance with the *California Building Energy Efficiency Standards* modeling compliance. These standards require modeling of most buildings to demonstrate compliance tradeoffs allowed within the standards. Both the building industry and Energy Commission staff generally agree that these models do not accurately represent the efficiency of geothermal heat pump systems. This inaccurate representation presents a barrier to the industry because the model does not sufficiently estimate GHP energy consumption to allow for direct comparison to the energy consumption of conventional heating, ventilation, and air conditioning systems."

"To date, many in the GHP industry have successfully adapted the Energy Commission-approved compliance models for GHP. However, developing an ACM could greatly improve the accuracy for modeling this technology. For example, an ACM could standardize and improve current calculation methods to include soil water/moisture migration — the largest heat transfer mechanism — soil diffusivity, precipitation, known aquifer data, and other water sources. Also, an ACM could potentially be developed to include the combination of providing both domestic hot water and space conditioning, another aspect of GHPs that are currently not well captured.

"…industry representatives suggest that industry, utilities, and the Energy Commission need to come together to swiftly make corrections or provide new rules sets to the *Building Energy Efficiency Standards*."

PG&E GeoExchange Project report*: Title 24 Options for Ground-Coupled Heat Pumps (1999)*

"Closed-loop GHPs, which represent the majority of systems being installed in California, are typically rated according to ARI-330 which specifies ground loop return water conditions of 32°F and 77°F for heating and cooling mode operation, respectively. For typical California residential conditions, the ARI-330 return water assumptions are too low, with more typical return water temperatures of 45-50°F for heating and 90-100°F for cooling.

Other Regulatory Requirements

The Department of Water Resources published Draft Standards for Geothermal Heat Exchange Wells in 1999. These standards have not advanced past the "draft" designation since they were originally published, yet they have been adopted by some jurisdictions. The following was excerpted from a February 2016 analysis of SB 995 (Pavley):

> "In 1996, the Legislature passed and the Governor signed AB 2334 Chapter 581, Statutes of 1996), which requires DWR to develop and submit to the Water Board a report containing recommended standards for GHEWs [ground heat exchange wells]. DWR issued a Draft of standards for GHEWs in 1999, with the goal of creating one bulletin (Bulletin 74-99) to cover all four types of wells (water wells, monitoring wells, cathodic protection wells and geothermal heat exchange wells). However, due to delays, Bulletin 74-99 was never formalized and the GHEW standards remain as a Draft."

The DWR website announced webinars held on June 20th and 25th, 2019 to solicit input on Bulletin 74. As of March 2020, the only document posted on the DWR website is the un-edited 1999 draft.

The standard excludes shallow systems, defined in Part I, Section 1.B.2.a as "any heat exchange system having an excavation whose bottom does not exceed a depth of 20 feet from ground surface" from the requirements of Parts II and III. Part II includes requirements for grouting, sealing, thermal fusing of piping, limitations on fluid type, and pressure testing. Part III covers procedures for destroying (abandoning) existing GHEs.

Part I of the standard requires conformance with Sections 13750.5 and 13751 of the California Water Code. Section 13750.5 requires that the driller possess a C-57 Water Well Contractors License. Section 13751 requires the contractor or driller to file a report with the department within 60 days of completion that includes:

A. A description of the well site and location.
B. A description of the bore hole diameter and depth and type of geothermal heat exchange system installed.
C. The methods and materials used to seal off surface or contaminated waters.
D. The methods used for preventing contaminated water in one aquifer from mixing with the water in another aquifer.
E. The signature of the well driller.

The primary barriers imposed by the standard for large-diameter shallow bore systems are:

- Excavators who use augers to bore shallow holes typically do not drill water wells and do not possess a C-57 license.
- The cost of reporting and challenges of meeting reporting requirements C and D.

The advantage of large-diameter, shallow bore GHE systems is that they avoid many of the costly requirements imposed by the DWR standard on deep bore systems.

APPENDIX B:
Detailed Equations

$$g\left(\frac{t}{t_s},\ \frac{r_b}{H}\right) = 2\pi k\left(\frac{T_b - T_g}{Q'}\right)$$

Equation 1

$$t_s = \frac{H^2}{9\alpha}$$

Equation 2

where:

T_b	mean bore wall temperature	(°C)
T_g	undisturbed ground temperature	(°C)
Q′	heat transferred per unit length of GHE	(W m^{-1})
r_b	radius of the bore hole	(m)
k	soil thermal conductivity	(W m^{-1} K^{-1})
g	g-function	(dimensionless)
t	time	(s)
t_s	time to reach steady state	(s)
H	height (or depth) of the GHE	(m)
α	soil thermal diffusivity = $\frac{k}{\rho C}$	(m^2 s^{-1})
ρ	soil density	(kg m^{-3})
C	soil specific heat capacity	(J kg^{-1} K^{-1})

$$\left(\frac{t}{t_s},\ \frac{r_b}{H}\right) = 2\pi k\left\{\frac{T_b - (R'_{total}Q') - T_g}{Q'}\right\}$$

Equation 3

$$R'_{total} = R'_{convection} + R'_{pipe\ conduction} + R'_{pipe-borewall\ conduction}$$

Equation 4

$$g\left(\frac{t}{t_s},\ \frac{r_b}{H}\right) = 2\pi k\left(\frac{T_{mf} - T_g}{Q'}\right)$$

Equation 5

$$T_{mf} = \frac{T_{in} + T_{out}}{2}$$

Equation 6

$$T_{tw}(t_n) = T_{ug}(d_m, t_n) + \sum_{i=1}^{n} \frac{(Q'_i - Q'_{i-1})}{2\pi k} g(t_n - t_{i-1})$$

Equation 7

where:

T_{tw} tube wall temperature

T_{ug} undisturbed ground temperature which includes impact of surface condition

t_n time interval for n^{th} time step

i arbitrary index

d_m GHE's average buried depth

$$T(\mathrm{z,t}) = \mathrm{T_m} + A_T . exp\left(-z.\sqrt{\frac{\pi}{t.\alpha}}\right).\cos\left[\frac{2\pi}{t_y}.\left(t - t_{shift} - \frac{z}{2}.\sqrt{\frac{t_y}{\pi.\alpha}}\right)\right]$$

Equation 8

where:

T_m the annual average air temperature (°C)

A_T the annual amplitude of the average air temperature cycle (°C)

t_y seconds in 1 year = 31,536,000 s

t_m seconds in 30 days = 2,592,000 s

z depth (m)

t_{shift}: time to account for the date of minimum surface temperature (s)

Equation 9

where

g combined g-function for GHEs of different boundary conditions

g1 g-function for GHE with boundary condition 1 (3 sides isothermal, 1 side adiabatic)

g2b g-function for GHE with boundary condition 2b (2 sides isothermal, 2 sides adiabatic)

x1 number fraction of GHEs of type 1 relative to total number of GHEs

x2b number fraction of GHEs of type 2b relative to total number of GHEs

Table B-1: Example of Site-Specific Data Required for Simulationx

System specific inputs	
Heat carrier fluid in the ground loop:	
Fluid type:	Water-Propylene Glycol
Mass fraction of antifreeze (%)	15%
Average temperature of the fluid	59°F (15°C)
Mass flow rate of the heat carrier fluid [kg/s] for one GHE:	0.05
Zone depths	
Depth of the head of the GHE [m]:	1
Depth of the model below the end of the GHE [m]:	20
Length of the GHE [m]	5.71
Inner pipe (1) diameters and conductivity:	Same as helical pipe
Helical pipe (2):	
Inside Diameter of pipe [mm]:	17.3
Outside Diameter of pipe [mm]:	22.2
Thermal conductivity of pipe [W/ (m K)]:	0.47
Bore hole diameter [m]:	0.9144
Inlet pipe (Helical or inner pipe)	Inner pipe (common practice to avoid vapor lock)
Pipe length [m]:	67.9 (for 22 ft depth)
Pitch between rings [m]:	0.2286
Outside helix diameter [m]:	0.8858
GHE field configuration	Multiple 6: 1 of each BC type
For each time step	
Heat load [W]	100
Condition (GHE On or OFF)	On throughout
Weather inputs	
Annual mean air temperature	59°F (15°C)
Annual semi-amplitude	0°F (0°C)
Time delay [days]:	0
Specific surface convective thermal resistance (m^2 K/W):	0.121
Absorptance coefficient	0
Emissivity	0
Input for each time step	
Global horizontal radiation [W/m^2]	0
T sky	59°F (15°C)
T air	59°F (15°C)

Thermal conductivity [W/ (m K)]:	1.56
Specific heat [J/ (kg K)]:	1559
Density [kg/m3]:	1239
Grouting material properties and ground layer above, below and GHE surrounding all are same as those given above	

Source: University of California, Davis

APPENDIX C:
Design and Installation Guide

LDSB ground heat exchange loops offer a more economical ground-coupled heat pump option compared to traditional deep-bore systems. LDSBs have proven to be effective in monitored projects since 2013. Like all ground loop systems, they must be sized large enough that late-season penalties for the gradually changing surrounding ground temperatures do not compromise annual performance in comparison with air-coupled heat pump systems. This Guide provides key advice on appropriate LDSB sizing for a range of California climates and typical soil types. It also conveys a preferred installation sequence, backfill process, and manifolding approach to join the multiple parallel shallow bores.

These recommendations were provided by a manufacturer for the LDSB heat exchangers and verified in two cases by the parametric simulations using the CaRM model. It should be noted that the parametric simulations were based on CBECC-Res 2013 load profiles and these recommendations are valid for similar load profiles in each climate zone. Ground temperature saturation and GHE performance depends on the total load exchanged with the ground. While equipment sizing may be the same for two building load profiles, if one profile has significantly more cooling our heating loads then a larger number of bores would be needed for that building to achieve similar performance.

Design Guide

Based on advice from a potential helix manufacturer, this Guide considers the following two LDSB configurations, each using a 24" diameter augured hole:

1. 22' deep hole, 20' helix with 2' earth cover on top, made from ¾" (nominal) high density polyethylene (HDPE) tube
2. 15' deep hole, 13' helix with 2' earth cover on top, made from 1/2" (nominal) HDPE tube

The second, shallower configuration requires more bore holes per ton than the first, and thus requires more land area. However, where adequate area is available, shallower may have economic advantages for the following reasons:

1. Faster boring: Available large-bore excavators drill, grab a bite of earth, bring it out, dump it, and go back for more. Each successive "bite" takes longer, so deeper is a bit more expensive to excavate. (On the other hand, fewer holes means fewer moves to set up for the next hole, so the total time equation bears further study.)
2. Smaller tube size: When the 22' and 15' options have equal tubing surface area in the ground, the thinner wall of the ½" tubing in the 15' holes means better heat exchange and lower tubing cost.

Key design recommendations are as follows:

1. Number of Bore holes: Select the appropriate bore hole quantity per ton vs. climate and surrounding soil condition using Table C-1, found below, for 22' deep holes. Multiply the appropriate tabulated value by the system capacity in tons, and round up if necessary, to the next integer to determine the total number of bore holes.

2. Bore hole Layout: Arrange the bore holes in a straight line whenever possible, to access the largest possible volume of surrounding earth. In suburban settings, placing the holes on or along a fence line is advantageous. Upsize the bore hole quantity by 10% (as tabulated) when holes are arranged in a grid pattern.
3. Bore hole Spacing: Provide minimum spacing of 8' between bore holes. Increased spacing between bores can improve performance if land area is available but the parametric results did not show that to have a significant impact.
4. Irrigation and Ground Moisture: Table C-1 and Table C-2 assume that moisture level within the 24" bore hole diameter is kept at a minimum of 15%. This can be accomplished without significantly increasing water use either by distributing all of a home's gray water (preferably by pumping, to assure distribution to all holes) into the bore field, or by installing each LDSB in a full-height, sealed 28" diameter polyethylene bag, with occasional water addition from a supply water source (summer) and/or a rainwater collection source (winter). If no irrigation is provided, upsize the bore hole quantity by 25% (as tabulated).

Table C-1: Installation Guide for Bore Field Sizing Bore Hole Quantity per Ton for 15' Deep Holes

Type	Field Characteristics	CZ 1,3,4,5,6,7	CZ 2,8,9,10	CZ 11,12,13	CZ 14,15,16
1	Basic Sizing, Line Pattern	2.6	3.3	4.0	5.0
2	Basic w/o Irrigation	3.1	4.1	5.0	6.3
3	Type 1, Grid Pattern	2.7	3.6	4.4	5.5
4	Type 2, Grid Pattern	3.4	4.5	5.5	6.9

Source: University of California, Davis

Table C-2: Installation Guide for Bore Field Sizing Bore Hole Quantity per Ton for 22' Deep Holes

Type	Field Characteristics	CZ 1,3,4,5,6,7	CZ 2,8,9,10	CZ 11,12,13	CZ 14,15,16
1	Basic Sizing, Line Pattern	1.7	2.1	2.5	3.1
2	Basic w/o Irrigation	2.1	2.6	3.1	3.9
3	Type 1, Grid Pattern	1.9	2.3	2.8	3.4
4	Type 2, Grid Pattern	2.3	2.8	3.4	4.3

Source: University of California, Davis

1. Manifolds: Connect the bore hole field to the home or building, and interconnect the bore holes, using HDPE tubing buried at least 18" below ground. Manifold connections should be made with approved non-corrodible metallic connectors. Size manifold piping in accordance with Table C-3 below. From center "T", manifold size may be reduced based on tons of bore holes outboard. Either separate the supply and return lines by a minimum of 6" or insulate the return line from the ground to the heat pump. "Reverse return" piping will slightly improve system performance but is not required. Water from

the heat pump should enter the bottom of the helix and spiral upward before returning to the heat pump. This configuration provides preferred heat transfer and facilitates air removal when the system is being filled. It is desirable but not required to provide accessible valving to each bore hole for filling and purging the system. The installation guidelines below assume that individual bore hole valving is not provided.

Table C-3: Manifold Maximum One-Way Length in Feet vs. Connecting Pipe Size System Size, Tons

Nominal Pipe Size	**2**	**2.5**	**3**	**4**	**5**	**6**
1"	56	38	29	17	12	8
1.25"	200	133	105	59	42	29
1.5"	417	286	208	125	87	63
Note: Based on 2.5 gpm/ton flow and maximum manifold pressure drop of 2' water head.						

Source: University of California, Davis

Installation Guide

Well-planned, careful installation of the LDSB system is necessary for reliable performance. This Guide assumes that the helix manufacturer(s) delivers a product designed for installation in accordance with the sequence below, and that maintains proper spacing between tubes in the helical pattern during and after backfill. Sequential installation steps for the bore hole field are:

1. Soil Test: Verify the soil type by either a) hiring a contractor to sample to at least two-thirds of the selected bore hole depth, or b) relying on prior sampling taken within reasonable proximity of the bore hole site.
2. Layout: Based on the number of bore holes determined from the Design Guide above, lay out the bore hole field, preferably such that the midpoint of the field (which hopefully forms a straight line) facilitates the shortest possible path for manifold piping to connect to the heat pump location. Use a ground market system to draw target marks at the centers of the bore holes.
3. Assemble the helical ground heat exchangers: The pre-coiled helical ground exchangers arrive tightly packed, with circumferentially-opposed markings that designate their connection points to their two vertical support/connection tubes fabricated from slotted 1” PVC pipes. Using the assembly jig supplied by the helix manufacturer, follow its assembly instructions to snap each marked location on the helix into its receiving slot on a PVC support pipe. After all tubes are snapped into place, insert the spreader bars that “ovalize” the cross-section and help prevent tubes from popping out of the slots during handling and backfill. Clip the bottom (inlet) “tail pipe” to the spreader bars so it exits through the top end of the helix, near the outlet pipe.
4. Drill Holes: Employ a ground-auger to drill the 24” holes to desired depth. Place the spoils (removed cuttings) in a location that does not interfere with drilling other holes, and that facilitates later removal to a permanent location. Enough spoils can remain to fill the top 2’ of the bore holes. Verify that at least the specified depth is achieved.

5. Place and Fill Heat Exchangers: Carefully slide each semi-rigid coil assembly into its bore hole, bottom end first. The bottom spreader bar will rest on the bottom of the excavated hole. Secure the two pre-marked (inlet, outlet) piping tails against one side of the bore hole, with their ends taped closed and projecting above ground.
6. Backfill: Place a sturdy, hopper-style backfill screen with maximum 2" openings over the hole, positioned to hold the piping tails safely away from possible damage. Deliver clean, (hopefully dry) fill sand through the screen and into the bore hole. Spray water onto the screen and into the hole if/as necessary to expedite the backfill process. Continue until the top coil of the helix is covered. Remove the screen, level the top of the sand, coil the two tails in the hole, and place a protective round disc horizontally in the hole atop the tails.
7. Excavate Trenches: Use a narrow backhoe bucket or chain trencher to dig manifold trenches approximately 21" deep. The trenches should interconnect all bore holes and provide a path to the indoor heat pump location.
8. Place and Connect Manifolds: Install continuous manifold piping in the trenches to connect from the heat pump location to the nearest bore hole. Use "T" connectors to join the "from heat pump" manifold to the bottom inlet "tail" at each bore hole, taking care that flow will proceed either horizontally or downward to all holes. Also use "T" connectors to join the "to heat pump" manifold to the top outlet "tail" at each bore hole, taking care that flow will proceed either horizontally or upward from all holes. Take care to separate "to" and "from" pipes in the trenches and insulate the "to heat pump" manifold with ¾" insulation if pipes are less than 4" apart.
9. Pressure Test: At the heat pump end of the two manifolds, cap one connection and through apply a pressurized air source to the other connection. Maintain 80 PSI test pressure for two hours before backfilling trenches. Leave system at pressure for two days after initial test, and
10. Backfill: Use soil removed from the bore holes and trenches to backfill all exposed outdoor piping. Backfill to slightly above original grade to compensate for future settling of the disturbed soil. Remove remainder of bore hole soil to a permanent location.
11. Purge and Fill: Install valving at the heat pump that allows fill and purge while bypassing the heat pump. Use high pressure/high-capacity submersible pump in a portable reservoir of at least 20 gallons to pump the fill liquid (water or propylene glycol anti-freeze) through the ground loop system in the proper flow direction and back into the reservoir. Continue pumping until no air emerges at the return. Then change valve positions to purge the loop circulating pump (not the submersible) and heat pump heat exchanger with the return flow from the ground. Again, proceed until all air is removed. Close valves and establish final loop pressure in the 15-30 PSI range. The ground loop is now ready to operate.

Title 24 Draft Compliance Option

The following discussion considers the compliance option for ground-coupled heat pumps in California Title 24 codes.

Regulatory Requirements for Ground-Coupled Heat Pumps

Ground-Coupled Closed Loop Heat Pump Industry Test Standards

AHRI 330-98, "Standard for Ground Source Closed-Loop Heat Pumps" develops performance at the following standard rating conditions:

Cooling

- Entering indoor air: 80°F (27°C) dry bulb, 67°F (19°C) wet bulb
- Entering fluid temperature: 77°F (25°C)
- Fluid flow rate: As specified by manufacturer

Heating

- Entering indoor air: 70°F (21°C) dry bulb, 60°F (16°C) wet bulb, max
- Entering fluid temperature: 32°F (0°C)
- Fluid flow rate: As specified by manufacturer

Indoor coil airflow rate is based on external resistances that vary from 0.10 to 0.20 inches water column depending on the unit capacity or at a lower airflow if specified by the manufacturer.

The standard also provides for part-load ratings and tests at extreme conditions.

Federal Standards and California Title 20 Requirements

Ground-coupled heat pumps (GCHPs) are not federally regulated. Title 20 Section 1605.3(c)(1) states: "The mandatory efficiencies for ground-source heat pumps are a minimum coefficient of performance (COP) for heating and EER for cooling." It is presumed these standards are based on AHRI 330-1998, copied below.

Table C-4: Ground-Source Heat Pump Standards from AHRI 330-1998

Appliance	Rating Condition	Minimum Standard
Ground water-source heat pumps (cooling)	59°F entering water temperature	16.2 EER
Ground water-source hear pumps (heating)	50°F entering water temperature	3.6 COP
Ground-source heat pumps (cooling)	77°F entering water temperature	13.4 EER
Ground-source heat pumps (heating)	32°F entering water temperature	3.1 COP

Source: __AHRI 330-1998_

The California Modern Appliance Efficiency Database (MAEDBS) lists 6,517 "ground-source" heat pumps with unique model numbers. The coefficient of performance ranges from 3.1 to 5.6 and EERs range from 13.8 to 42.

Title 24 Compliance for Ground-Coupled Heat Pumps

To be accurate, compliance methods should account for the performance of the both the heat pump and how it responds to water temperatures from the ground heat exchanger, and how the soil and return water temperature is affected by the load imposed on the heat exchanger by the heat pump.

Current ACM Methods

Earlier Title 24 compliance methods used an equation to convert the COP at 32°F to HSPF and used the EER at 77°F entering water temperature as a proxy for SEER. Current requirements and modeling assumptions found in the Residential ACM Manual and the CBECC-Res User's Manual are listed below.

- 2019 Residential ACM Reference Manual – Section 2.4.2: "A ground-source heat pump system, which uses the earth as a source of energy for heating and as a heat sink for energy when cooling, is simulated as a minimum efficiency split-system equivalent to the standard design with default duct conditions in place of the proposed system. The mandatory efficiencies for ground-source heat pumps are a minimum coefficient of performance (COP) for heating and EER for cooling." Current minimum federal standards for heat pumps are HSPF 8.2 and SEER 14. AHRI 210/240 evaluates HSPF at 47°F, 35°F, and 17°F (26°C, 19°C, and 9°C); and evaluates SEER at 82°F (28°C)."
- 2016 CBECC-Res User Manual, Chapter 8 (Version 8.2.4): "Ductless mini-split, multi-split, Variable Refrigerant Flow (VRF) and ground source heat pumps—Until an exceptional method is approved, these systems are modeled as equivalent to a standard design system with no penalty and no credit."

  CBECC-Res inputs for GCHPs include COP, heating capacity, EER, and cooling capacity. Standard rating conditions for entering water temperatures are 77°F (25°C) for cooling and 32°F (0°C) for heating. These inputs are not used by the software and are only useful for verifying the equipment meets minimum federal standards. "Standard design" heat pumps have a SEER of 14 and an HSPF of 8.2.

  There are several inaccuracies with modeling air-source and ground-source heat pumps the same way. First, ground-source heat pump performance ratings are used in the compliance model only to verify they meet federal standards, not to develop a performance map. Second, ground-source heat pump performance is a function of ground loop temperature, not outdoor air temperature. There are no edibility criteria to require properly sized ground loops. Third, properly sized ground-source heat pumps do not require resistance heat for backup or defrost cycle operation. The ACM calculation for air-source heat pumps includes energy use for backup resistance heat, and AHRI 210/240 ratings include defrost cycle compressor and resistance heating energy.

Ideal Compliance Modeling Methods

"Designers have been asking the Energy Commission for a method to directly input heat pump coefficient of performance (COP) and EER in approved software since 1997."
—Pat Splitt

Accurate modeling of ground-source heat pumps and ground heat exchanger (GHE) designs would allow the value of these systems to be recognized. Though water temperature is perhaps more critical to determining GCHP performance than air temperature is for air source heat pumps, there have been no efforts to apply rudimentary performance maps such as is current practice for air source equipment (using SEER at 82°F (28°C) and EER at 95°F (35°C)).

Ideally, the compliance model would account for heat pump performance at varying entering water temperatures and include a GHE model that would calculate entering water temperatures on an hourly time step.

The GHE model could use a derivative of the EnergyPlus G-Function method or a simplified version of CaRM to calculate heat pump entering water temperatures based on soil type, ground loop design, and hourly building load. Soil types are provided in several resources, including CEC-500-2014-060. The variety of GHE designs should be constrained and limited by eligibility criteria. The number of required heat exchangers should be prescriptively required based on the greater of the heating or cooling design load and soil type.

Heat pump energy use could be calculated using MAEDBS listed COPs and EERs and modified on an hourly basis using equations that determine performance at non-standard entering water conditions. A generic performance map could be used in lieu of requiring detailed performance information specific to each product.

Proposed Interim Compliance Approach

According to Bruce Wilcox, future versions of the ACM will include improved performance maps which might accommodate GCHPs. A similar approach could be applied as used for variable capacity heat pumps (VCHPs) or "mini-splits" wherein a percentage improvement over minimum standard efficiencies could be used. Designs would have to meet specific eligibility criteria for GHE design. The problem with this method is that there is a much wider variation in GCHP performance than for VCHPs (COPs range from 3.1 to 5.6 and EERs from 13.8 to 42). The efficiency adjustments could be developed using CaRM with a heat pump model, or EnergyPlus simulations.

Pathways for Adding GCHP Rulesets to the ACM

- Codes and Standards Enhancement Reports: On a three-year cycle California utilities sponsor teams (Statewide Utility Codes and Standards Enhancement or CASE teams) to identify, recommend, and support code change proposals. Recommendations are described in CASE reports which document feasibility, energy savings and costs, and market impacts. Following stakeholder input through workshops and docket postings and Commission staff coordination, CASE reports are accepted by the Energy Commission and final language is developed for adoption in a Commission business meeting.
- Exceptional Method Process: The Warren-Alquist Act requires that industry representatives, not the Energy Commission, develop compliance options for technologies not explicitly required in the Building Energy Efficiency Standards. This process includes a review process, development, and verification of new compliance software. California Administrative Code Part 1, Chapter 10, Sections 10-109 and 10-110 provides for applications for approval of compliance software and exceptional methods to be made to the Energy Commission, and for the Commission to approve methods that analyze devices that cannot be adequately modeled using the public domain computer programs. Applications are required to include all information needed to verify the method's accuracy. The Commission is required to determine if the accepted application is complete within 75 days, after which the application will be made available for public review. Within 90 days of receiving a complete application the Executive Director submits a written recommendation which will be placed on the consent calendar for the next business meeting. A fee may be charged to cover processing and review costs. Despite these timelines, it has historically taken more than one year to fully process an application.

- Energy Commission Staff Initiatives: On occasion, Energy Commission staff direct consultants to conduct research on selected topics or technologies to refine compliance methods. For example, extensive research by Energy Commission consultants was completed on mini-split heat pumps. Co-funded by PG&E, this work resulted in the change in compliance methods from using minimum standard federal performance values to improved values which will be applied under the 2019 Title 24, Part 6 Standards.

APPENDIX D:
Additional Advantages of GSHP Systems

Geo-Heat Pumps for California Buildings: Ready for Prime Time

By Dick Bourne, PE

The project summarized in this report is the most valuable effort so far in California to evaluate the potential for geo-exchange systems to help meet the State's "zero-carbon by 2045" goal. 2045 is a scant 25 years away, and many localities have committed to even more aggressive timelines. Geo-heat pumps (GHPs) should become a major solution (and sooner is better) because of the following "coming realities" of the energy playing field for buildings:

1. New buildings will be all-electric; the zero-carbon future virtually disallows combustion of fossil fuels.
2. Most buildings will be heated by heat pumps, which multiply efficiency by extracting heat from the outdoor environment or from waste heat leaving the building.
3. Currently, the most common HVAC heat pumps extract heat from the outdoor air and deliver it to indoor air; hence they are labeled "air-to-air heat pumps" (AHPs).
4. AHPs have congenital performance weaknesses that prevent them from achieving the energy performance of properly designed and installed GHPs.
5. The economics of energy efficiency technologies must consider competition with renewables; a factor that will increasingly favor energy efficient GHPs.

This paper will further develop the last two of these coming realities, adding context both to: a) the choice between AHPs and GHPs, and b) the relationship between energy efficiency and renewables.

Heat Pump Choices

Most California homes already have two air-to-air heat pumps, both used for cooling. First is the refrigerator, which cools (extracts heat from) its freezer and fresh food sections and discharges that heat (plus the heat equivalent of the compressor's electricity use) into the surrounding space- usually the kitchen. So cooking, the refrigerator, and active cooks make the kitchen a hot spot! Second is the air-conditioner, which extracts heat from inside the home and discharges it (again, plus the heat equivalent of the compressor's electricity use) to the outdoors. An AHP (air-to-air heat pump) for space heating is simply an air-conditioner with a reversing valve and controls that allow its cycle to work the opposite way, extracting heat from outdoors and delivering it (plus compressor energy) into the home. Some basics:

- The coefficient of performance (COP) of a heat pump describes the heat pump efficiency "multiplier"- how much the heat pump multiplies the energy used by the compressor, compared to simple indoor electric heaters, which have a COP of 1.0. Typical heat pump COPs are 1.5 to 6, depending on temperatures and heat pump design.
- The heat pump COP varies continually depending on the temperatures of the "source" and "sink" where heat is being extracted and discharged, respectively. The greater the "sink minus source" temperature difference, the lower the COP.

- So, for AHPs, the colder it is outdoors, the lower the heating efficiency, and the warmer it is outdoors, the lower the cooling efficiency.

Why are GHPs more efficient than AHPs?

GHPs extract heat from a closed water loop in the ground, and the ground is more moderate in temperature than outdoor air. Therefore, GHPs have achieved widespread success in the Midwest US, where winters are very cold, and summers are very hot. Instead of extracting heat from sub-zero air in mid-winter, the GHP extracts heat from the ground at depths that never freeze; and discharges heat to the ground which in summer is usually is nearer to indoor temperature. Exchanging heat with outdoor air encumbers AHPs with added features that make them more prone to failure and performance degradation in the field compared to GHPs. Table D-1 shows typical degradation factors and impacts on both AHPs and GHPs.

Table D-1: AHP/GHP Performance Comparison

Penalty Source	AHP Cause	AHP Impact	GHP Cause	GHP Impact
Extreme Weather	in table-based simulations	NA	NA	
Short Cycling	based on forced air; H & C	8.3%	same as AHP if forced air	8.3%
Defrost	50% of ORNL study; H only	6.5%	NA	
Supplemental Heat	ORNL study; H only*	5.0%	NA	
Crankcase Heater	ORNL study; H & C	4.3%	NA	
Dirty Outdoor Coil	Mowris, 40% blockage; H & C	6.5%	NA	
Total Heating		30.6%		8.3%
Total Cooling		19.1%		8.3%

*** Extremely variable with thermostat use; 5% is a conservative value for Sacramento.**

Source: University of California, Davis

What other factors favor GHPs over AHPs?

GHPs have other advantages over AHP that are more difficult to quantify, as tabulated below in Table D-2.

Table D-2: Other Considerations*

	AHP	GHP
Outdoor Space and Noise	yes	no
Outdoor Degradation	yes	no
Needed Roof Area for ZNE PV	more	less
Outdoor Service	coil cleaning	none
Expected Years Life	15	25

Refrigerant	field-filled	factory-filled
Likely Ozone Impact	significant	low
Components	outdoor unit	indoor unit
	equipment pad	
	indoor unit	
	refrigerant lines	
Wiring Needs	outdoors and indoors	indoors only

*** showing differences only**

Source: University of California, Davis

So, why don't all-electric homes typically use GHPs?

Historically, there are two major reasons that GHPs are seldom installed in California:

1. Cost! Installing the necessary tubing in the ground is expensive, particularly with the "deep bore" technology required in urban and suburban (that is, non-rural) neighborhoods. GSHPs with deep bores do not pass typical "payback" tests.
- Contractors: Partly due to high cost and drilling complexity, there are only a few contractors in a given market area with ground loop installation skills.

Why are GHP prospects better for the future?

Here are some key considerations:

1. Non-quantitative advantages: For the reasons tabulated above, GHP offers many owner advantages beyond its energy savings and benefits toward carbon reduction; these have not been in play historically because of high ground loop initial costs.
2. Results of this Project: These reported results will improve prospects in two ways:
    - They confirm that the much lower-cost shallow bore helix ("SBH", in comparison with deep bores) can perform well in California applications, bringing GHP into a reasonable cost range
    - They include excellent modeling tools that facilitate proper GHE sizing for a full range of applications; these tools should streamline acceptance of this emerging technology in the California energy standards.
3. Incentives: Congress has continued to legislate GHP incentives that match photovoltaic (PV) solar incentives (formerly 30% of installed cost, down to 26% for 2020); but even with this incentive, GHP has been too expensive for the "production builders". The low cost of the SBH changes that equation and (see 6. below) brings it into competition with PV.
4. Better Buildings: As the energy efficiency of existing buildings is improved over time, whether by retrofitted changes or by altered occupant behavior, the GHP performance advantage over AHP increases. There are two causes of this growing advantage: first, reducing thermal loads worsens AHP average efficiency because operation becomes more concentrated in the most extreme weather; and second, reduced annual loads result in less ground temperature swing for GHPs, increasing average efficiency.
5. AHP Shortcomings: As noted above, AHPs are inherently more complicated and prone to field problems than GHPs, and our average of all known field studies suggests that

absent pre-monitoring remedial work, AHP efficiencies typically fall well below their rated values. When lower costs and higher GHP volumes (and publicity) make the public more familiar with GHP technology, there will be more focus on its operational and reliability advantages compared to the inherently more finicky AHPs.

6. The Renewables Benchmark: In the near future when all new buildings will be all-electric and required to meet a zero-net energy (ZNE) standard, economics will favor higher-efficiency systems and equipment like GHPs. The cost benchmark for efficiency equipment is the "installed cost per annual kWh generated" for renewables, given the spending choice between saving and generating electricity. But with the California renewables share of total generation growing, the cost per kWh for batteries will need to be added on the generation side. (The "duck curve" discussion makes this point.)
    - Where today the pre-incentive PV installed cost per annual kWh is roughly $2.50, the cost of today's most common battery pack (Tesla Powerwall) raises the total renewable generation cost to $4.17 per annual kWh generated.
    - Based on Climate Zone 12 (Sacramento) results shown in this report for the optimal configuration, GHP costs $3.72/annual kWh saved, based on ideal AHP performance; less than the $4.17 cost of generation including batteries.
    - If field-data-based performance corrections are applied for heating (30.6% AHP, 8.3% GHP) and for cooling (19.1% AHP, 8.3% GHP), GHP savings increase to 1027 kWh/year and the GHP unit cost drops to $1.69 per annual kWh saved- less than the current $2.50/annual kWh saved for PV without batteries (see 6.a. above). (To clarify that these numbers are conservative, note that in this field-based scenario, overall annual AHP operating costs, at today's typical $0.20/kWh IOU rate, would be $520, for a $43/month average. Most homeowners would expect to spend more to heat and cool the ~2400 sq. ft. sample home.)
    - In this scenario, the non-quantitative GHP benefits (Table 2) accrue at no cost, and potential volume cost reductions remain, suggesting an excellent GHP future in California. Particularly valuable is the increased available roof area to add PV, thus increasing the likelihood of serving an electric vehicle.
7. Open Source: This technology currently has no proprietary protection; no patents, and no known patents pending. So, it is available to all entrepreneurs willing to compete to bring it to market. This also means there is no reason not to either mandate its efficiency level as soon as sufficient market volume is achieved to verify the economics presented here.

Higher GHP Volume and Participation: Entering the production builder marketplace will increase production levels and competition, reducing GHP system and installation costs and prices. Newer and better ground technology strategies will evolve, increasing GHP advantages over AHPs. State of California incentives, and continuing federal GHP incentives, would help "prime the pump" as they clearly have with photovoltaics. PV has accomplished a major descent on its cost curve over the last 20 years, and a similar opportunity is now there for GHP systems

APPENDIX E:
LDSB-GSHP Integration User Guide for EnergyPlus

EnergyPlus has a variety of built-in models for different geometries of GSHP systems that require minimal user input such as soil properties and G-function coefficients included as parameters in the building energy model. EnergyPlus also has the capability to model novel ground heat exchangers that are not included in EnergyPlus. This report examined a shallow depth, helical ground heat exchanger that was modeled using a Python Plugin in EnergyPlus. The input parameters, setup required, and algorithm are briefly described in this guide and illustrated by EnergyPlus IDF objects and python code. Specifically, the following steps are needed to model the shallow GSHP systems in EnergyPlus.

Step-1: Create an IDF as if modeling a GSHP coupled to a built-in ground heat exchanger model. This would include everything related to modeling the building such as internal loads, geometry, setpoints, etc. The water-to-air heat pump must also be specified and placed on the demand of a PlantLoop. The supply side of the PlantLoop where the GHE is specified should be left blank to fill in with no other GHE related objects specified as all GHE and ground temperature modeling will occur in the Python Plugin.

Step-2: The following EnergyPlus objects are for the Python Plugin to model the behavior of the GHE and control the supply side of the PlantLoop.

- DistrictCooling
- DistrictHeating
- EnergyManagementSystem:* objects
- ExternalInterface
- ExternalInterface:Schedule
- Output:Variable objects

The Python code records the amount of heat exchanged between the PlantLoop fluid and the source side of the heat pump from all previous timestep via Output:Variable values to calculate the inlet outlet fluid relationship of the GHE being modeled at the current timestep. The EnergyManagementSystem objects use the current GHE inlet temperature to calculate the GHE outlet temperature, and the GHE outlet temperature setpoint is met by the DistrictCooling and DistrictHeating objects.

Step-3: Define the G-function values, monthly deep ground temperatures, timestep, PlantLoop properties, and some soil properties in the Python Plugin code.

- The GHE Fluid Specific Heat (J/kg.K)
- The Number of GHEs
- The Length of the Bore hole (m)
- The Grout Thermal Conductivity (W/m. K)
- The Flow Rate through the Heat Pump (kg/s)

The G-function coefficients should be determined from data points that can be obtained from the CaRM numerical model for the G-function as shown in Figure E-1.

Figure E-1: The Variation of G-Function as a Function of Ln(T/Ts)

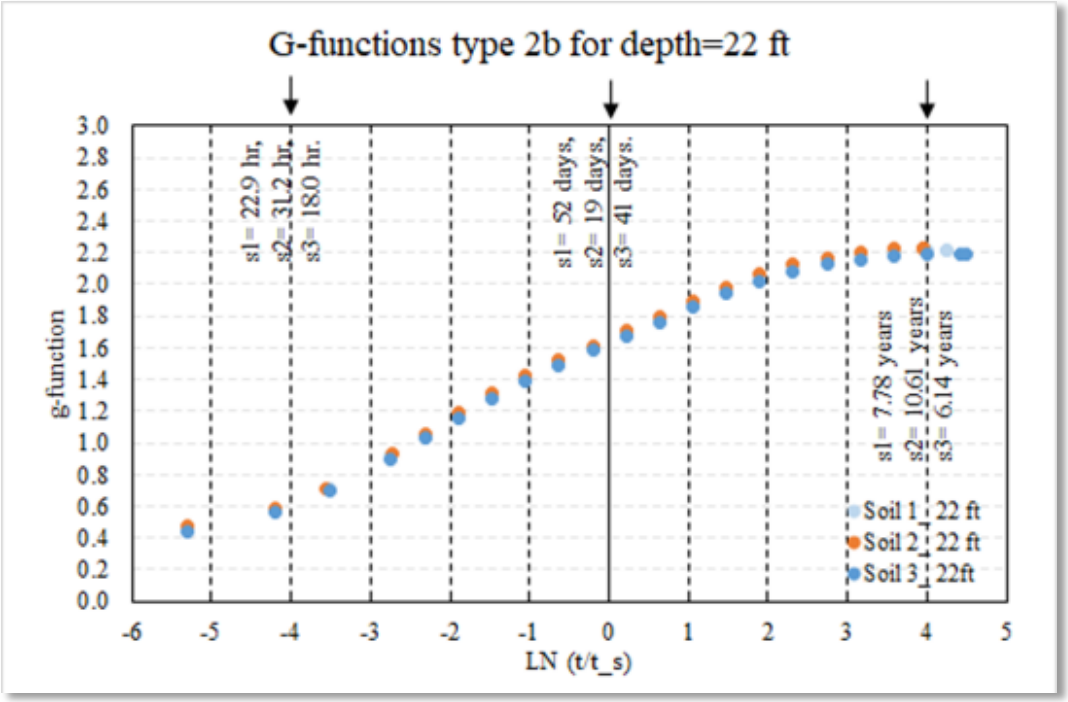

The variation of G-function as a function of Ln(T/Ts) estimated from the numerical model developed for shallow GSHP systems. Ts is a characteristic time period for the GHE which is used for the logarithmic horizontal axis for a more aesthetic graph. Ts = 51.91 days in this case, but the G-function can accept arbitrary time units.

Source: University of California, Davis

Step-4: Iteratively simulate the IDF with its associated Python Plugin and determine number of GHEs, GSHP flow rate, fluid type, heat pump capacity, etc. until the model behavior is satisfactory.

Numerical Algorithm: A common use of the G-function values is to compute the bore hole boundary temperature from the previous amounts of heat transferred to the ground. In the case of a U-tube GHE, the heat transfer through the grout from the bore hole wall to the pipe is numerically solved after calculating the bore hole wall temperature. The helical GHE, however, does not have a simple numerical solution due to the more complex geometry. Instead, the G-functions provide an output related directly to the mean fluid temperature inside the GHE since the helix portion is close to the bore hole wall.

The three main equations and some intermediate algebra lead to the GHE fluid inlet outlet relationship for the n'th timestep based on values from all previous timesteps (Figure E-2, below.)

t_n: Simulation time at the n'th timestep

Δt: length of one timestep

T_{mf}: Mean fluid temperate inside GHE

T_g: undisturbed deep ground temperature

Q': Heat absorbed by the ground per meter of GHE in one bore hole

k: grout thermal conductivity

g(t): value of G-function with time input t which is normalized into LN(t/T_s)

T_s: GHE time constant

T_{in}: temperature of fluid going into the GHE

T_{out}: temperature of fluid going out of the GHE

H: vertical length of GHE helix

$\dot{m}$: fluid mass flow rate through pipe in one bore hole

C_p: fluid specific heat

Figure E-2: Equations Used for Applying G-Functions Predicting Mean Fluid Temperature

$$T_{mf}(t_n) = T_g(t_n) + \sum_{i=1}^{n} \frac{Q'(t_i) - Q'(t_{i-1})}{2\pi k} g(t_n - t_{i-1})$$

$$T_{mf}(t_n) = \frac{T_{in}(t_n) + T_{out}(t_n)}{2} \qquad Q'(t_n) = \frac{T_{in}(t_n) - T_{out}(t_n)}{H} \dot{m} C_p$$

Substituting for $T_{mf}(t_n)$ and $Q'(t_n)$ into the top equation and rearranging solves gives $T_{out}(t_n)$ in terms of $T_{in}(t_n)$, which are the two unknowns.

$$T_{out}(t_n) = m * T_{in}(t_n) + b \qquad m = \left(\frac{\dot{m}C_\rho}{2\pi kH} g(\Delta t) - \frac{1}{2}\right) \Big/ \left(\frac{\dot{m}C_\rho}{2\pi kH} g(\Delta t) + \frac{1}{2}\right)$$

$$b = \left(T_g(t_n) - \frac{Q'(t_{n-1})}{2\pi k} g(\Delta t) + \sum_{i=1}^{n-1} \frac{Q'(t_i) - Q'(t_{i-1})}{2\pi k} g(t_n - t_{i-1}) \right) \Big/ \left(\frac{\dot{m}C_\rho}{2\pi kH} g(\Delta t) + \frac{1}{2}\right)$$

Source: University of California, Davis

The calculation of m and b are done in Python and communicated to EnergyPlus to specify the outlet fluid setpoint of the DistrictHeating and DistrictCooling objects based on the fluid temperature of the inlet of the DistrictHeating and DistrictCooling objects. The inlet and outlet fluid temperatures of the water-to-air heat pump in EnergyPlus are then solved to be consistent with the inlet and outlet fluid temperatures of the DistrictHeating and DistrictCooling objects representing the GHE.